GPS-BASED MULTI-SENSOR SYSTEMS FOR STRUCTURAL HEALTH MONITORING

WENTAO YANG

Ph.D

The Hong Kong Polytechnic University

2018

The Hong Kong Polytechnic University

Department of Land Surveying and Geo-Informatics

GPS-BASED MULTI-SENSOR SYSTEMS FOR STRUCTURAL HEALTH MONITORING

Wentao Yang

A Thesis Submitted in Partial Fulfilment of the Requirements for the

Degree of Doctor of Philosophy

March 2017

CERTIFICATE OF ORIGINALITY

I hereby declare that this thesis is my own work and that, to the best of my knowledge and belief, it reproduces no material previously published or written, nor material that has been accepted for the award of any other degree or diploma, except where due acknowledgement has been made in the text.

(Signed)

(Name of student) Yang Wentao

ABSTRACT

Structural health monitoring (SHM) is to use sensors to extract structural characteristics information, such as stress, strain, deformation, displacement, velocity and acceleration. However, the deformation signals are usually very weak and contaminated by noise, as they distribute in different space and time domains, and are acquired by different ways and different sensors. Therefore, it is necessary to process them to get the characteristic information which is sensitive to structural damage. Based on GPS observations, this thesis brings in other sensors and establishes proper mathematical models to form an integrating algorithm for structural health monitoring, which can combine the information obtained by more than two sensors to achieve a higher observation accuracy.

The thesis first analyzes the problems in GPS, tilt-meters, and accelerometers when applied to monitoring structural health. It then proposes some integration methods for combined use of these sensors. The main innovations of the thesis are as follows,

1) A platform for integrating the multi-GPS antenna and tilt-meter instruments has been studied. The priori information that the distance between instruments is a constant, is taken as constraints and added to the observation equations of GPS and the tilt-meter, in which a new data processing model is proposed. Verification experiments show that when the GPS observation is abnormal, the

integration algorithm can improve the precision by 37%, and the improvement in the elevation direction is the most significant.

2) This study proposed to combine stacked multi tilt-meters and GPS for applications such as monitoring high-rise buildings and landslides. A new least squares algorithms with constraints are proposed. An adaptive factor is given to adjust the contribution of the GPS observation and the tilt-meter observation to the parameter estimation, which provides a new way for multi sensor data fusion. The case study show, when the GPS observation is abnormal, the standard deviation of results obtained by the adaptive fusion algorithm was reduced by about 40% in all the three directions (north, east and elevation).

3) Based on an analysis of existing methods for fusing GPS, accelerometer and tilt-meter observations in monitoring structural dynamics, a Kalman filter-based model with constraints is established for integrating the different sensors data. Experiment results show that the new algorithm can improve the precision by 60% when the GPS observation is abnormal and accuracy is poor (less than 10mm).

4) An adaptive filtering algorithm with constraints is presented for the fusion of GPS, accelerometer and tilt-meter when the weighting scheme is iteratively estimated. Simulation experiments with different GPS observation precisions and different numbers of satellites in simulation experiments show that the proposed algorithm can significantly improve the reliability of the monitoring

system, especially when the GPS observation is abnormal and satellites are insufficient.

The thesis offers some new techniques for real-time monitoring of structures such as dams, high-rise buildings, and slopes for protecting lives and properties.

Keywords *Structural health monitoring; Deformation monitoring; GPS; Accelerometer; Tilt-meter; Adaptive Filter; Stochastic Constraint; Constraint Filter*

ACKNOWLEDGEMENTS

First and foremost, I would like to thank my advisor, Prof. Xiaoli Ding. His consistent advice and support have been encouraging, tireless and fundamental to the research summarized in this thesis. He gave me all of the necessary conditions to pursue and complete my PhD.

I also want to thank Prof. Wu Chen, Prof. John SHI Wen-zhong, Prof. LIU Zhi-zhao, George for their encouragement and understanding.

I acknowledge all the staff members in the department of Land Surveying and Geo-Informatics for their help and encouragement during my study, especially W.K. HO, Vaness Yu, and Ziki Cheung who helped me a lot.

I would like to thank my teachers in Central South University, Prof. Jianjun Zhu and Prof. Wujiao Dai, for their continuous support, encouragement and understanding. Thanks is also given to my teachers Yixian Wu, Benqing Xiang, Shenghao Yang in my middle school for their enlighted study. Thanks to Wenkun Yu, Biyan Chen, Gangcai Feng, Linghong Ke, Bochen Zhang, Xiaowei Zhou, Mi Jiang, Jun Hu andJennifer Collins who helped make my study in Hong Kong Polytechnic University.

In the end, thank all of my kinsfolk and my friends, for everything.

TABLE OF CONTENTS

CERTIFICATE OF ORIGINALITY ..... **III**

ABSTRACT ..... **V**

ACKNOWLEDGEMENTS ..... **VIII**

TABLE OF CONTENTS ..... **X**

LIST OF FIGURES ..... **XII**

LIST OF TABLES ..... **XVII**

LIST OF ABBREVIATIONS ..... **XIX**

CHAPTER 1 INTRODUCTION **1**

1.1 Structural Health Monitoring 1
1.2 GPS Technology in SHM 6
1.3 Multi-sensor Monitoring Technology in SHM 10
1.3.1 Integrating GPS and Accelerometer *10*
1.3.2 Integrating GPS and Tilt-meter *13*
1.3.3 Integration GPS with Pseudolites *13*
1.3.4 Integration GPS with other Satellite Positioning Systems *15*
1.4 Data Processing Technology in SHM 16
1.4.1 Gross Error Detection and Reliability Theory *17*
1.4.2 Wavelet Analysis Method *17*
1.4.3 Artificial Neural Network *20*
1.4.4 Genetic Algorithms *22*
1.4.5 Hilbert-huang Transform *23*
1.5 Research Objectives 25
1.5.1 Objectives *26*
1.5.2 Organization *28*

CHAPTER 2 SENSORS IN STRUCTURAL HEALTH MONITORING **31**

2.1 GPS 31
2.1.1 GPS Tropospheric Effects *37*
2.1.2 GPS Multi-path Effects *44*
2.1.3 Zero Baseline Tests *59*
2.2 Tilt-meter 62
2.2.1 The Measuring Principle of the Tilt-meter *62*
2.2.2 Error Model of the Tilt-meter *65*
2.2.3 Tests of Tilt-meter Accuracy *67*
2.3 Accelerometer 69
2.3.1 Principle of the Accelerometer *70*
2.3.2 MEMS Accelerometer Error Model *71*
2.3.3 Six Position Calibration of the Dynamic Accelerometer *72*
2.3.4 Tests of Accelerometer Accuracy *74*
2.4 Other Sensors 77
2.4.1 Hydrostatic Level *77*
2.4.2 Ultrasonic Flaw Detector *78*
2.4.3 Electronic Total Station *79*
2.5 Summary 80

CHAPTER 3 MULTI-ANTENNA GPS AND SINGLE TILT-METER FUSION **83**

3.1 Hardware Deployment 84
3.2 Observation Equations 84
3.2.1 Tilt-meter Observation Equations *84*

3.2.2 Constraint Equations ... *87*
3.2.3 Combined Adjustment Model ... *89*
3.3 Simulation Experiment ... 91
3.3.1 Influence of the Tilt-meter Accuracy on the Algorithms ... *93*
3.3.2 The Effect of Number of Satellites on the Algorithms ... *96*
3.3.3 Influence of GPS Data Accuracy on the Algorithms ... *101*
3.4 Case Study ... 104
3.5 Discussions and Conclusions ... 107

CHAPTER 4 MULTI TILT-METER AND SINGLE GPS DATA FUSION ... 109

4.1 Principles of Data Fusion Method ... 109
4.2 Observations Equations ... 110
4.2.1 Deformation Linearisation ... *110*
4.2.2 Torsion Correction ... *111*
4.2.3 Displacement Conversion ... *112*
4.2.4 Selection of Adaptive Factors ... *117*
4.3 Simulation Experiment ... 118
4.3.1 Impacts of Tilt-meter Precision on the Algorithms ... *119*
4.3.2 Influence of Number of Satellite on Algorithm ... *123*
4.4 Case Study ... 127
4.5 Discussions and Conclusions ... 133

CHAPTER 5 MULTI SENSOR DATA FUSION METHOD ... 135

5.1 Multi Sensor Data Fusion ... 135
5.2 Kalman Filtering Model ... 136
5.3 The Solution Methods for Constrained Filtering ... 139
5.4 Adaptive Filter Method for Constrained Filtering ... 142
5.5 Simulation Study and Analysis ... 146
5.5.1 Influence of GPS Data Accuracy on the Algorithms ... *148*
5.5.2 Influence of number of Satellites on the Algorithms ... *151*
5.6 Case Study ... 155
5.7 Discussions and Conclusions ... 159

CHAPTER 6 CONCLUSIONS AND FUTURE WORK ... 161

6.1 Conclusions ... 161
6.2 Recommendations for Future Work ... 162

REFERENCES ... 165

LIST OF FIGURES

2.1	Diagram of single epoch algorithm without integer ambiguity	34
2.2	Diagram of the multi-path effects	45
2.3	Variations of ZBL on the north coordinate	61
2.4	Variations of ZBL on the east coordinate	61
2.5	Variations of ZBL on the elevation coordinate	61
2.6	Variations of ZBL on the distance domain	62
2.7	Principle of the gravity tilt-meter	63
2-8	Transformation from tilt-meter coordinate system to GPS coordinate system	64
2-9	Tilt-angle static observation of X axis	68
2-10	Tilt-angle static observation of Y axis	68
2-11	Tilt-angle dynamic observation of X axis	69
2-12	Tilt-angle dynamic observation of Y axis	69
2-13	Acceleration static observation of X axis	75
2-14	Acceleration static observation of Y axis	75
2-15	Acceleration static observation of Z axis	75
2-16	Acceleration dynamic observation of X axis	76
2-17	Acceleration dynamic observation of Y axis	76
2-18	Acceleration dynamic observation of Z axis	77
3-1	Hardware of the integrated system	84
3-2	Variations in the north direction with different tilt-meter accuracies (precision: GPS, 8 mm; number of satellite, 9; Tilt-meter, 0.001 to 0.01 degree)	94
3-3	Variations in the east direction with different tilt-meter accuracies (precision: GPS, 8 mm; number of satellite, 9; Tilt-meter, 0.001 to 0.01 degree)	95
3-4	Variations in the elevation direction with different tilt-meter accuracies (precision: GPS, 8 mm; number of satellite, 9; Tilt-meter, 0.001 to 0.01 degree)	95
3-5	Comparison of the algorithms in terms of the variation in the north direction (precision: GPS, 8 mm; tilt-meter, 0.003 degree; number of satellite, 4)	97
3-6	Comparison of the algorithms in terms of the variation in the east direction (precision: GPS, 8 mm;	97

	tilt-meter, 0.003 degree; number of satellite, 4)	
3-7	Comparison of the algorithms in terms of the variation in the elevation direction (precision: GPS, 8 mm; tilt-meter, 0.003 degree; number of satellite, 4)	98
3-8	Comparison of the algorithms in terms of the variation in the north direction (precision: GPS, 8mm, tilt-meter, 0.003 degree; number of Satellite, 8)	99
3-9	Comparison of the algorithms in terms of the variation in the east direction (precision: GPS, 8 mm, tilt-meter, 0.003 degree; number of Satellite, 8)	99
3-10	Comparison of the algorithms in terms of the variation in the elevation direction (precision: GPS, 8 mm, tilt-meter, 0.003 degree; number of Satellite, 8)	100
3-11	Comparison of the algorithms in terms of the variation in the north direction (precision: GPS, 10 mm; tilt-meter, 0.003 degree; number of satellite, 4)	102
3-12	Comparison of the algorithms in terms of the variation in the east direction (Precision: GPS, 10 mm; tilt-meter, 0.003 degree; number of satellite, 4)	102
3-13	Comparison of the algorithms in terms of the variation in the elevation direction (precision: GPS, 10 mm; tilt-meter, 0.003 degree; number of satellite, 4)	103
3-14	Tilt angles from tilt-meter and GPS observations	104
3-15	Variations of the distances calculated from GPS observations	105
3-16	Variations in the elevation direction from GPS observations only (left panels) and from the integrated system (right panels)	106
3-17	Enlarged section of Fig. 3-16.	106
4-1	Diagram of Linear displacement & tortuosity displacement	110
4-2	Linear displacement in each section	110
4-3	Integration platform diagram	111
4-4	Diagram of the conversion from tilt variation to displacement variation	112
4-5	Comparison of the algorithms in terms of the	119

variation in the north direction (precision: GPS, 8 mm; tilt-meter, 0.001 degree; number of satellite, 9)
4-6 Comparison of the algorithms in terms of the variation in the east direction (precision: GPS, 8 mm; tilt-meter, 0.001 degree; number of satellite, 9) 120
4-7 Comparison of the algorithms in terms of the variation in the elevation direction (precision: GPS, 8 mm; tilt-meter, 0.001 degree; number of satellite, 9) 120
4-8 Comparison of the algorithms in terms of the variation in the north direction (precision: GPS, 8 mm; tilt-meter, 0.01 degree; number of satellite, 9) 121
4-9 Comparison of the algorithms in terms of the variation in the east direction (precision: GPS, 8 mm; tilt-meter, 0.01 degree; number of satellite, 9) 121
4-10 Comparison of the algorithms in terms of the variation in the elevation direction (precision: GPS, 8 mm; tilt-meter, 0.01 degree; number of satellite, 9) 122
4-11 Comparison of the algorithms in terms of the variation in the north direction (precision: GPS, 5 mm; tilt-meter, 0.003 degree; number of satellite: 4) 123
4-12 Comparison of the algorithms in terms of the variation in the east direction (precision: GPS, 5 mm; tilt-meter, 0.003 degree; number of satellite: 4) 124
4-13 Comparison of the algorithms in terms of the variation in the elevation direction (precision: GPS, 5 mm; tilt-meter, 0.003 degree; number of satellite: 4) 124
4-14 Comparison of the algorithms in terms of the variation in the north direction (precision: GPS, 5 mm; tilt-meter, 0.003 degree; number of satellite: 9) 125
4-15 Comparison of the algorithms in terms of the variation in the east direction (precision: GPS, 5 mm; tilt-meter, 0.003 degree; number of satellite: 9) 125
4-16 Comparison of the algorithms in terms of the variation in the elevation direction (precision: GPS, 5 mm; tilt-meter, 0.003 degree; number of satellite: 9) 126
4-17 Experiment instrument platform 127
4-18 Comparison of the algorithms in terms of the 128

	movement in the north direction (Use all the visible satellites)	
4-19	Comparison of the algorithms in terms of the movement in the east direction (Use all the visible satellites)	128
4-20	Comparison of the algorithms in terms of the movement in the elevation direction (Use all the visible satellites)	129
4-21-a	Sky view of satellites	129
4-21-b	Satellites observed after mask	129
4-22	Comparison of the algorithms in terms of the variation in the north direction	130
4-23	Comparison of the algorithms in terms of the variation in the east direction	131
4-24	Comparison of the algorithms in terms of the variation in the elevation direction	131
5-1	Comparison of the algorithms in terms of the variations in the north direction (precision: GPS, 10mm; tilt-meter, 0.02 degree; accelerometer, 0.002g; number of satellite, 4)	148
5-2	Comparison of the algorithms in terms of the variations in the east direction (precision: GPS, 10mm; tilt-meter, 0.02 degree; accelerometer, 0.002g; number of satellite, 4)	149
5-3	Comparison of the algorithms in terms of the variations in the elevation direction (precision: GPS, 10mm; tilt-meter, 0.02 degree; accelerometer, 0.002g; number of satellite, 4)	149
5-4	Comparison of the algorithms in terms of the variations in the north direction (precision: GPS, 5mm; tilt-meter, 0.02 degree; accelerometer, 0.003 g; number of satellite, 4)	151
5-5	Comparison of the algorithms in terms of the variations in the east direction (precision: GPS, 10mm; tilt-meter, 0.02 degree; accelerometer, 0.002 g; number of satellite, 4)	152
5-6	Comparison of the algorithms in terms of the	152

	variations in the elevation direction (precision: GPS, 5mm; tilt-meter, 0.02 degree; accelerometer, 0.003 g; number of satellite, 4)	
5-7	Instruments and experiment environment	154
5-8	Movement in the north direction of the dynamical experiment	155
5-9	Movement in the east direction of the dynamical experiment	155
5-10	Movement in the elevation direction of the dynamical experiment	156

LIST OF TABLES

2-1	Six position orientation and the gravity acceleration of each axis.	73
3-1	WGS84 coordinates and plane coordinates of three known points (A1, A2, A3).	91
3-2	Standard deviations of three algorithms when the accuracy of the tilt-meter changes. (unit: mm) (precision: GPS, 8 mm; number of satellite, 9*; Tilt-meter,0.001 to 0.015 degree*).	93
3-3	Standard deviations of three algorithms when different numbers of satellites are used. (unit: mm) (precision: GPS, 8 mm; tilt-meter, 0.003 degree; number of satellites, 4 to 9).	95
3-4	Standard deviations of the three algorithms with different GPS precisions. (unit: mm) (precision: GPS, 10 mm; tilt-meter, 0.003 degree; number of satellite, 4; GPS, 5 to 15 mm).	100
3-5	Standard deviation of variations from GPS algorithm and from GPS/Tilt-meter algorithm.	107
4-1	Standard deviations of the three algorithms with different accuracies. (unit: mm) (precision: GPS, 8 mm; tilt-meter, 0.001 degree; Tilt-meter, 0.001 to 0.015 degree).	119
4-2	Standard deviations of the three algorithms with different visible satellite number. (unit: mm) (precision: tilt-meter, 0.01 degree; GPS, 8 mm; number of satellites, 4 to 9).	123
4-3	Standard deviation of variations from GPS/Tilt algorithm and from adaptive algorithm	131
5-1	Standard deviations of the four algorithms with different GPS precisions. (unit: mm) (Precision: Precision: GPS, 2 to 15 mm; tilt-meter, 0.002 degree; accelerometer, 0.002g).	147
5-2	Standard deviations of the four algorithms with different numbers of satellites. (unit: mm) (Precision, GPS, 10 mm; tilt-meter 0.002 degree;	150

accelerometer, 0.002g; number of satellites, 4 to 9)
5-3 standard deviations of the four algorithms with different numbers of satellites. (unit: mm) (Precision, GPS, 10 mm; tilt-meter 0.005 degree; accelerometer, 0.002g; number of satellites, 4 to 9) 152
5-4 Standard deviations of the four algorithms in the dynamical experiment. (unit: mm) 156

LIST OF ABBREVIATIONS

BDS	Beidou Satellite Navigation System	9
BP	Back Propagation	20
C/No	Carrier-to-noise Power Density	48
DDs	Double Differences	55
DLL	Delay-locked Loop	47
EMD	Empirical Mode Decomposition	24
GA	Genetic Algorithm	22
GPS	Global Positioning System	6
HHT	Hilbert-Huang Transform	23
ICA	Independent Component Analysis	24
IMF	Intrinsic Mode Functions	24
IMS	Intrinsic Mode Signal	24
IMU	Inertial Measurement Unit	11
MEDLL	Multi-path Elimination Delay Lock Loop	48
MEMS	Micro-Electro-Mechanical System	70
PLL	Phase-locked Loop	47
RTK	Real Time Kinematic	7
SAAS	Saastamoinen Model	39
SHM	Structural Health Monitoring	1
SNR	Signal to Noise Ratio	25
UPS	Uninterruptible Power System	11
VLBI	Very long baseline interferometry	44
WVR	Water Vapor Radiometer	44
ZBL	Zero Baseline	59

CHAPTER 1 INTRODUCTION

1.1 Structural Health Monitoring

*Civil infrastructures such as bridges, buildings, and pipelines must be maintained to ensure public safety. Structural health monitoring (SHM) aims to give at every moment during the life of a structure, a diagnosis of the "state" of the constituent materials, of the different parts and of the full assembly of these parts constituting the structure as a whole (***Daniel et al., 2006***). SHM involves the observation of a system over time using periodically sampled dynamic response measurements from an array of sensors, the extraction of damage-sensitive features from these measurements, and the statistical analysis of these features to determine the current state of system health (***Hoon et al., 2001***). SHM refers to the measurement of the operating and loading environment and the critical responses of a structure to track and evaluate the symptoms of operational incidents, anomalies, and/or deterioration or damage indicators that may affect operation, serviceability, or safety reliability (***Aktan et al., 2000***). By establishing threshold displacements or drift ratios and identifying changing dynamic characteristics, procedures can be developed to use such information to ensure public safety and/or take steps to improve the performance of the structures (***Celebi et al., 1998***).*

At present, rapid economic development brings more high-rise buildings, large water conservation projects and bridges. Real-time dynamic deformation

monitoring and diagnosis for deformable bodies, structure damage detection, structural safety assessment, and disaster prevention and control have become increasingly important for modern engineering and it has become a research hot spot. The SHM system can collect structural health status data in real time and identify the location and damage extent by some damage identification algorithms. Therefore, it can effectively evaluate the structure safety, completely predict the evolution of structure status and provide early-warning for emergencies. In addition, monitoring data quality evaluation, deformation inner rules analysis, prediction model for structural property changes and structure rest life are important study areas of civil engineering surveying.

Installing appropriate sensors in the structure is common for SHM. These usually consist of corrosion sensors, strain gauges, corrosion sensors, barometers, hygrometers, pluviometers and fiber optic sensors. These instruments can be roughly divided into three categories:

*1) Structural sensors, which can identify structural pressure strength, shear strength, elasticity and plasticity, temperature shrinkage, chemical shrinkage and conduct crack detection. For example, corrosion of steel elements can be investigated by nondestructive evaluation technologies such as eddy currents, ultrasonic waves, and electrochemical impedance spectroscopy (***Fildes et al., 1995***). **Suresh et al.** (**2004**) employed surface-bonded piezo-impedance transducers to perform structural identification and damage diagnosis for*

structural components, such as the concrete bridge, during a destructive loading test.

2) Environment sensors, which can collect temperature, humidity, rainfall, wind speed, stress and other parameters. **Staszewski et al.** *(***1997***) demonstrated that temperature and ambient vibrations can affect the performance of piezoelectric sensors in composite plate tests.*

3) Geodetic monitoring sensors, such as Global Positioning System (GPS), robotic total station, crack meter, tilt-meter. GPS is a common geodetic monitoring technical tool used in recent years. It has the ability to work under adverse weather conditions whilst providing measurements of relative displacements in near real-time and helping to identify the dynamic characteristics of vibrating systems. So, they have been widely used in the deformation monitoring of man-made structures.

*A lot of studies have been conducted in the last 30 years revolving around those sensor technologies. In 1987, some sensors were installed on the Foyle Bridge in Derry, Northern Ireland, a three-span continuous steel box girder bridge (522 m long), to monitor the girder vibration, deflection and strain under the effect of wind and vehicle load, while also simultaneously monitoring the wind and temperature fields. It is one of the earliest complete monitoring systems which real-time monitoring and analysis was well utilized and data shared on the internet (***Sloan et al., 1993***). Since then, a lot of SHM systems were installed on bridges including the Skarnsundet Bridge in Norway, a cable-stayed bridge*

*(main span 530 m), the Sunshine Skyway Bridge (main span 440 m) in USA, Faroe, a sea-crossing cable-stayed bridge and the Great Belt East, a suspension bridge (main span 1624 m) in Denmark, the Tampico cable-stayed bridge in Mexico, Flintshire, a single tower cable-stayed bridge in UK, Confederation, a continuous rigid frame bridge in Canada, the Akashi Kaikyo Bridge in Japan, the Seo-Hae cable-stayed bridge in South Korea, Rama 8, a single tower cable-stayed bridge in Thailand(***Chueng et al., 1997; Sumitro et al., 2001; Sohn et al., 2003***). **Ko et al.** (**2005**) summarized large-scale bridges in China instrumented with real-time monitoring systems, such as the Jiang Yin Bridge, the first Nanjing Yangtze River Bridge, the second Nanjing Yangtze River Bridge, Run Yang Yangtze River Bridge and the Sutong Yangtze River Bridge, the Tsing Ma Bridge, the Kap Shui Mun Bridge and Stonecutters Bridge, Human Bridge and the Zhanjiang Bay Bridge.*

*The Tsing Ma Bridge in Hong Kong, which is a railway-highway combined suspension bridge with a total length of 2160 m and a main span of 1337 m, also includes a functioning SHM system. It is an important transport tie connecting Hong Kong's new airport to the downtown area. Considering Hong Kong's frequent typhoon weather and the large loading applied from the vehicles and railway to the bridge structure, a large SHM system was installed during the construction (***Lau et al., 1999**; **Ko et al., 1999***). The SHM system mainly monitor the influence of wind, vehicle and temperature on the bridge. The wind load is measured by 6 anemometers installed on the deck and on top of pylons.*

*The vehicle load is measured by weight machines and the temperature is measured by 115 temperature sensors installed on the deck and pylon. The global structure response is measured by accelerometer sensors, displacement sensors, level range finders and GPS systems. In total, 12 one-way, 3 two-way and 2 three-way accelerometer sensors were installed on Tsing Ma bridge deck and the main cable and 2 displacement sensors and 9 level range finders were installed on the deck and pylon of bridge. The local structure response is measured by laid strains. Altogether, 110 strain gauges were pasted on the deck and pylon. In addition, a system for data collection, transmission and processing was also installed on the bridge which can facilitate real-time monitoring on main pylon, rope, rope anchor head, suspenders, deck and bridge supports. Observations of the last five years show that the wind effect, temperature and transport loads are far below the value specified in the design, and the strain-displacement reaction of the key parts are much lower than that stated in the design. Besides the Tsing Ma Bridge, two other major cable-stayed bridges in Hong Kong had SHM systems installed. The total number of sensors installed on these three bridges is approx. 900 (***Lau et al., 1999***).*

*SHM systems are also widely applied in building management. It was reported that more than 150 buildings in California, more than 100 buildings in Japan, and more than 40 buildings in Taiwan have been fitted with instruments with strong motion monitoring systems for seismic excitation/response measurement and post-earthquake damage assessment (***Huang et al., 2001; Li et al., 2003; Huang et al., 2006***).* **Brown et al.** *(***1998***) deployed a long-term monitoring*

program on the Republic Plaza building in Singapore, which was constructed with a reinforced concrete core and a structural steel frame. Large number of stress and strain gauges were embedded inside the core wall and columns to detect variation with increasing dead loads during construction. This allowed for a full-scale measurement on a number of high-rise structures under strong wind conditions. **Li et al.** *(***2007***) devised a GPS-based SHM system for high-rise buildings which simultaneously and continuously measures the wind speed, wind direction and building's displacement responses under strong wind conditions.*

Normally, most structural designs and monitoring system designs are integrated in modern architecture to ensure that engineers design the system including sensing, signal processing, data management and offer valuable information for evaluating structural integrity, durability and reliability. These would provide most benefit to owners with regard to asset management.

1.2 GPS Technology in SHM

*With the continuous developments in hardware and software, GPS has been shown to perform well in the bridge structural vibration monitoring and deformation of land movements, landsides, earth structures (***Forward et al., 2001***), dams (***Hudnut and Behr, 1998***), buildings (***Lovse et al., 1995; Guo et al., 1997***), and bridges (***Fujino et al., 2000; Roberts, 1997; Roberts et al., 1999***).*

As early as November 1993, **Lovse et al.** *(***1995***) had measured the vibration of the Calgary Tower (height 160m) under great winds in west Alberta with GPS. The results show that the vibration frequencies in the North-South and East-West directions are both 0.3Hz, within the safe range of 0.1-10Hz, and the amplitudes are ±15cm and ±5cm in these two directions, respectively.* **Celebi et al.** *(***1998, 1999, 2002***) used real time kinematic (RTK) GPS with a frequency of 10 Hz to conduct a simulation experiment of vibration measurement for a simple structural model.* **Kijewski et al.** *(***2003) and Michael et al. (2005***) used GPS to monitor a building in Chicago city and extracted necessary data to accurately determine the damping coefficient of high-rise buildings. They also found that GPS measurements have some low frequency systematic errors that are difficult to separate by filtering. In order to test the accuracy of RTK GPS measurements,* **Tamura et al.** *(***2002***) designed a small electronic vibration device to simulate high-rise structure vibrations with different frequencies and amplitudes. The actual vibration displacement was measured by a precise linear converter. Their results show that the GPS measurements consist with the actual vibration displacement when the amplitude is above 2 cm and the frequency is lower than 2 Hz. Then they monitored the deformation of a steel tower with a height of 108 meters under high wind speed and extreme temperatures. They found the average displacement grows proportionally to the square of the mean wind speed when wind speeds are high and the maximum displacement of the tower is 4 cm with an approximate circle trajectory when there is no wind.* **Janusz et al.** *(***2011***) made a container, from which water can leak from the bottom at a slow*

speed, to simulate the quasi-static test. The test shows that GPS could measure dynamic displacements accurately if the amplitude of motion is not less than 5 mm in the horizontal plane or not less than 10 mm in the vertical direction, provided that the motion frequency is less than or equal to 1 Hz. In 1996, **Guo et al.** *(***1997***) used two single-frequency GPS receivers with a sampling rate of 10 Hz to monitor the Di Wang Commercial building (height 325m) in Shenzhen, China. They verified the dynamic analysis results of the original structural design and results accord with the structural calculation value.* **Chen et al.** *(***2001***) and* **Huang et al.** *(***2001***) used dual-frequency GPS receivers with a sampling rate of 10Hz to measure the vibration of the same building for two days. In order to further improve the accuracy, they employed wavelet filter and Multi-resolution analysis to de-ionise and separate long-period multipath errors, which can reveal micro structural vibration (1~2mm) in GPS monitoring results.* **Dai et al.** *(***2007***) proposed a single epoch algorithm with deformation characteristics and maximum deformation constraints, which greatly reduces single epoch ambiguity search space and computation load of candidate coordinates, and improves the calculation efficiency.* **Wang et al.** *(***2011***) used GPS RTK and total station, the single epoch GPS positioning technology and the three-dimensional measurement technology to deploy real-time track and monitoring on the whole process of a landslide. The results confirm that the horizontal precision and vertical precision of RTK surveying can be between 15 mm and 20 mm when the base stations and mobile stations can observe more than 7 satellites and the RTK data links work well. In 2015,* **Meng et al.** *(***2016***) established a GPS monitoring*

system for deformation and wind speed for the Forth Road Bridge. With 4 GPS receivers and 2 ultrasonic anemometers, the system can measure the three dimensional displacement and wind speed for bridge key parts in real-time, and can monitor settlement of bridge substructure by earth observation technologies. **Xiao et al.** *(***2016***) studied the deformation monitoring algorithms with millimeter level precision based on the Beidou satellite navigation system (BDS), and proposed more efficient search method for BDS constellation structure with independent double difference observation values.* **Ye et al.** *(***2016***) analysed the success rate of single epoch ambiguity resolution in different calculation models of GPS and BDS and proposed an algorithm for deformation data processing based on Beidou tri-band observations.*

*However, when the SHM is used for monitoring dams, bridges and high-rise buildings, GPS positioning accuracy is highly sensitive to multipath effects when GPS signals reflected by nearby objects arrive at a receiver's antenna (***Axelrad, 1996***). Additionally, when monitoring high-rise structures, the tropospheric effects cannot be effectively mitigated by the double-difference operations in GPS data processing.*

*Many studies have been done to reduce these errors, some improve hardware like receivers and antennas to refrain the multi-path noises, some use semi-parametric models and the penalized least square method are used to model multipath errors (***Jia et al., 2000***), details can be find in section 2.1.*

1.3 Multi-sensor Monitoring Technology in SHM

SHM consists of local monitoring and global monitoring. Local monitoring mainly observes important structure parts or components by sensors, and global monitoring observes macroscopic deformation, displacements and vibrations of large civil engineering structures by monitoring technologies, such as the GPS, surveying robots (total stations) and laser scan micrometer. Combining GPS surveying with other sensors, including extensometers, tilt-meters, accelerometers, surveying total stations and photogrammetric, is another way to reduce multi-path errors and increase the positioning accuracy.

1.3.1 Integrating GPS and Accelerometer

*Integrating GPS with an accelerometer is a potential method for mitigating multipath effects and increasing the positioning solution accuracy. While GPS can detect long wavelength deformations, the accelerometer, with its higher data rate and short-term stability, is capable to accurately identify higher frequency movement. In semi-static or dynamic applications with very small rotations, the combination of GPS and accelerometer can provide necessary information for reliable long-term millimeter accuracy positioning (***Tolmanand, 1997***). Many methods have been proposed to integrate the two datasets for obtaining more accurate and reliable seismic waves (displacement, velocity and acceleration). There are two critical issues in the integration. One is the precise correction of the strong-motion's baseline shifts caused by tilting and/or rotation of the seismic sensors, and the other is the suitable constraint of the high resolution*

*accelerations to get more reliable seismic waves (***Rui et al., 2015***). Using RTK GPS and accelerometer,* **Celebi et al.** *(***1998, 1999, 2002***) simultaneously monitored in real-time the vibration of a 44-story building in Los Angeles and a 34-story building in San Francisco. The results show that GPS and accelerometer both can measure the fundamental vibration frequencies of the buildings (0.25Hz) when the amplitude is small, but GPS provides more accurate measurements when amplitudes are large.* **Meng et al.** *(***2004***) combined GPS and accelerometer to monitor the deformation of bridges, then process the data by the adaptive filtering method and extracted reliable results. By adding suppressor and lightning rod components,* **Yi et al.** *(***2010***) improved the above multi-sensor monitoring device to reduce multipath errors and effectively avoid lightning strikes.* **Meng et al.** *(***2011***) made a precise time data logger (PTDL) to embed the uninterruptible power system (UPS) time of the GPS receivers into acceleration signals, so the multi sensor synchronization problem can be resolved.* **Moschas et al.** *(***2011***) also successfully monitored the vibration response of iron towers and steel bridges by integrating accelerometers with the GNSS receiver.*

In recent years, the INS became increasingly important in deformation monitoring, as the inertial measurement unit (IMU) is able to deploy short-term high precision independent positioning. As INS and GPS are complementary to each other, they are integrated as a GPS/INS system. If GPS drop-outs, INS will be calibrated when GPS lose satellites. After the outage, the INS can provide estimates of position and velocity for the GPS receiver to speed up data

*reacquisition (***Bjornar Vik, 2000***). The integrated solution of GPS and INS offers better long term accuracy than a stand-alone accelerometer and is suitable for demanding applications.* **Chen et al.** *(***2013***) applied GPS/INS positioning to monitor the railway track irregularity, therefore improving the monitoring efficiency.* **Portovello et al.** *(***2003***) studied the dynamic displacement monitoring method for bridge structures based on the integration of GPS and accelerometer. To reduce the multipath errors and observation noises,* **Han et al.** *(***2015***) established a model to remove system trends and noise based on empirical mode decomposition. They also built an acceleration displacement reconstructing model with regularisation parameters. They analysed the correlation between GPS intrinsic mode function components and reconstructing acceleration displacement to extract the bridge deformation information.The displacement can be obtained by the double integration of acceleration signals, but the double integration method leads to errors in the calculation of velocities and displacements. Accelerometer measurements cannot be used to recover the permanent displacements at centimeter level, and even if they could, it is questionable if it can be done in real-time (***Celebi, 2000***). In other words, the accuracy level of displacements calculated from accelerations has not been widely verified by observations. In addition, this method cannot measure the total inertia offset of buildings. Thus, monitoring the global response via accelerometers can only provide an indication of resonant response and fails to capture static and quasi-static behaviors (***Kijewski et al., 2006***).*

1.3.2 Integrating GPS and Tilt-meter

Tilt-meter has high precision levels and are designed to measure very small horizontal tilts. They has been used extensively for monitoring volcanoes, responses of dams to filling, small movements of potential landslides, and structure responses to influences like loading and foundation settlement. **Yigit et al.** *(***2008***) measured a tall building (Rixos) using a tilt-meter, and analysed its consistency with the GPS results in both the time and frequency domains under the action of a hurricane.* **Ma et al.** *(***2014***) determined the slope slip surface by combining the ground-based GPS and underground sliding tilt-meters. A slide failure mode and the sliding zone's depth of the corresponding surface monitoring hole was determined by the underground displacement data.*

At present, most researches on multi-sensor integrations directly integrate the coordinates of tilt-meter result with that of GPS result (coordinate domain integration), without considering the integration of the observation ranges. It would be better if the weighting across multiple sensor errors can be considered.

1.3.3 Integration GPS with Pseudolites

The geometry of the satellite constellation has a direct influence on the accuracy of GPS positioning, which should be considered when the sky view of the antenna is obstructed by trees, high buildings or mountainous terrain, etc. One way to improve the GPS satellite geometry and the availability of ranging signals is to use pseudolites to transmit GPS-like signals. Pseudolites are ground-based

*transmitters that can be configured to emit GPS-like signals to enhance the GPS (***Elrod et al., 1996; Wang et al., 2001***). In the test range at Yuma Proving Ground (USA), four ground transmitters provide the simulated GPS satellite signals to test GPS receivers. These ground transmitters are the so-called pseudolites (***Harrington et al., 1976***). These first pseudolites were designed to transmit GPS L1 signals, though the navigation message for these pseudolites was different from that of the GPS satellites.*

Cohen et al. *(***1993***) developed a low cost GPS L1 C/A code pseudolite for an automatic landing system CAT III. In the mid-1990s, commercial pseudolite hardware products became available on the market. The first commercial pseudolite product was manufactured by the Integri Nautics Company (www.integriNautics.com). In 2001, another manufacturer, Navicom, launched a new pseudolite product called NGS1T (***Soderholm et al., 2001***).*

*Although they transmit similar ranging signals with GPS satellites, pseudolite signals can be much stronger. If the transmitters are far from the receiver antenna, the pseudolite signals will be too weak to be tracked. This is referred to as the 'near-far' problem caused by the higher dynamic range of the signal strength, which a user receiver will experience when the receiver is in motion in proximity to pseudolite signal transmitters (***Cobb et al., 1997***). Based on a signal processing technique that does not require receiver hardware modification,* **Madhani et al.** *(***2001***) proposed a successive interference cancellation approach to mitigate the near-far problem.* **Dai, et al.** *(***2000***)*

presented an integrated system of GPS and PL for deformation monitoring and demonstrated that the accuracy of the height component could be improved to the same level as that of the horizontal components with appropriately located pseudolites.

1.3.4 Integration GPS with other Satellite Positioning Systems

The reliability of the satellite-based navigation systems is essentially dependent on the redundancy and geometry of the measurements system. The integration of GPS, COMPASS and GLONASS has advantages as follows.

a) The geometry strength of satellite constellation will be improved. The Position Dilution of Precision (PDOP) value will drop dramatically because more satellites are visible.

*b) The positioning accuracy will be improved, especially for carrier phase based RTK positioning, because much more redundant double difference measurements can be used to mitigate systematic errors such as multi-path errors and small cycle slips (***Wang et al., 1996. Nobuaki et al., 2001***).*

c) The ambiguity solution will be faster. Even single epoch solution can be attained. And thus the corresponding success rate will also be improved dramatically.

Similar to the GPS system, GLONASS and COMPASS systems consist of space segment, control segment and user segment. The user equipment is able to measure pseudo-ranges and pseudo-range rates.

1.4 Data Processing Technology in SHM

The SHM uses sensors to extract structure information in different space and time domains, such as stress, strain, deformation and displacement, velocity and acceleration. Because many kinds of sensors appearing in SHM observation are heterogeneous sensors, their observation equations have different error forms. In particular, different observation information needs to give a suitable weight to make data fusion, they cannot simply use a set least squares to estimate parameters. Some new needs data processing algorithms must be studied. However, following factors affect the information collection:

a). Incomplete survey information.

b). Low measurement accuracy and signal noises.

c). Non-sensitivity of the survey information to the local deformation of object.

As the collected signals are usually weak or contaminated, they should be processed before being used to get sensitive characteristics of structure damage. The SHM includes deformation monitoring, data pre-processing and deformation analysis and prediction. The data processing method directly affects the validity and reliability of the monitoring results. With the emergence of new surveying and mapping technologies, the traditional single monitor mode has changed to

multiple-monitor mode, which integrate point, line and space monitoring. For example, GPS observation and measurement errors has complex signal characteristics, such as multi-path error, tropospheric delay and ionosphere delay. Many cleaning methods for deformation monitoring data have been studied. A lot of new data processing methods for SHM were proposed, for example, digital filtering, adaptive Kalman filtering, wavelet analysis method, fractal geometry, and fuzzy methods.

1.4.1 Gross Error Detection and Reliability Theory

Observation errors, including accidental errors, system errors and gross errors (abnormal values, singular values, outliers), seriously affect the observation quality. Gross errors are large random errors. Detecting and controlling gross errors are important to the survey and mapping data processing. A common method for gross errors processing based on the reliability theory is to put the gross error into a function model or a stochastic model, then use the Least-Squares combined with hypothesis testing methods to detect gross errors. This method chooses appropriate weight functions to reduce the weight of observations containing gross errors by iterative adjustment.

1.4.2 Wavelet Analysis Method

As the wavelet analysis has the multi-scale spatial and temporal resolution and its time scale can be set as needed, it can describe the intrinsic characteristics of signals more accurately and can be used to extract non-stationary vibration

signal waveform characteristics to get the original signals. Because of its signal magnifying and focusing ability, the wavelet transform can be used to identify and analyse structural deformation signals. Wavelet analysis on the structure observation can identify whether the structure is health and can accurately find the exact moment that the injury occurs. Using the Mexican hat wavelet, **Segawa et al.** *(***2001***) analysed input acceleration and the response of acceleration to identify parameter changes (such as stiffness and damping) caused by structural damages.* **Hera et al.** *(***2002***) studied the health monitoring benchmark with the wavelet analysis theory. He deployed the discrete wavelet transform to acceleration responses and determined the moment the damage occurs by decomposing the anomaly of the high-frequency wave. The results demonstrate the high sensitivity to local stiffness loss of this method and verify that the wavelet analysis is especially suitable for online monitoring. By means of Wavelet decomposition and reconstruction,* **Huang et al.** *(***2002***) extracted deformation characteristics from the contaminated observation data sequence. They overcame the limitations of traditional methods in solving non-stationary and non-equal time-interval observation data series filter.* **Li et al.** *(***2003***) applied a wavelet analysis to the dynamic reflection in a shaking table test of a two-story wood frame house.* **Qin et al.** *(***2006***) reconfigured the transform survey data to signals, and then used the wavelet analysis to filter out high-frequency noises.* **Pan et al.** *(***2007***) applied the wavelet neural network, which combines wavelet analysis and artificial neural network, to process the deformation data.* **Hu et al.** *(***2008***) proposed a complex wavelet analysis*

method to reduce the analysis time and difficulty of TDR monitoring signals by decreasing the computational load of the wavelet function. **Wang et al.** *(***2011***) brought up a hierarchical threshold de-noising method about autocorrelation analysis of the wavelet detail coefficients and determined the maximum levels of wavelet decomposition by the minimum frequency of useful signals.* **Li et al.** *(***2011***) employed wavelet transform to de-ionise and extract deformation trends and frequencies and did a wavelet analysis to the wind-induced vibration of bridges. As the hard-threshold method is not continuous and the soft-threshold has bias,* **Yao et al.** *(***2011***) presented an effective wavelet threshold de-noising model for GPS dynamic deformation monitoring data.* **Luan et al.** *(***2015***) processed the wavelet de-noised data by the Kalman filtering algorithm, which improves the reliability of prediction and analysis about bridge deformation.* **Wu et al.** *(***2007***) proposed a Kalman filtering and smoothing technique, which was capable of dealing with multi-rate estimates, to accurately estimate the velocity and displacement from noise contaminated measurements of acceleration and displacement, which were gathered by accelerometer and GPS receivers, respectively.* **Bei et al.** *(***2002***) applied wavelet analysis to deformation monitoring and proposed a new standard for evaluating the effect of wavelet de-ionising.* **Wang et al.** *(***2016***) conducted a spectral analysis and wavelet de-noising to bridge vibration time series and got the main vibration frequency range and the two main cycles under the bridge load. They obtained the de-ionised time series by using high frequency soft-threshold methods on each layer.*

Wavelet functions are discrepant in structures, characteristics and analysis effects, so selecting a proper wavelet function is always important. However, there is still no general principle for wavelet function selection available and most researchers select wavelet functions by their personal experience now. On the other hand, assessment of the structural damage also needs further research.

1.4.3 Artificial Neural Network

*The back propagation (BP) neural network algorithm is a multi-layer feedforward network trained according to error back propagation algorithm and is one of the most widely applied neural network models (***Li et al., 2012***). By training the network weights and thresholds, arbitrary non-linear mapping from input to output can be realised. Basic principles of applying neural network to deformation monitoring are: taking the physical parameters (such as natural frequencies, mode shapes) got by numerical methods (such as the finite element method, energy law) or filed measuring as input training variables of the training samples, and the structural damage (location, degree) as output variables, train the neural network with training samples to make it remember these knowledge, based on the organization, the abilities of self-learning and adaptation of the neural network. And make the natural network master the nonlinear mapping between input variables (such as the natural frequencies, mode shapes) and output variables (location, degree of structure damage), and to detect the structural damage. There are many relating optimisation algorithms, such assimilated annealing, genetic algorithms, Ant Colony algorithm*

and Particle Swarm, which have been applied to the prediction model of neural network to improve the prediction accuracy of deformation data processing.

Ko et al. *(***2001***) used the back-propagation neural network to detect the damage of the Kap Shui Mun Bridge in Hong Kong. They proposed new indicators, and applied the 3-step hierarchical damage identification consisting of the early damage warning, damage detection and localisation and estimation of damage phases.* **Yan et al.** *(***2009***) introduced two new parameters, scaling factor and translation factor, into the wavelet neural network to make it be flexible and effective in function approximation and well in fault tolerance.* **Xu et al.** *(***2012***) optimized the weights and thresholds for BP neural network by the particle swarm optimization and established a model for dam deformation monitoring based on of the optimized BP neural network.* **Zhou et al.** *(***2012***) built a new BP network by introducing the nonlinear optimization method, which can be used to process and predict the structure deformation data with uncertainty and nonlinearity.* **Fan et al.** *(***2013***) used the optimized neural network to establish a deformation prediction model and trained and tested its reliability and feasibility with related data. The results verified that the generalized regression neural network algorithm can quickly find suitable smoothing factors and predict motion data effectively.* **Liu et al.** *(***2014***) optimized the initial weights and threshold of the neural network model by the particle swarm optimization algorithm and took the available deformation monitoring data as the input parameters to establish a deep foundation pit deformation forecasting method by introducing nonlinear inertia weight*

decreasing strategy and learning factor dynamic adjustment method. **Hu et al.** *(***2014***) proposed an improved particle swarm optimization algorithm (IPSO), which considers the optimal particle effects on the neighborhood particle swarm speed.* **Wu et al.** *(***2015***) came up with a new method based on non-equal time-interval gray combination GA-BP model with weight.*

With the growing application of neural network in deformation monitoring, some problems appeared.

a) For large and complex structures, network training is time consuming and needs a large number of injury samples. The network convergence is slow and sometimes only the local convergence is obtained.

b) Model selection: For different structures, different network models bring different results, therefore, selecting a network model according to the structural characteristics needs further study.

c) Network size. There is no uniform method to determine the network size for different structures. In practice, trying the size one by one is the only way now.

1.4.4 Genetic Algorithms

The Genetic algorithm (GA) is a search algorithm based on natural selection and the mechanisms of population genetics. A simple GA is comprised of three operators: reproduction, crossover, and mutation. Reproduction is the process of survival-of-the-fittest selection. Crossover is the partial swapping between two

*parent strings to produce two offspring strings. Mutation is the occasional random inversion of bit values that generates non-recursive offspring (***Lee et al., 2005***). It has easy operation and robustness and a searching space throughout the entire solution space, which can significantly improve the efficiency of random searching in the parameter space.*

Although great improvement has been achieved in genetic algorithms, its basic theory is not perfect. On top of this, there is a great gap between theory and application, which also requires a lot of in-depth research, specifically:

a) Convergence theories of GA are incomplete.

b) Holland schema theorem still cannot clearly explain the premature phenomena and cheating problem.

c) The genetic algorithm has low searching efficiency and complex calculation process.

1.4.5 Hilbert-Huang Transform

Hilbert-Huang transform (HHT), was developed on the basis of the Hilbert transform is a time-frequency analysis method for specific nonlinear and non-stationary time series analysis. It overcomes the limitations of traditional Hilbert transform, and first describes the basic concepts of instantaneous frequency and time-frequency analysis. It is a new adaptive method for analysing non-stationary and nonlinear data. The HHT method consists of two steps: first, use

the signal empirical mode decomposition (EMD) to get a list of intrinsic mode functions (IMF) or intrinsic mode signal (IMS), and then use the Hilbert transform on the IMF to obtain the Hilbert-Huang spectrum, called the Hilbert spectrum. As it takes instantaneous frequency as the basic amount and the Eigen-mode signal time as the basic domain signal, the HHT method out performs traditional methods in reflecting the time domain of signals.

Yang et al. *(***2001***) applied HHT to the structure damage identification in civil engineering and pointed out that combining EMD and Hilbert spectrum analysis can accurately detect the injury time and the frequency change of structure self-vibration before and after the damage. By this method, the acceleration signal of only one point is needed in detecting the moment of structural damage.* **Guo et al.** *(***2007***) analyzed the dam monitoring data from the time and frequency domains with the HHT.* **Li et al.** *(***2007***) verified that the HHT can effectively extract dynamic characteristics and structure damage information from the structure responses to diagnose the structure health status. For the mode mixing problem caused by intermittent signals in the EMD method of HHT,* **Xu et al.** *(***2010***) studied the decomposition process and noise control based on noise-assisted decomposition method-ensemble empirical mode decomposition (EEMD).* **Fan et al.** *(***2010***) used the EMD to process deformation data of high-rise buildings, which can eliminate noise and extract the deformation characteristics. Combining the EMD and Independent Component Analysis (ICA),* **Luo et al.** *(***2012***) proposed the EMD-ICA method with reference signals to weaken the multipath effect.* **Wu et al.** *(***2016***) used the model correlation*

criterion to determine the signal level and noise level by ICA-based filtering noise reduction method in EMD. They effectively determined the cut-off point between signal level and noise level with low Signal to Noise Ratio (SNR) and mitigated most noises while keeping useful information.

HHT has a lot of shortcomings in the application to SHM. As there is no universal and practical guidelines for EMD decomposition, the mode mixing problem caused by intermittent signal will affect the decomposition effect and damage the IMF's true physical meaning. In the health monitoring data processing for large engineering structures, how to remove noise from nonlinear and non-stationary signals to get comprehensive structural damage signals and how to solve the mode mixing problem caused by intermittent signals and signal interactions need significant further study.

1.5 Research Objectives

By measuring the operating and loading environment as well as the critical responses of a structure, SHM can track and evaluate the stability and safety of the structure. As traditional single-sensor based monitoring technologies have different defects, they are unable to conduct long-term structural health monitoring:

a) GPS signals are affected by satellite constellation geometry and signal propagation path. It is not easy to characterize the effect by mathematical means. The multi-path and tropospheric errors can't be mitigated completely.

b) Besides the high frequency noise, there are low-frequency systematic errors in GPS displacement series, which overlap with the frequency of the overall inertia displacement produced by engineering structures under the effect of temperature and force. So, it is difficult to achieve real-time and high precision structure monitoring only by the GPS technology.

c) At present, most researches on multi-sensor integrations directly integrate the coordinates of tilt-meter with that of GPS (coordinate domain integration), without considering the integration in the GPS observation range. It would be better if the model errors could be brought into the integration and the weighting across multiple sensor errors can be considered.

d) The under-developed sensing technology leads to incomplete monitoring information. Some factors influencing the structure health are very difficult to detect. Furthermore, the detection is costly and cannot be monitored in real time. Health monitoring systems with incomprehensive information focus on collecting either static indicators or dynamic indicators. With the improvement of surveying and mapping technology, monitoring methods are developed from single mode to multiple mode integrating point, line and plane monitoring. But the data processing of SHM cannot satisfy the development from static analysis to dynamic analysis.

1.5.1 Objectives

This study focuses on integrating GPS, tilt-meter and accelerometer sensor as well as their applications in monitoring the stability of structures, such as high-rise buildings, dams and bridges. The main objective of this study is to develop algorithms for GPS, tilt-meter and accelerometer sensor integration, to monitor the deformations and dynamics of structures, detailed as follows:

a) To develop multi-sensor data integration algorithms and achieve a multi-sensor system integrating GPS, tilt-meter and accelerometer to monitor the deformation of structure, such as building, bridge and slope.

b) To propose a new data fusion model and algorithm, corresponding GPS observation equations and tilt-meter observation equations will be established. To give a method for combined adjustment, taking the distance between sensors as the constraints and the virtual observations. To establish a model combining the GPS observation equation and tilt-meter observation equation, and give the weighted least square algorithm. To analyze the influence of different sensor precisions on the algorithm with simulation examples and compare the computational results for many accuracy combinations. To verify the effectiveness of the algorithm by examples.

c) To combine multi tilt-meters and GPS and form the distance constraint equation with random noise by the tilt-meter. Least squares algorithms with stochastic constraints are to be constructed. To give an adaptive factor to adjust the contribution of the observation of GPS and the observation values of the tilt-meters to the parameter estimation, which provides a new way for multi sensor

data fusion. To analyze the reliability of the algorithm with an example when the GPS observation information is not sufficient, in which the influence of different precision of the sensor on the algorithm is analyzed and the calculation results for many precision combinations is given. The accuracy of the algorithm should also be analyzed.

d) To study the fusion methods of GPS, accelerometer and tilt-meter in the dynamic observation model, and propose a new fusion method. This method should establish a combined filtering model by GPS/Accelerometer sensors and a filter model with constraints given by tilt-meter observation. Then the filtered solution is projected into the space formed by the constraint equation. The validity of new constraint filtering algorithm will be analyzed by an example.

e) To study the adaptive filtering algorithm on three sensor fusion models about GPS, accelerometer and tilt meter. To give an adaptive factor to reasonably balance the proportion of dynamic information and observation information, and restrain the abnormal information in observation model and dynamic model.

1.5.2 Organization

This thesis is organized as follows:

Chapter 1 begins with a review of the research on structural health monitoring, including applications of hardware combinations and data processing developments as well as problems in SHM. The purpose and significance of this study and the research content are also presented in this chapter.

Chapter 2 studies the multi-sensor technology used in SHM. Emphasis is given to the multi sensor combination technology based on GPS, the main error sources of GPS, tilt-meter and accelerometer. GPS observation model, error equation of GPS, tilt-meter and accelerometer are studied in this chapter. This chapter finishes with an inner precise calibration for the GPS, tilt-meter and accelerometer sensor.

In the third chapter, a fusion method of multi-GPS observation and single tilt-meter data is developed. We design the combination form of multiple GPS antennas and a dual axis tilt-meter are installed on a fixed position of the platform. Based on the method of combined adjustment and taking the distance between sensors as the constraints for prior information and as the virtual observation, this chapter establishes the main model combining GPS with tilt-meter, which is solved by the weighted least squares.

Chapter 4 explores some combination forms of multiple tilt-meter and GPS, and develops a distance constraint equation with random noise. The least squares algorithm with stochastic constraints is presented, in which an adaptive factor is proposed to adjust the contribution of GPS and tilt-meter observations to parameter fusion estimation, which provides a new approach for multi-sensor data fusion.

We propose in Chapter 5 a new method for sensor fusion, based on the study of the fusion methods of GPS, accelerometer and tilt-meter in the dynamic observation model. Firstly, a combined filter model is established by GPS and

Accelerometer, and then the filtering model with constraints is constructed taking the measurements of the tilt-meter as the constraints. In the calculation, a new constraint filtering method is obtained by projecting the filtered solution in the space of the constraint equation. Based on the adaptive filtering and constrained observation equations, the adaptive filtering algorithm of fusion models of GPS, accelerometer and tilt-meter is obtained. By means of the adaptive factor calculation method, the dynamic information and the observation information is reasonably balanced and the abnormal information in the observation model and the dynamic model is suppressed. Many simulation examples are constructed to analyze the accuracy of the three sensors and the reliability of the algorithm when the GPS observation is not sufficient.

Chapter 6 summarizes the research work and gives a prospect for the future research.

CHAPTER 2 SENSORS IN STRUCTURAL HEALTH MONITORING

Included within this chapter is a review of the basic principles, methods and current research of deformation monitoring sensors involved in this thesis. From utilizing information gathered from GPS, accelerometer, tilt-meter and the error sources in SHM, an all-encompassing review is provided inclusive of current research related to this field.

2.1 GPS

GPS can work under adverse weather conditions, providing measurements with a high level of automation, non-inter-visibility and high precision. Due to this it has been widely used in deformation monitoring for manmade structures, such as high-rise buildings, dams, and bridges.

The function of GPS carrier phase observation can be written as

$$\lambda\varphi_i^j(t) = R_i^j(t) + c\left[\delta t_i(t) - \delta t^j(t)\right] - \lambda_\Phi N_i^j(t_0) - \delta_{i,I}^j(t) + \delta_{i,T}^j(t) + \delta_{i,M}^j(t) + \varepsilon_i^j \quad (2\text{-}1)$$

where, $\varphi_i^j(t)$ *is the phase measurement, i.e. the output of the receiver;* λ *is the carrier wave length;* $R_i^j(t)$ *is the geometric distance between satellite* S^j *and* T_i *at epoch time t;* $\delta t_i(t)$ *is the GPS receiver clock error;* $\delta t^j(t)$ *is the satellite clock error;* $N_i^j(t_0)$ *is the integer ambiguity of the carrier when it was locked by the receiver;* $\delta_{i,I}^j(t)$ *is the ionospheric refraction effect on the pseudo-range*

measurement code; $\delta_{i,T}^{j}(t)$ *is the tropospheric refraction effect on the pseudo range measurement code;* $\delta_{i,M}^{j}(t)$ *is the multi-path effect;* ε_{i}^{j} *is the unmolded random error.*

By using differential positioning methods, monitoring stations and reference stations to observe the same satellite at the same time, their observation difference is the single different observation between GPS stations, which can eliminate satellite clock errors and reduce the ionospheric and tropospheric effects, especially those effects of short baseline application. The single difference observation can therefore be written as

$$\Delta\Phi_{12}^{j} = \Delta R_{12}^{j} + c\Delta t_{12}(t) - \lambda\Delta N_{12}^{j} - \Delta_{12,I}^{j} + \Delta_{12,T}^{j} + \Delta_{12,M}^{j}(t) + \Delta\varepsilon_{12}^{j} \qquad (2\text{-}2)$$

Where:

$$\Delta\Phi_{12}^{j} = \lambda\varphi_{2}^{j}(t) - \lambda\varphi_{1}^{j}(t)$$

$$\Delta R_{12}^{j} = R_{2}^{j}(t) - R_{1}^{j}(t)$$

$$\Delta t_{12}(t) = \delta t_{2}(t) - \delta t_{1}(t)$$

$$\Delta N_{12}^{j} = N_{2}^{j}(t) - N_{1}^{j}(t)$$

$$\Delta_{12,I}^{j} = \delta_{2,I}^{j}(t) - \delta_{1,I}^{j}(t)$$

$$\Delta_{12,T}^{j}(t) = \delta_{2,T}^{j}(t) - \delta_{1,T}^{j}(t)$$

$$\Delta_{12,M}^{j}(t) = \delta_{2,M}^{j}(t) - \delta_{1,M}^{j}(t)$$

$$\Delta\varepsilon_{12}^{j} = \varepsilon_{2}^{j} - \varepsilon_{1}^{j}$$

Selecting the satellite with the highest altitude angle as the reference satellite, the difference between single difference observables and reference satellite observation is the GPS double difference observations. Assuming ground-based observation stations T1 and T2 observe two GPS satellites S^j, S^k *at the same time, the double difference observables can be written as:*

$$\nabla\Delta\Phi_{12}^{jk} = \nabla\Delta R_{12}^{jk} - \nabla\Delta N_{12}^{jk} + \nabla\Delta_{12,I}^{jk} + \nabla\Delta_{12,T}^{jk} + \nabla\Delta_{12,M}^{jk}(t) + \nabla\Delta\varepsilon \qquad (2\text{-}3)$$

where:

$$\nabla\Delta\Phi_{12}^{jk} = \Delta\Phi_{12}^{k} - \Delta\Phi_{12}^{j}$$

$$\nabla\Delta N_{12}^{jk} = \Delta N_{12}^{j} - \Delta N_{12}^{k}$$

$$\nabla\Delta_{12,I}^{jk} = \Delta_{12,I}^{k} - \Delta_{12,I}^{j}$$

$$\nabla\Delta_{12,T}^{jk} = \Delta_{12,T}^{k} - \Delta_{12,T}^{j}$$

$$\nabla\Delta_{12,M}^{jk} = \Delta_{12,M}^{k} - \Delta_{12,M}^{j}$$

$$\nabla\Delta\varepsilon = \Delta\varepsilon_{12}^{k} - \Delta\varepsilon_{12}^{j}$$

As shown in Figure 2.1, A is as the reference point, B is the monitoring points obtained during the first observation, i.e. the initial monitoring point; C is the new monitoring point after the displacement and J and K are the satellite codes.

According to (2-3), the double difference observables equation based on points A and C can be written as:

$$\nabla\Delta\Phi_{AC}^{jk} = \nabla\Delta R_{AC}^{jk} - \nabla\Delta N_{AC}^{jk} + \nabla\Delta_{AC,I}^{jk} + \nabla\Delta_{AC,T}^{jk} + \nabla\Delta_{AC,M}^{jk}(t) + \nabla\Delta\varepsilon \qquad (2,4)$$

Point A is the reference point with coordinates (x_A, y_A, z_A)*. Point C is the deformation monitoring point with changing coordinates, which can only be approximated by the coordinates of point B* (x_B, y_B, z_B)*.*

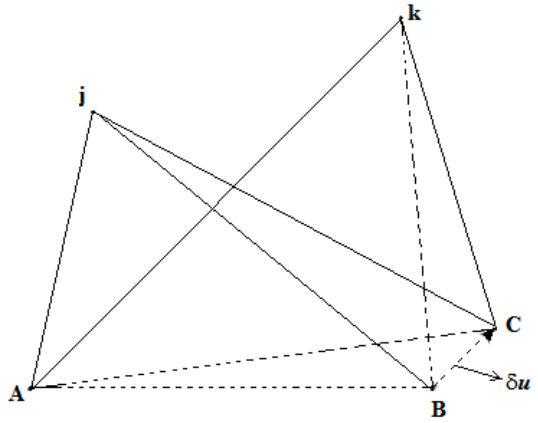

Fig. 2.1 Diagram of single epoch algorithm without integer ambiguity

Assume the displacement between points B and C are $\delta u = (\Delta x, \Delta y, \Delta z)$*, and the coordinates of satellites J, K are* (x_j, y_j, z_j) *and* (x_k, y_k, z_k)*.*

$$\nabla\Delta\Phi_{AC}^{jk} - \nabla\Delta\Phi_{AB}^{jk}$$

$$= \sqrt{(x_k - x_B - \Delta x)^2 + (y_k - y_B - \Delta y)^2 + (z_k - z_B - \Delta z)^2}$$

$$- \sqrt{(x_j - x_B - \Delta x)^2 + (y_j - y_B - \Delta y)^2 + (z_j - z_B - \Delta z)^2} \qquad (2\text{-}5)$$

$$- \sqrt{(x_k - x_B)^2 + (y_k - y_B)^2 + (z_k - z_B)^2}$$

$$+ \sqrt{(x_j - x_B)^2 + (y_j - y_B)^2 + (z_j - z_B)^2}$$

i. e.

$$R_B^j = \sqrt{(x_j - x_B)^2 + (y_j - y_B)^2 + (z_j - z_B)^2}$$

$$R_B^k = \sqrt{(x_k - x_B)^2 + (y_k - y_B)^2 + (z_k - z_B)^2}$$

If δu is very small, decompose (2-5) at $(\Delta x, \Delta y, \Delta z) = (0,0,0)$, then we have

$$\nabla\Delta R_{AC}^{jk} - \nabla\Delta R_{AB}^{jk} = -(\frac{x_k - x_B}{R_B^k}\Delta x + \frac{x_j - x_B}{R_B^j}\Delta x) - (\frac{y_k - y_B}{R_B^k}\Delta y \qquad (2\text{-}6)$$

$$+ \frac{y_j - y_B}{R_B^j}\Delta y) - (\frac{z_k - z_B}{R_B^k}\Delta z + \frac{z_j - z_B}{R_B^j}\Delta z)$$

let

$$l_B^k = \frac{x_k - x_B}{R_B^k}, l_B^j = \frac{x_j - x_B}{R_B^j}, m_B^k = \frac{y_k - y_B}{R_B^k}, m_B^j = \frac{y_j - y_B}{R_B^j}, n_B^k = \frac{z_k - z_B}{R_B^k}, n_B^j = \frac{z_j - z_B}{R_B^j}$$

(2-6) can be written as:

$$\nabla\Delta R_{AC}^{jk} - \nabla\Delta R_{AB}^{jk} = -l_B^k\Delta x + l_B^j\Delta x - m_B^k\Delta y + m_B^j\Delta y - n_B^k\Delta z + n_B^j\Delta z \qquad (2\text{-}7)$$

Thus, from (2-4) we get

$$\nabla\Delta\Phi_{AC}^{jk} - \nabla\Delta R_{AB}^{jk} + \nabla\Delta N_{AC}^{jk} = -l_B^k\Delta x + l_B^j\Delta x - m_B^k\Delta y + m_B^j\Delta y - n_B^k\Delta z + n_B^j\Delta z + \nabla\Delta_{AC,I}^{jk} + \nabla\Delta\varphi_{AC,T}^{jk} + \nabla\Delta_{AC,M}^{jk}(t) + \nabla\Delta\varepsilon \qquad (2\text{-}8\text{-}a)$$

As the baseline is short (less than 10km) in the SHM, the residual ionosphere error can be eliminated, $\nabla\Delta_{AC,I}^{jk} = 0$*. By GPS observation model (2-8-a), we see*

$$\boldsymbol{L}_{GPS}(t) = -l_B^k\Delta x + l_B^j\Delta x - m_B^k\Delta y + m_B^j\Delta y - n_B^k\Delta z + n_B^j\Delta z + \nabla\Delta\varepsilon$$

where:

$$\boldsymbol{L}_{GPS} = \nabla\Delta\Phi_{AC}^{j\mathrm{k}} - \nabla\Delta R_{AB}^{j\mathrm{k}} + \nabla\Delta N_{AC}^{j\mathrm{k}} - \nabla\Delta\varphi_{12,T}^{jk} - \nabla\Delta_{AC,M}^{jk}$$

And its matrix form is

$$\boldsymbol{L}_{kGPS} = \boldsymbol{E}_{kGPS}\begin{bmatrix}\Delta x_k\\ \Delta y_k\\ \Delta z_k\end{bmatrix} + \boldsymbol{v}_{1k} \qquad (2\text{-}8\text{-}b)$$

where:

$$\boldsymbol{E}_{kGPS} = \begin{bmatrix} l_B^2 - l_B^1 & m_B^2 - m_B^1 & n_B^2 - n_B^1\\ l_B^3 - l_B^1 & m_B^3 - m_B^1 & n_B^3 - n_B^1\\ \cdots & \cdots & \cdots\\ l_B^n - l_B^1 & m_B^n - m_B^1 & n_B^n - n_B^1\end{bmatrix}$$

Other errors are usually smaller than half the wavelength, so (2-8) can be used to inverse ambiguities and then provide the single epoch solution but only if the deformation of monitoring points is small.

2.1.1 GPS Tropospheric Effects

For high-rise structure deformation monitoring, the height difference between their baseline ends is very larger. With the same temperature, pressure, water vapor content and the satellite altitude angle, the larger the elevation, the greater the residual tropospheric delay effect. Troposphere is the lowest and the non-ionised level of the atmosphere, which is primarily composed of nitrogen and oxygen as it is a non-dispersive medium of radio waves (frequencies up to 15 GHz). Thus, the signal propagation in it is frequency independent.

Precise GPS applications are affected by the tropospheric effect, called the tropospheric delay. This section will study the principle of tropospheric effects and their elimination methods. Generally, the tropospheric effects can be mitigated in three ways.

The first method is to use empirical modes to estimate atmospheric delay, such as Hopfield mode and Sasstamonien mode. These methods need meteorological parameters (temperature, pressure and relative humidity or vapor pressure).

The second way is to estimate the tropospheric effects by least squares or Kalman filter with position parameters.

And the third approach uses environment instruments such as water vapor radiometer to calculate the wet component in the experiment mode. The estimation accuracy is high, but such equipment is expensive and is difficult to use in GPS dynamic measurement.

2.1.1.1 Basic Principles

Tropospheric delay is the geometric distance difference between the signal propagation path and the satellite to the receiver. It can be described as:

$$dTrop = L - R = \int_S n(s)ds - \int_R dr = \int_R (n(s) - 1)ds - |\int_S ds - \int_R dr| \quad (2\text{-}9)$$

where $n(s)$ *is the refractive coefficient on propagation path,* S *and* R *are the electromagnetic wave optical path and the geometric distance between two antennas, respectively.* $\int_S N(s)ds$ *is the path delay on velocity change.* $\int_R dr$ *is the optical path curvature and its value can be ignored if the satellite altitude is larger than 10 degrees (***Li et al., 2001***). About 90% of the tropospheric delay is caused by dry gas in the atmosphere, known as the dry component. The remaining 10% is caused by water vapor, known as the wet component. The zenith tropospheric delay is also commonly used in the direction of wet and dry weight and the corresponding mapping function.*

$$dTrop = ZTD_d MP_d(E) + ZTD_w MP_w(E) \quad (2\text{-}10)$$

where ZTD *is the direction of the zenith tropospheric delay,* $MP(E)$ *is the mapping function of the wet component and dry component, respectively. For a mid-latitude stand on the sea level, the zenith delay in dry weight is about 2.3 m,*

*and that of wet weight is around1 ~ 80 cm. For low altitude angle of the satellite, the total tropospheric delay can be up to 30 m (***Li et al., 2001***).*

2.1.1.2 Empirical Model Methods

Many zenith tropospheric delay correction models have been developed from the tropospheric model correction algorithm. These models generally consider the error characteristics and sources, and use a large amount of observation data to fit the half experience and half theory formula. At present, the most extensively used model is the Saastamoinen model (SAAS), which can be described as:

$$\begin{gathered} D_{Trop} = Z_d m_d(E) + Z_w m_w(E) \\ Z_d = \frac{0.002277}{f(\varphi, H)} \cdot P \\ Z_w = \frac{0.002277}{f(\varphi, H)} \cdot (\frac{1225}{T} + 0.05) \cdot e \\ f(\varphi, H) = 1 - 0.0026 \cdot cos(2\varphi) - 0.00028 \cdot H \end{gathered} \qquad (2\text{-}11)$$

*where D_{Trop} is the tropospheric delay(meter) from satellite to site; Z_d and Z_w are the dry component and wet component of the zenith tropospheric delay, respectively; $m_d(E)$ and $m_w(E)$ are the projection functions of the dry and wet components of the tropospheric delay(meter), respectively; E is the satellite elevation angle (radian); P is the atmosphere pressure (mbar); φ is the latitude of site (radian); H is the elevation (m); e is the vapor pressure of atmosphere, which can be calculated by relative humidity (***Kleijer, 2004***).*

$$e = e_0 \, exp\left\{\frac{L}{R_v}\left(\frac{1}{T_0} - \frac{1}{T}\right)\right\}\frac{RH}{100} \qquad (2\text{-}12)$$

where $e_0 = 6.11 mbar, T_0 = 273.16^o$, *T is the temperature(k), L is the latent heat, RH is the relative humidity(%).*

*The standard atmosphere model can be used to calculate temperature, humidity and pressure (***Berg et al., 1948***).*

$$\begin{aligned} T &= T_0 - 0.065H \\ P &= P_0(1 - 2.26 \times 10^{-5}H)^{5.225} \\ RH &= RH_0 exp(-6.396 \times 10^4 H) \end{aligned} \qquad (2\text{-}13)$$

where T is the atmosphere temperature; RH is the relative humidity; P is the atmosphere pressure; T_0, P_0 *and* RH_0 *are standard meteorological elements.*

*The SAAS model (***Saastamtrinen et al., 1972***) considers the dry air pressure in the troposphere represented by thermostatic vertical gradient, and it increases the height and precision of the troposphere corrections. The RMS estimation in the model was made by Elgered (***Elgered et al., 1991***). His results show that the error of the refractive index constant is about 2.4 mm, the uncertainty of the universal gas constant is 0.1 mm, and the refractive changes effect of the average molar mass in the dry air is 0.1 m. If more accurate meteorological elements are provided, the delayed correction accuracy in sub-millimeter level of the dry weight could be achieved (***Davis et al., 1985***). As the SAAS model has high accuracy and is not affected by temperature errors, the dry weight delay model is superior to other models (***Mendes et al., 1995***).* **Dai et al.** *(***2007***) compared to residuals of tropospheric delay with different elevation. If the elevation difference is more than 100 m, the tropospheric delay residual is about 0.05 m.*

And when the height difference is 300 m, the residual is 0.1 m, which cannot be simply eliminated by the relative position technology. As the empirical model has a low accuracy, the tropospheric delay cannot be eliminated completely by it. In addition, the temperature and humidity parameters cannot be detected, as most GPS observation stations have no environment sensors.

2.1.1.3 Parameter Estimation Methods

*Since the dry component accounts for 80% of the tropospheric delay, the dry weight is relatively stable in terms of time and space. Its refraction change rate in the zenith direction is about 2 cm/hour, which is significantly weakened by the model correction. However, the wet weight refraction accounting for 20% of the entire delay is not stable, and its refraction change rate in the zenith direction is 3 to 4 times larger than that of the dry weight (***Bock et al., 2001***). For the dry delay, the accuracy of the tropospheric refraction correction model is about 80%. The correction model is derived in an approximation situation, with an assumption that the atmosphere is an ideal gas in the hydrostatic equilibrium state.*

a) Single-Parameter Estimation Method

If the zenith delay of the station is corrected by the model approach, there will be some deviation between the correction and the real value. Let the deviation be a constant, the tropospheric delay correction can be expressed as:

$$D^s = (D_d^Z + D_w^Z + \varepsilon)MF(E) \qquad (2\text{-}14)$$

*D_d^Z is the dry component of the zenith tropospheric delay, D_w^Z is the wet component of the zenith tropospheric delay, $MF(E)$ is the mapping function of the wet and dry components. With a high-altitude-angle satellite, at a mid-latitude position on the sea level, the dry component of the zenith tropospheric delay is about 2.3 m, and the wet component is 1 ~ 80 cm. But with a low-altitude-angle satellite, the total tropospheric delay can be up to 30 m in the same position (***Li et al., 2001***).*

b) Multi-Parameter Estimation Method

In order to show troposphere refraction changes with higher precision, one parameter will be added during the estimation after the model correction. This is the multi-parameter estimation method:

$$D^s(t) = \left(D_d^z + D_w^z + \varepsilon(\Delta t)\right)MF(E) \quad t_{i-1} \le t \le t_i, t_i = t_{i-1} + \Delta t \qquad (2\text{-}15)$$

c) Stochastic Process Method

According to the results of the water vapor radiometer, the refraction of the wet weight in the zenith direction can be described by a first-order Gaussian Markov process.

$$\frac{d\rho(t)}{dt} = -\frac{1}{\tau_\rho}\rho(t) + W(t) \qquad (2\text{-}16)$$

where τ_ρ is the relevant time of the stochastic process, $W(t)$ is the zero-mean Gaussian white noise, and the variance is σ_w^2.

d) Subsection Linear Method

By the subsection linear methods, an unknown parameter is assigned at the epoch interval, and the wet delay varying with time is represented by a discrete stochastic process of the step size $K \cdot \Delta t$ *, if the tropospheric refraction of the station in the zenith direction changes linearly with time.*

Parameters $\rho(i)$ *and* $\rho(i+k)$ *should be estimated and their state equations are:*

$$\begin{gathered} \rho(i+k) = m(k \cdot \Delta t)\rho(i) + W(i+k) \\ m(K \cdot \Delta t) = e^{\frac{k-\Delta t}{\tau}} \\ \sigma_w^2(i) = \frac{1}{2}\tau \cdot \sigma_w^2\{1 - \{m(k \cdot \Delta t)\}^2\} \end{gathered} \tag{2-17}$$

Also, in the wet delay between i and i+k, the jth epoch can be written as

$$\begin{gathered} \rho(j) = \rho(i) + \frac{j-i}{k}[\rho(i+k) - \rho(i)] \\ i \le j \le (i+k) \end{gathered} \tag{2-18}$$

Tropospheric refraction parameters $\rho(j)$ *and* $\rho(i+k)$ *in the zenith direction of the station are reduced if k is appropriately selected, so the least squares method can be used to estimate the parameters.*

2.1.1.4 External Correction Methods

External correction methods measure the water vapor impact on the satellite signal propagation path by using an external device. Using this method, the component of zenith hydrostatic delay is described by the experience meteorological model, and the valuation is made based on the surface

*measurements and the standard atmospheric parameters (***Elgered et al., 1991***). On the other hand, the delay components of wet path are gained by the conversion of the lumped water vapor measured in distance.*

*Microwave radiometer technology was used in the 1970s to measure the amount of tropospheric water vapor, so it is often named as water vapor radiometer (WVR). WVR has been widely used as a path delay correction in GPS and very long baseline interferometry (VLBI) measurements (***Han et al., 2000***).*

Although external correction methods achieve high accuracy (better than 1cm in the zenith direction), it needs costly and bulky instruments, which do not have the capability to monitor for a whole day. Furthermore, it is difficult to set a wide range of intensive observation station networks to achieve operational observations.

2.1.2 GPS Multi-path Effects

Multi-path errors distort the pseudo-range and the carrier phase observations and affect the GPS observations, especially in the case of smooth reflective surfaces like building roofs. The accuracy of the GPS-derived position solution highly depends on the geometry of the tracked satellites-receiver. Additionally, in cases of monitoring urban canyons, dam in valleys or structural near high-rise buildings, the number of visible satellites may not be sufficient to reliably determine the position.

This section will study principles of the multi-path effect as well as its reduction methods, including the GPS antenna design, signal processing in GPS receiver, weight model and filter approach in data processing.

2.1.1.1 Basic principle

As shown in Figure 2.2, the basic theory assumes that the signal travels directly from the satellite to the receiver antenna. In addition to the direct signals and the original line-of-sight (LOS), there are signals reflected by the objects near the antenna and reach the antenna through indirect paths. These signals interfere with direct signals.

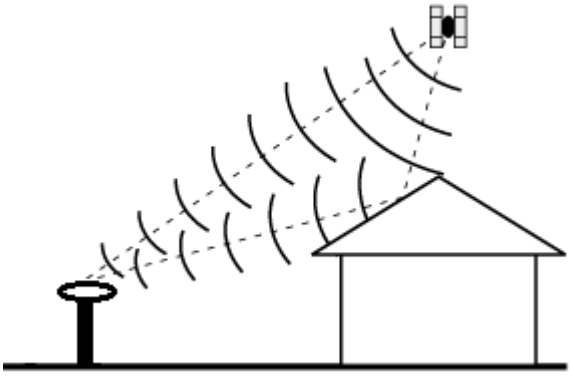

Fig. 2.2 Diagram of the multi-path effects (Dai, 2009)

The LOS and reflected signals can be written as:

$$S_{LOS} = Asin(\omega_0 t) \qquad (2\text{-}19)$$

$$S_M(t) = \alpha_1 \cdot A \cdot sin(\omega_0 t + \Delta_1) \qquad (2\text{-}20)$$

where α_1 *is the reflection coefficient,* Δ_1 *is relative phase offset,* ω_0 *is angular frequency signal. The received combined signal can be described as*

$$S_{total}(t) = A \cdot sin(\omega_0 t) + \alpha_1 \cdot A \cdot sin(\omega_0 t + \Delta_1) \quad (2\text{-}21)$$

or

$$S_{total}(t) = \alpha_c \cdot A \cdot sin(\omega_0 t + \Delta_c) \quad (2\text{-}22)$$

$$\alpha_c = \sqrt{(1 + 2\alpha\, cos\, \theta + \alpha^2)}$$
$$\Delta_c = arctan(\frac{\alpha sin\Delta}{1 + \alpha cos\Delta}) \quad (2\text{-}23)$$
$$\Delta = \frac{4\pi s}{\lambda} sin\beta$$

where β is the incident angle of the reflected signal, s is the distance from the antenna to the reflection surface, λ is the signal wavelength. The biggest phase shift caused by multi-path is a quarter wavelength, which is 4.8 cm for L1 carrier phase and 6.2 cm for L2 carrier phase.

2.1.1.2 Multipath-Rejecting GPS Antenna

*An effective and simple method to eliminate the multi-path effect is to use multipath-rejecting GPS antenna (e.g. advanced pinwheel compact controlled reception pattern antennae and choke-ring antennae) or multi-path resistant receivers with correlation techniques (***Zhong et al, 2010***). This kind of antenna can be grouped to three categories.*

*a) Change the antenna shape to reduce the signal gain in the approximating horizontal direction. By doing this, the multi-path effect in the horizontal direction can be partially reduced (***Schupler et al., 1994***).*

b) Theoretically, direct GPS signals are right-handed polarization, and the reflected signal is left-handed polarization. Thus specially designed antennae can suppress left-handed polarization signals and eliminate the multi-path. But in practice, the antenna is dextral polarized and fails to suppress left-handed polarization signals.

*c) Chock-ring antennae can efficiently suppress the multi-path effect but this kind of antennae are large and expensive. Additionally, they are powerless for large angle multi-path errors (***Young et al., 1998***).*

2.1.1.3 Signal Processing in GPS Receiver

*Signal processing in GPS receiver can be improved by reducing the multipath effects during the processing. Receiver signal tracking loop consists of the delay-locked loop (DLL) and the phase-locked loop (PLL). Each of them has a GPS signal automatic correlation function code recogniser and a carrier phase discriminator. To achieve higher accuracy, multipath effects are usually reduced in the automatic correlation function code recognizer to generate direct signals (***Dierendonck et al., 1997***). Multi-path Elimination Delay Lock Loop(MEDLL) can deal with the multipath of both the DLL and PLL, so it can effectively reduce the multi-path effect in the pseudo range and phase observations (***Van Nee, 1992***). However, it has large calculation loads and needs high-performance processors.*

2.1.1.4 Signal-to-Noise Ratio Method

Bilich et al. *(***2004***) presents observations of SNR data from a continuously operating GPS station named CASA, which shows strong evidence of ground and monument multipath. The SNR data at CASA demonstrate daily repeatability and a seasonal trend that multi-path error strongly depends on the antenna environment changes. When the SNR data show variability due to multi-path, SNR observations are consistent with positioning post fit phase residuals. This indicates that SNR-based corrections for geodetic applications may be feasible. As both the phase observation value and SNR are relative to the reflector position and orientation, a weighting GPS observation based on SNR or carrier-to-noise power density (C/No) is obtained to estimate the geometry information of the reflector, and phase observation value of the multi-path error (***Axelrad et al., 1996; Reichert et al., 2001***).*

*C/No is the ratio of carrier signal energy to noise in 1 Hz bandwidth. It is correlated to the multi-path effect, antenna gain and attenuation of antenna cable, satellite signal emission levels and troposphere delay. The value of C/No is usually 45 db - Hz. Based on C/No observations, Brunner (***Brunner et al., 1999***) established a stochastic model* $SIGMA - \varepsilon$.

$$\sigma^2 = C_i \cdot 10^{-\frac{C/No}{10}} \qquad (2\text{-}24)$$

Thus

$$C_i = B_i \cdot (\frac{\lambda_i}{2\pi})^2 \qquad (2\text{-}25)$$

where B is the phase tracking loop bandwidth(Hz), λ is the carrier phase wavelength(m). $C_{L1} = 0.00224\ m^2$ Hz and $C_{L2} = 0.00077\ m^2$ Hz.

The SNR of GPS phase observations and satellite altitude angle are highly relevant due to the fact that mapping relationships between C/No and satellite leads to altitude being defined. Because of diffraction or other signal interference, the C/No will be smaller than the normal. Keeping this in mind, a C/No and satellite altitude relation template $SIGMA - \Delta$ can be established with a fixed receiver antenna in the open environment:

$$\sigma^2 = C_i 10^{-(\frac{c}{No_{measured}} - \alpha\Delta)/10} \qquad (2\text{-}26)$$

where Δ is the difference between the template and observed value, α is the empirical coefficient, which is 2 in most cases.

2.1.1.5 Filter Approach

*If the GPS antenna location and its surrounding environment are fixed, GPS multi-path will change with the satellite position. Usually the multi-path has a similar cycle with the satellite operation, which is11 hours, 58 minutes 2 seconds in this study. The multi-path cycle is a sidereal day, namely 23 hours 56 minutes 4 seconds. Since the geometry between the GPS satellites and a specific receiver-reflector location repeats every sidereal day, multi-path tends to exhibit the same pattern between consecutive days (***Satirapod et al., 2005***). This repetition can be used to verify the presence of multi-path, through the analysis of observations made at a static receiver on different days.* **Geo et al.** *(***2000***)*

studied an adaptive finite-duration impulse response filter, based on a least-mean-square algorithm. It is a useful multi-path mitigation strategy that use data of two adjacent days to reduce the standard deviations of the pseudo-range multi-path time series to about one fourth of its magnitude before correction, and to about half in the case of carrier phase. And this algorithm is suitable for real-time applications. **Khoonphool et al.** *(***2003***) proposed a multi-path mitigation technique based on the use of wavelet decomposition. In this technique, the optimal level for wavelet decomposition of multi-path disturbance has been identified, and the results indicate that carrier-phase multi-path can be removed by using threshold in the denoised signal. When using GPS to monitor the structure health, the time series is obtained by (2-8) and this contains the deformation information of both structure and non-structure bodies. In general, the deformation of the structure body is very small (mm level). And the non-structural deformation information (i.e. the GPS error) is mainly caused by the residual tropospheric delay, multipath effect and the measurement of random noise, and is difficult to mitigate.*

Wavelet transform is a time-scale analysis method, which performs well in the local transform of both time and frequency domains. It has been widely used in deformation signal extraction and multipath effect reduction. Wavelet analysis contains the local short time Fourier transform, providing a scalable and translational window for multi-scale analysis, which is called Multi-Resolution analysis. It can capture the overall and local information of signals.

Let $\psi(t) \in L^2(R)$ *be a wavelet function, in which* $L^2(R)$ *is a square-integrable real space, and its Fourier transform is:*

$$C_\psi = \int_R \frac{|\psi(\omega)|^2}{\omega} d\omega < \infty \qquad (2\text{-}27)$$

where $\psi(t)$ *is the basic wavelet or the mother wavelet. The wave function system is composed of a cluster of basic wavelet functions after stretching or translating.* $\psi_{a.b}(t)$*, also known as the sub wavelet sequence* $\psi(t)$*, can be obtained after stretching and translating the basic wavelet function.*

$$\psi_{a.b}(t) = \frac{1}{\sqrt{a}} \psi\left(\frac{t-b}{a}\right), a, b \in R, \qquad a \neq 0 \qquad (2\text{-}28)$$

where a *is a stretching factor used to determine the position of the window on the frequency axis and the window shape in the basic wavelet transform.* b *is a translating factor affecting the window position on the phase plane. Function* $f(t) \in L^2(R)$ *is defined as the continuous wavelet transform.*

$$W_f(a,b) = \langle f, \psi_{a,b}(t) \rangle = |a|^{-\frac{1}{2}} \int_R f(t) \overline{\psi(\frac{t-b}{a})} dt \qquad (2\text{-}29)$$

The time frequency window of wavelet transform is two rectangular $[b - a\Delta\psi, b + a\Delta\psi] \times [(\pm w_0 - \Delta\psi)/a, (\pm w_0 + \Delta\psi)/a]$*, and the window center is* $(b, \pm w_0/a)$*. The width of the time window and the frequency window are* $2a\Delta\psi$ *and* $2\Delta\psi/a$*, respectively.*

In SHM, signals are usually a kind of discrete wavelet sequence, written as:

$$\psi_{j.k}(t) = 2^{-\frac{j}{2}}\psi(2^{-f}t - k), j, k \in Z \quad (2\text{-}30)$$

It is a special case of (2-28) when, $a = 2^j, b = k \cdot 2^j$. *The corresponding discrete wavelet transform is:*

$$W_f(j,k) = \langle f, \psi_{j,k} \rangle = 2^{-\frac{j}{2}} \int_R f(t)\overline{\psi(2^{-f}t - k)}dt \quad (2\text{-}31)$$

Details of the signals can be analyzed with different resolutions. Decompose the signal into different frequency details, and obtain the corresponding approximate components. Stretch the basic wavelet function to form a series of closure W_j, *then the scale space* V_j *is expressed as*

$$V_j = \cdots + W_{j-2} + W_{j-1} \quad (2\text{-}32)$$

Let f_s^j *be the approximate signal of function* $f(t)$ *in the scale space* V_j, f_d^j *be the details obtained by f(t) projecting on the wavelet space* W_j, *we get:*

$$f_s^j = \sum_k c_{j,k}\phi_k(2^{-j}t) = \sum_k c_{j,k}\phi_{j,k}(t) \quad (2\text{-}33)$$

$$f_d^j = \sum_k d_{j,k}\psi_k(2^{-j}t) = \sum_k d_{j,k}\psi_{j,k}(t) \quad (2\text{-}34)$$

where f_s^j *is the low frequency part of the signal,* f_d^j *is the high frequency part of the signal,* $c_{j,k}$ *is the scale expansion coefficient, and* $d_{j,k}$ *is the wavelet expansion coefficient.*

$$c_{j,k} = \langle f(t), \phi_{j,k}(t) \rangle \quad (2\text{-}35)$$

$$d_{j,k} = \langle f(t), \psi_{j,k}(t) \rangle \quad (2\text{-}36)$$

After decomposition, the wavelet analysis is used to calculate the scale and wavelet coefficients $c_{j,k+1}$, $d_{j,k+1}$. *We get:*

$$c_{j,k} = \sum_k h_0(m-2k)c_{j+1,k} + \sum_k h_1(m-2k)d_{j+1,k} \quad (2\text{-}37)$$

$$m = 2k + n$$

$$c_{j+1,k} = \sum_k h_0(m-2k)c_{j,m} \quad (2\text{-}38)$$

$$d_{j+1,k} = \sum_k h_1(m-2k)d_{j,m} \quad (2\text{-}39)$$

The analysis of the multipath effect on the GPS observation begins with some sampled observations. If the sampling rate is f_s, *the Nyquist sampling rate is* $f_s/2$, *which is the highest frequency in the sampling sequence. Wavelet analysis is composed of wavelet decomposition and reconstruction. Decomposition is to get the adjustment coefficient of each frequency band, and reconstruction is to reconstruct the corresponding frequency band signals based on the decomposition of the coefficients. The formula for inverse transform or reconstruction of wavelet transform is:*

$$f(t) = \frac{1}{C_\psi} \int_{-\infty}^{+\infty} \int_{-\infty}^{+\infty} \frac{1}{2a^2} W_{f(a,b)} \psi(\frac{t-b}{a}) dadb W_{j-1} \qquad (2\text{-}40)$$

As $\psi_{a,b}(t)$ *works as the observation window of the analyzed signal,* $\psi(t)$ *should also fulfill the following requirements for general functions.*

$$\int_{-\infty}^{+\infty} |\psi(t)| dt < \infty \qquad (2\text{-}41)$$

In addition, in order to maintain the same values in the reconstruction, the Fourier transform of $\psi(w)$ *of* $\psi(t)$ *should also meet the following conditions.*

$$A \leq \sum_{-\infty}^{+\infty} \left|\psi\left(2^{-j}w\right)\right|^2 \leq B, \qquad -\infty < A \leq B < +\infty \qquad (2\text{-}42)$$

Satirapod et al. *(***2005***) applied a wavelet decomposition technique to extract multi-path errors from GPS observations, which is then applied directly to the GPS observations to correct for the multi-path effects. The results show that the proposed method can significantly mitigate the multi-path effects at a permanent GPS station.* **Souza et al.** *(***2004***) proposed a wavelet transform to reduce the high frequency multi-path of the pseudo-range and carrier phase GPS double differences (DDs). This transform decomposes the DD signal to separate the high frequencies due to multi-path effects. After the decomposition, the wavelet shrinkage is performed by thresholding to eliminate the high frequency component. Then the signal can be reconstructed.* **Zhong et al.** *(***2008***) proposed*

*a method based on the technique of cross-validation for automatically identifying wavelet signal layers and this is developed and used for separating noise from signals in data series and also applied to mitigate GPS multipath effects. A multipath model and the sidereal day-to-day repeating property of GPS multipath signals is used to remove multipath errors from observations of subsequent days by taking advantage of the sidereal repeatability of multipath signals and to improve the quality of the GPS measurements (***Zhong et al, 2009***).*

Because of the noise and multipath effect in the GPS double difference phase observables, the deformation of the monitoring point and the multipath effect have lower frequencies than the noise. Through the wavelet analysis, noise can be decomposed into components with different frequencies. By the wavelet decomposition and reconstruction process, the signal can be filtered and de-noised to extract low-frequency signals.

2.1.1.6 Multipath Effect Elimination based on EMD Method

The essence of EMD is to obtain the inherent volatility model by the data time scale characteristics and then decompose the data into some combinations of IMF and residual trend. This is a continuous iterative process to adaptively decompose residual components. Each decomposition produces an IMF and a new residual component. The residual component will be further decomposed so the original signal can be expressed as the sum of IMF components and final residual components. Let $X(t)$ *be the original signal. Firstly, extract the mode function* $c_1(t)$ *and the residual function* $r_1(t)$. $r_1(t)$ *is then considered as a new*

original signal. And the above steps will continue to extract $C_2(t)$, $r_2(t)$, $C_3(t)$, $r_3(t)$...$c_n(t)$ and $r_n(t)$. If the residual function is a constant, a monotone function, or a function that contains only one extreme point, from which no proper IMF component can be extracted, the decomposition stops. That is:

$$X(\boldsymbol{t}) = \boldsymbol{c_1}(\boldsymbol{t}) + \boldsymbol{r_1}(\boldsymbol{t}) = \sum_{\boldsymbol{j=1}}^{\boldsymbol{2}} \boldsymbol{c_j}(\boldsymbol{t}) + \boldsymbol{r_2}(\boldsymbol{t}) = \cdots = \sum_{\boldsymbol{j=1}}^{\boldsymbol{n}} \boldsymbol{c_j}(\boldsymbol{t}) + \boldsymbol{r_n}(\boldsymbol{t}) \qquad (2\text{-}43)$$

In each decomposition step of $r_{i-1}(t)$, mode function $c_i(t)$ contains the high frequency part, and the residual function $r_i(t)$ contains the low frequency part, which indicates that the EMD method has the characteristics of a scale filter.

a) Filtering De-noising Algorithm based on EMD

Assume the contaminated signal $Y(t)$

$$\boldsymbol{Y}(\boldsymbol{t}) = \boldsymbol{X}(\boldsymbol{t}) + \boldsymbol{n}(\boldsymbol{t})$$

where $\boldsymbol{X}(\boldsymbol{t})$ is the original signal, $n(t)$ is the Gauss white noise. The purpose of EMD de-noising algorithm is to find $\widetilde{\boldsymbol{X}}(\boldsymbol{t})$, the best estimate of $\boldsymbol{X}(\boldsymbol{t})$. The basic idea is that most contaminated signals concentrate at low frequencies. The higher the frequency, the less the energy the signal has. Therefore, there must be a k_0, after which the IMF signal is the dominant mode. And the initial purpose of EMD filtering is to find k_0. Let $\widetilde{\boldsymbol{X}}(\boldsymbol{t})$ be the de-noised signal with a length of n, then the algorithm reconstructs the signal from the k-th IMF. This is similar to a low-pass filter design.

$$\widetilde{\boldsymbol{X}}_{\boldsymbol{k}}(\boldsymbol{t}) = \sum_{\boldsymbol{j}=\boldsymbol{k}}^{\boldsymbol{n}} \boldsymbol{c}_{\boldsymbol{j}}(\boldsymbol{t}) + \boldsymbol{r}_{\boldsymbol{n}}(\boldsymbol{t}), k = 1,2,\cdots,n \tag{2-44}$$

Here, if k is 1, the noise signal is the same with the original signal, which contains no noise. **Boundraa et al.** *(***2007***) proposed the CMSE criterion for continuous mean square errors based on EMD decomposition.*

$$\begin{aligned} MSE\left(\widetilde{\boldsymbol{X}}_{\boldsymbol{k}}(\boldsymbol{t}), \widetilde{\boldsymbol{X}}_{\boldsymbol{k+1}}(\boldsymbol{t})\right) &= \frac{1}{m}\sum_{\boldsymbol{i}=\boldsymbol{1}}^{\boldsymbol{m}} [\boldsymbol{c}_{\boldsymbol{k}}(\boldsymbol{t}_{\boldsymbol{i}}) - \boldsymbol{c}_{\boldsymbol{k+1}}(\boldsymbol{t}_{\boldsymbol{i}})]^2 \\ &= \frac{1}{m}\sum_{\boldsymbol{i}=\boldsymbol{1}}^{\boldsymbol{m}} [\boldsymbol{c}_{\boldsymbol{k}}(\boldsymbol{t}_{\boldsymbol{i}})]^2, k = 1,2,\cdots,n-1 \end{aligned} \tag{2-45}$$

According to the above formula, the CMSE value is equal to the energy density of the k-th IMF component, i.e. the mean square error (MSE) of the IMF component. If k is any number between 2 to n-1, the CMSE value can be calculated in turn. Determine k as k_0 *at the point that CMSE value has the first significant change (the point of noise energy distribution), and take it as the starting point of the clean signal.*

$$k_0 = \underset{2\le k\le n-1}{argmin}\, CMSE\left(\widetilde{\boldsymbol{Y}}_{\boldsymbol{k}}(\boldsymbol{t}), \widetilde{\boldsymbol{Y}}_{\boldsymbol{k+1}}(\boldsymbol{t})\right) \tag{2-46}$$

Then reconstruct the signal with all IMF begin with k_0

$$\tilde{X}_{k_0}(t) = \sum_{j=k_0}^{n} c_j(t) + r_n(t) \tag{2-47}$$

b) Soft Threshold De-noising

The original signal $\boldsymbol{X}(\boldsymbol{t})$ *after EMD decomposition is used to calculate the de-noising soft threshold of each IMF component.*

$$MAD_j = median\{\left|\boldsymbol{c_j}(\boldsymbol{t}) - median(\boldsymbol{c_j}(\boldsymbol{t})\right|\} \quad (2\text{-}48)$$

where $median()$ *is the value of the middle position in an ascending sequence. If the element number is odd, choose the middle element. If it is even, then average the value of the two middle elements. Then calculate the noise of IMF (i.e., mean square error).*

$$\hat{\sigma}_j = MAD_j/0.6745 \quad (2\text{-}49)$$

And then calculate each IMF de-noising soft threshold

$$\tau_j = \hat{\sigma}_j\sqrt{2lgL} \quad (2\text{-}50)$$

where L is the signal length. Finally eliminate the noise of IMF components.

$$\hat{c}_j(t) = \begin{cases} c_j(t) - \tau_j & if\ c_j(t) \geq \tau_j \\ 0 & if\ \left|c_j(t)\right| < \tau_j \\ c_j(t) + \tau_j & if\ c_j(t) \leq \tau_j \end{cases} \quad (2\text{-}51)$$

where j represents the j-th IMF component, $j = 1,2,\cdots,n$*. The soft threshold de-noise filter considers that the decomposed signal contains Gauss white noise, so its de-noising performance is good. But further de-noising performance verification is still needed, when the signal contains coloured noise.*

2.1.3 Zero Baseline Tests

*The satellite signals received by the GPS receiver is interfered by the channel deviation, then the delay of the phase locked loop and the deviation of the code tracking loop is seen. The caused error is called the internal noise of the receiver, which has a great influence on the performance of the receiver. Zero baseline (ZBL) tests are applied to determine the performance of GPS receivers, associated antennas and cabling, and data processing software. These tests are carried out by connecting two GPS receivers to a single antenna by a signal splitter. ZBL tests can verify the precision of the receiver measurements as well as validate the data processing software (***Meng et al., 2002***).*

In this study, a ZBL test was carried out at the rooftop of a six-story building on the campus of the Polytechnic University. Two GPS receivers (GPS-615), a kind of dual frequency receiver that provides updates five times per second, were employed in the initial ZBL tests. The GPS antenna (HX-CSX601) was installed at a point with known coordinates. With a dedicated low noise cable (about 3m), the antenna was connected to two receivers by a commercial eight channel signal splitter. The receiver has 120 dynamic channels configurable for optimized singles or dual frequency GPS and GLONASS satellite signals, and it is tracking for high performance satellite positioning with maximum availability.

A notebook with two USB to the serial port cable is used to collect raw GPS data from receivers. The data sampling rate is 1 Hz. The raw data will be converted to RINEX data format for post-processing.

The displacement sequence can be determined by a known baseline method. Since there is no displacement in the zero baseline application, the variations shifting sequence is thought to be caused by receiver noise.

Figures 2.3, 2.4, *and* 2.5 *are coordinate variations in the north, east and elevation directions, respectively. In the north direction, the standard deviation is 1.1 mm, and the maximum and minimum variations are 6.4 and -5.3 mm. In the east direction, the three equivalents are 1.9 mm, 10.2 mm and -12.8 mm. In the elevation direction, they are 1.8 mm, 11.8 mm and -10.5 mm. Additionally, Figure* 2.6 *shows the baseline variations. The distance variations are the root of the squared sum of the residuals in the three directions at each epoch. The standard deviation for variations in the distance domain is 1.74 mm, and the maximum residual is 14.8 mm.*

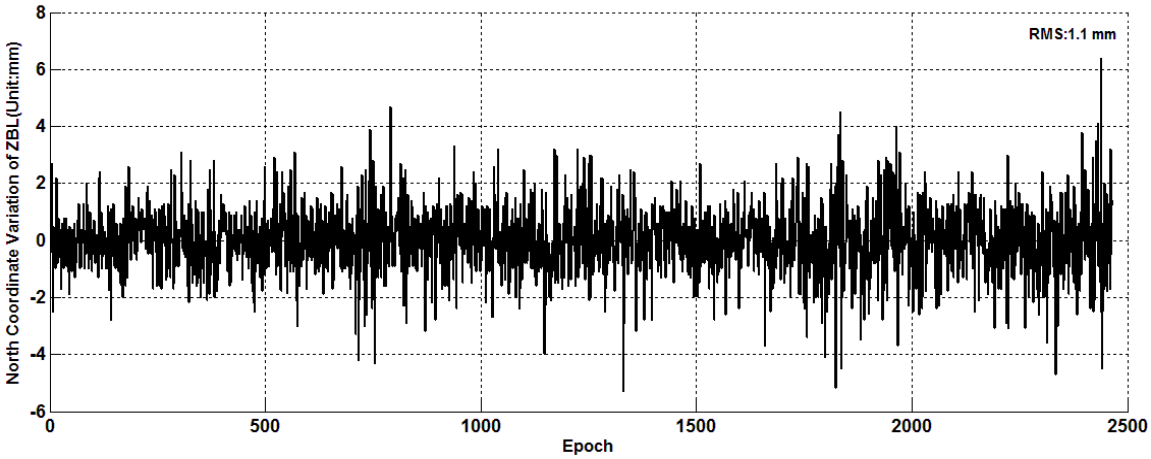

Fig. 2.3 Variations of ZBL on the north coordinate

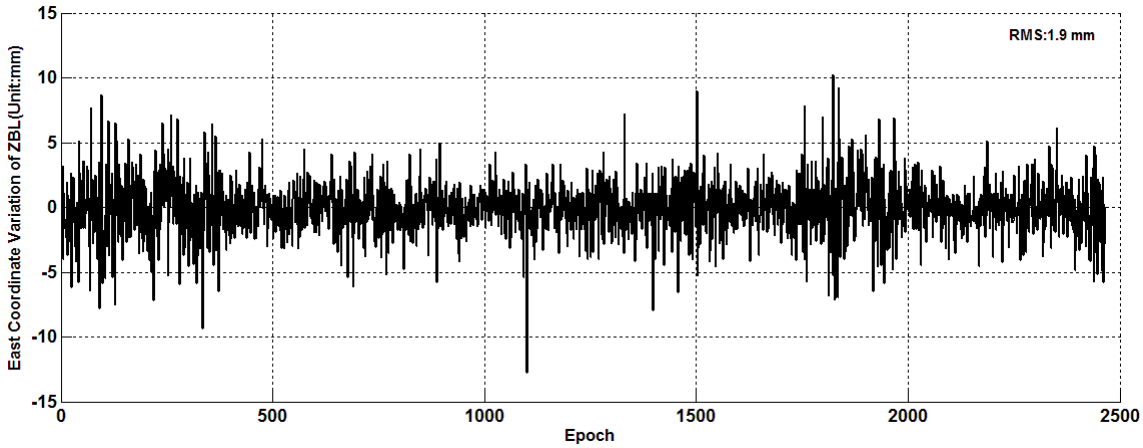

Fig. 2.4 Variations of ZBL on the east coordinate

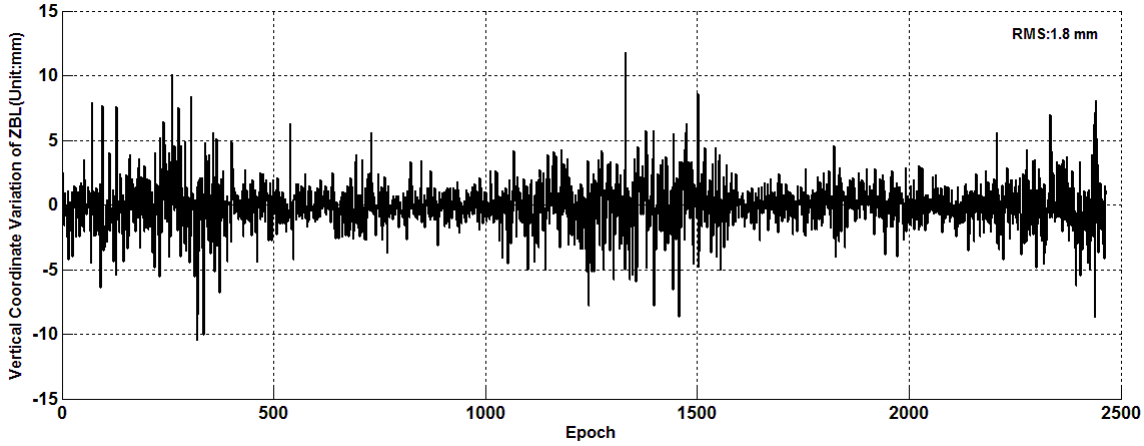

Fig. 2.5 Variations of ZBL on the elevation coordinate

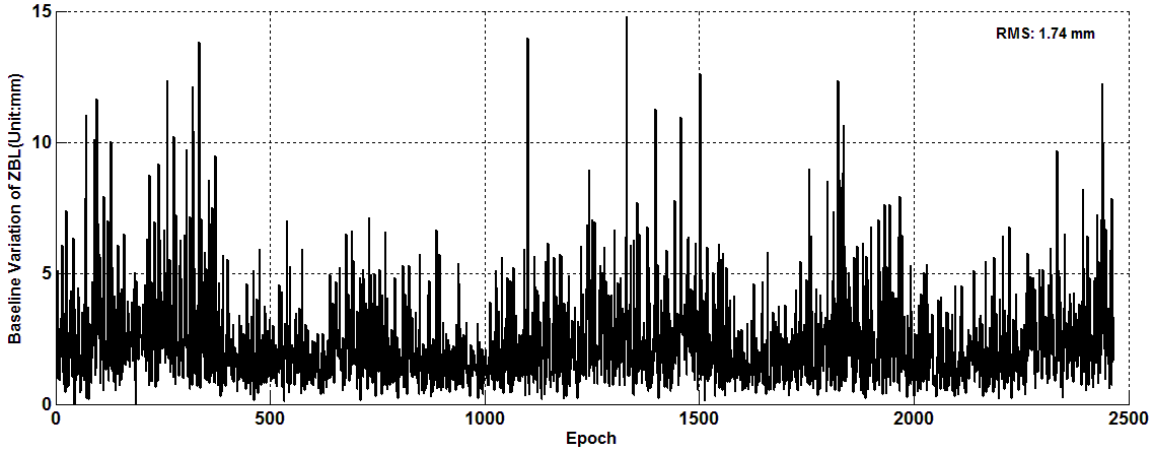

Fig. 2.6 Variations of ZBL on the distance domain

2.2 Tilt-meter

A tilt-meter is an instrument to measure the displacement by the precise inclination angle, which has been widely used in the displacement monitoring of the foundation pit, slope, foundation, bridge pier and so on. With the servo system of the force balance, the sensing element of tilt-meter can detect the inclination angle in the vertical direction. This section introduces the principles of the tilt-meter measuring and the corresponding statistical model.

2.2.1 The Measuring Principle of the Tilt-meter

2.2.1.1 Principle of the gravity tilt-meter

As shown in Figure 2.7, when the gravity is used for static measurements, there will be a tilt angel (θ_x, i.e. OX') between the OX axis and its original position, because of the flexible support.

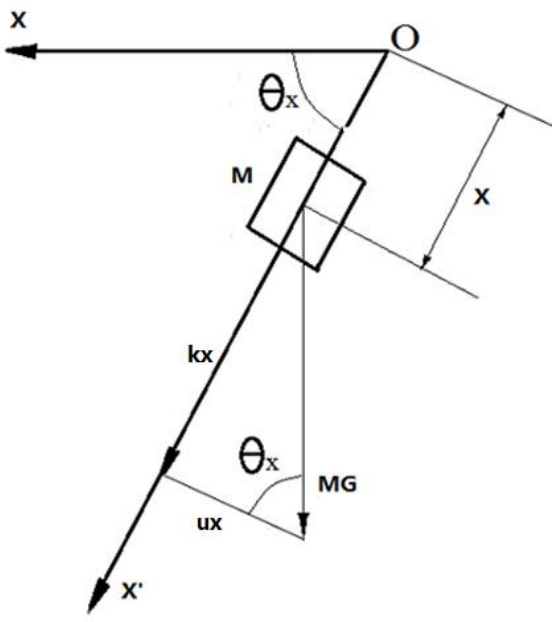

Fig. 2.7 Principle of the gravity tilt-meter

Because of gravity, the mass block m leaves the equilibrium position and produces a displacement X. $sin\theta_x = \frac{kx}{MG} = \frac{a_x}{g}$ *(2-52)*

and

$$sin\theta_y = \frac{ky}{mg} = \frac{a_y}{g} \quad (2\text{-}53)$$

where x and y are the displacement of mass block on the X axis and Y axis, k is the equivalent elastic coefficient of spring, m is equivalent mass(kg) of the object, θ_x *and* θ_y *are the tilt angles on the X and Y axes, respectively, and* a_x *and* a_y *are the projection of g on the X and Y axes.*

$$sin\theta_x = \frac{A_x}{A_g}, sin\theta_y = \frac{A_y}{A_g} \quad (2\text{-}54)$$

where, $\boldsymbol{A_x}$ *and* $\boldsymbol{A_y}$ *are the outputs of tilt-meter on the X and Y axis, respectively.* $\boldsymbol{A_g}$ *is output when the tilt is 90 degrees (i.e. when the projection on the axis of gravity is g). The tilt angle of the X and Y axes can be calculated by the output value on the X and Y axes.*

$$\theta_x = arcsin(\frac{A_x}{A_g}) \quad (2\text{-}55)$$

$$\theta_y = arcsin(\frac{A_y}{A_g}) \quad (2\text{-}56)$$

2.2.1.2 The axis tilt-meter measuring instrument

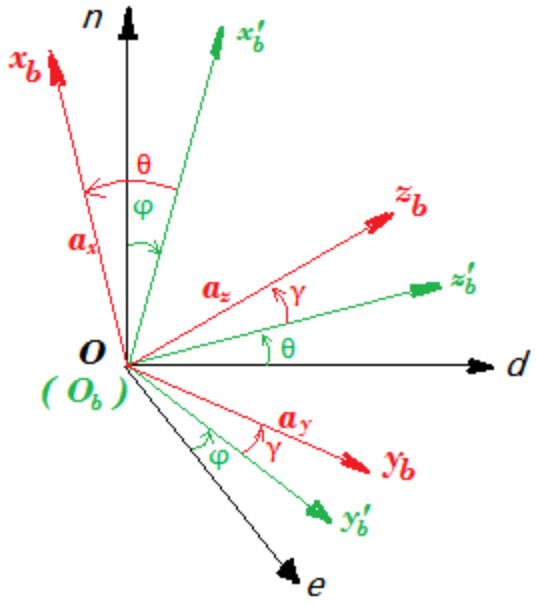

Fig. 2-8 Transformation from tilt-meter coordinate system to GPS coordinate system

Set the north-east-down coordinate system for "n, e, d", the sensor coordinate system for "front (x_b), right (y_b), down (z_b)". The transformation from the north-east-down coordinate system to the sensor coordinate system is as follows:

The tilt-meter first rotates angle φ around the d axis, go to the $O - x_b'y_b'd$ coordinate system, and then rotates angle θ around the y_b' axis, go to the $O - x_by_b'z_b'$ coordinate system, finally rotates angle γ around the x_b axis, go to the $O - x_by_bz_b$ coordinates. The coordinate transformation matrix is C_n^b

$$\boldsymbol{C}_n^b = \boldsymbol{C}_1\boldsymbol{C}_2\boldsymbol{C}_3 \qquad (2\text{-}57)$$

here

$$\boldsymbol{C}_1 = \begin{bmatrix} 1 & 0 & 0 \\ 0 & cos\gamma & sin\ \gamma \\ 0 & -sin\gamma & cos\gamma \end{bmatrix}, \boldsymbol{C}_2 = \begin{bmatrix} cos\theta & 0 & -sin\theta \\ 0 & 1 & 0 \\ sin\theta & 0 & cos\theta \end{bmatrix}, \boldsymbol{C}_3 = \begin{bmatrix} cos\varphi & sin\varphi & 0 \\ -sin\varphi & cos\varphi & 0 \\ 0 & 0 & 1 \end{bmatrix}$$

where θ, φ, γ, are the heading angle, pitch angle and roll angle, respectively.

Formulas (2-58) and (2-59) are the basic principle of measuring the tilt angle by the gravity. Measurements a_x, a_y, a_z from sensors are on the x, y, z axes, g is gravity acceleration. By formula (2-57), the relationship of the elevation angle and the rolling angle with the measured value is obtained. According to the formula, the pitching angle and roll angle are derived.

$$\theta = arcsin(\frac{-a_x}{g}) \tag{2-58}$$

$$\gamma = arctan(\frac{a_y}{a_z}) \tag{2-59}$$

By inputting the measurements on the three axes into the formula, the tilt angle can be obtained. As the formula shows, errors of a_x,a_y,a_z will affect the accuracy of the tilt-meter.

2.2.2 Error Model of the Tilt-meter

By the Taylor formula for (2-58) and (2-59), the pitch angle and roll angle measurement errors can be obtained.

$$\Delta\theta \approx \frac{1}{gcos\theta_0}\Delta a_x \tag{2-60}$$

$$\Delta\gamma \approx \frac{cos\gamma_0}{gcos\theta_0}\Delta a_y + \frac{sin\gamma_0}{gcos\theta_0}\Delta a_z \quad (2\text{-}61)$$

where $\Delta a_x, \Delta a_y$ and Δa_z are the measurement errors of accelerometers on the three axes. θ_0 and γ_0 are the real pitch angle and roll angle. $\Delta\theta$ and $\Delta\gamma$ are the errors of these two angles. g is the acceleration of gravity. The measurement error of accelerometer Δa obey the normal distribution with parameters μ and σ:

$$\Delta a \sim N(\mu, \sigma^2) \quad (2\text{-}62)$$

where μ is the zero bias of the sensor, σ is the standard deviation of the random error. Assuming error statistics on the x, y, z axes are independent from each other, $\Delta\theta$ and $\Delta\gamma$ meet the following requirements.

$$\Delta\theta \sim N(\frac{1}{gcos\theta_0}\mu_x, (\frac{\sigma(\Delta a_x)}{gcos\theta_0})^2) \quad (2\text{-}63)$$

$$\Delta\gamma \sim N(\frac{-cos\gamma_0}{gcos\theta_0}\mu_y + \frac{sin\gamma_0}{gcos\theta_0}\mu_z, (\frac{\sigma(\Delta a_y)cos\gamma_0}{gcos\theta_0})^2 + (\frac{\sigma(\Delta a_z)sin\gamma_0}{gcos\theta_0})^2) \quad (2\text{-}64)$$

where $\sigma(\Delta a_x), \sigma(\Delta a_y)$ and $\sigma(\Delta a_z)$ are the standard deviation of the measurement errors on the, y, z axes. $\Delta\theta$ is the measurement error of the pitch angle, $\Delta\gamma$ is the roll angle measurement error. Because the selected sensors are of the same type, Δa_y and Δa_z may have the same size. Calculate the mathematical expectation and standard deviation of $\Delta\theta$ and $\Delta\gamma$ by the statistical method.

$$E(\Delta\theta) = \frac{1}{g\cos\theta_0}\mu_x \tag{2-65}$$

$$E(\Delta\gamma) = \frac{-\cos\gamma_0}{g\cos\theta_0}\mu_y + \frac{\sin\gamma_0}{g\cos\theta_0}\mu_z \tag{2-66}$$

$$\sigma(\Delta\theta) = \frac{\sigma(\Delta a_x)}{g\cos\theta_0} \tag{2-67}$$

$$\sigma(\Delta\gamma) == \frac{\sigma(\Delta a_y)}{g\cos\theta_0} \tag{2-68}$$

The mathematical model of the tilt-meter measurement error suggests that the error of pitch angle measurement is related to the angle size, and the roll angle error is related to the pitch angle and roll angle.

2.2.3 Tests of Tilt-meter Accuracy

A MEMS tilt meter of RION(HCA526T) has been employed in this study, with the resolution of 0.001 degree, accuracy of 0.002 degree and the frequency of 20Hz. In order to verify its observation precision, the tilt-meter was fixed on a stable platform to conduct the observation and sampling for one consecutive day. Test results show that (Figures 2-9, 2-10), the standard deviation is 0.0027 degree on the X axis and 0.0024 degree on the Y axis.

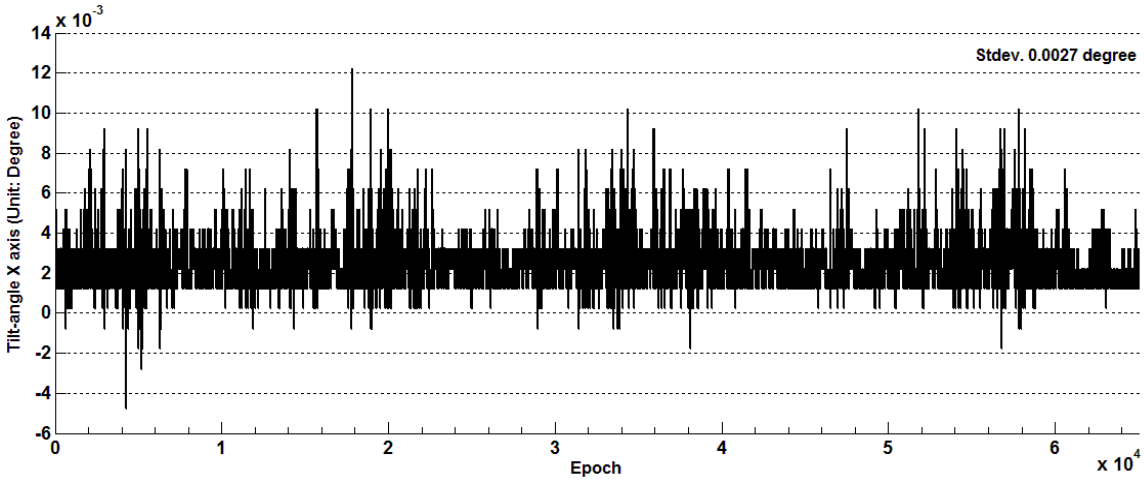

Fig. 2-9 Tilt-angle static observation of X axis

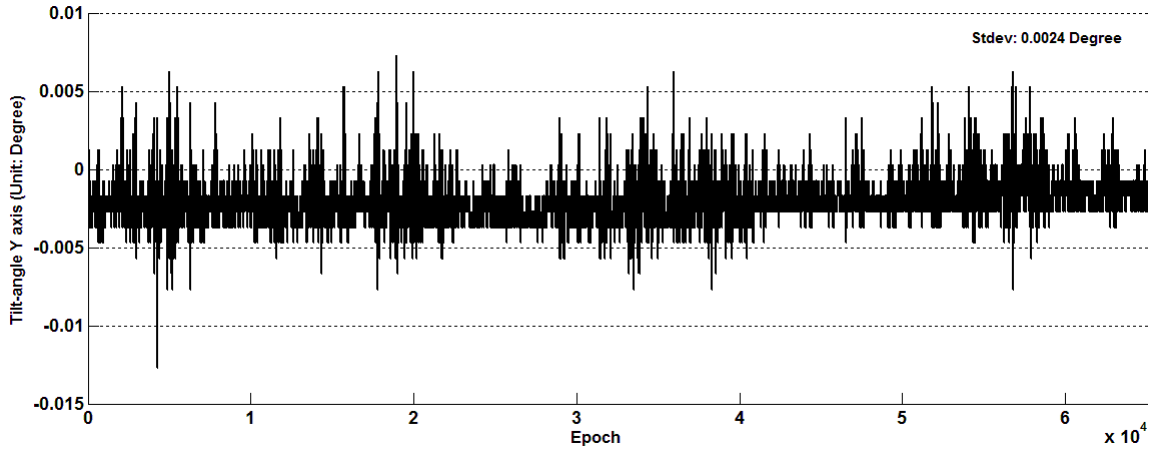

Fig. 2-10 Tilt-angle static observation of Y axis

As the obtained vibration data presented in figures 2-11 and 2-12 show, the platform vibrates at a frequency of 10 Hz for 60 seconds, and then vibrates at a lower frequency of 0.2 Hz for 90 seconds.

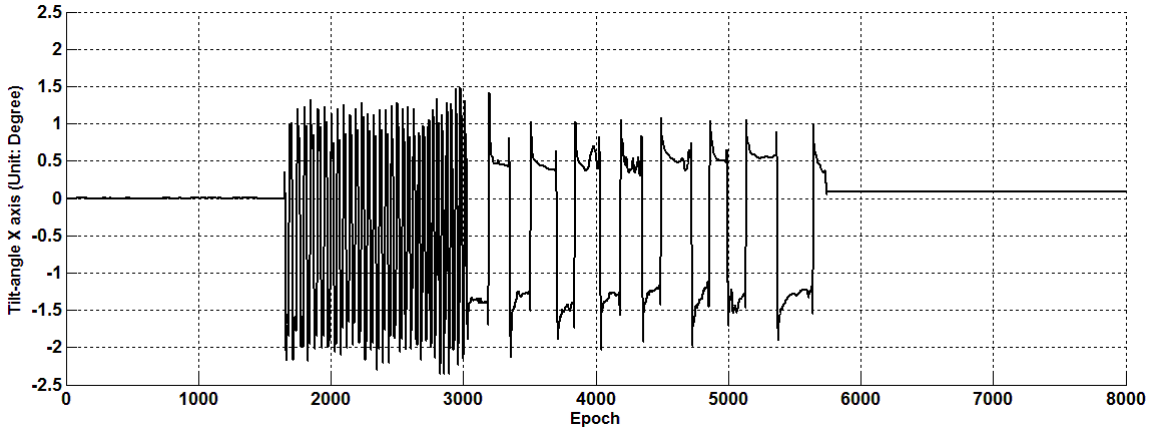

Fig. 2-11 Tilt-angle dynamic observation of X axis

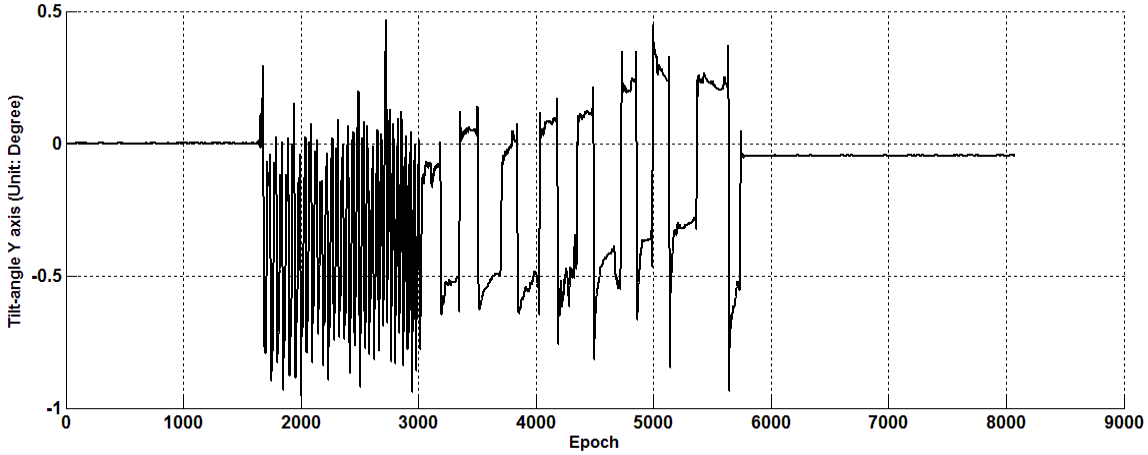

Fig. 2-12 Tilt-angle dynamic observation of Y axis

2.3 Accelerometer

Using the dynamic accelerometer to monitor the structure health one needs to identify the acceleration observation model. The accelerometer accuracy has an important influence on the speed and position of the structure monitoring solution. The main errors of the accelerometer are the zero offset and quadrature error, which mainly come from two aspects. One is the system error of the micro-electro-mechanical system (MEMS) accelerometer in the design or processing process. The other is the error caused by environmental changes. To

obtain more accurate deformation information, several kinds of accelerometer errors should be mitigated, such as scale factor error, installation error coefficient and zero error. This section focuses on the observation equation and error model of the dynamic accelerometer.

2.3.1 Principle of the Accelerometer

The commonly used accelerometers are gyro accelerometer and MEMS accelerometer. Gyro accelerometer measures displacement caused by Coriolis acceleration. Gyro accelerometer balances the moment of inertia with the gyroscopic moment, which has high precision and good stability. But the complex production process, large volume, high cost and long preparation time make gyro accelerometers usually only used in large scale navigation and guidance control systems. In SHM, MEMS accelerometer is often used. MEMS uses the position measuring interface circuit to measure the object displacement, and then converts the measurement to digital signals by analog-digital conversion (ADC). According to Newton's second law, F=MA, that is, the physical acceleration a (m/s^2) is proportional to the resultant force (F), and inversely proportional to its mass m (kg), and the acceleration direction is the same as the resultant force. Accelerometer is also an electromechanical device, and it has holes, cavities, springs and pipes, which are made by microfabrication technology. The accelerometer obtains the object's acceleration by measuring the displacement of the gravity center relative to the fixed electrode.

The MEMS accelerometer consists of a vibrating mass and an elastic beam. When there is acceleration input, the mass will be displaced due to the inertia force, and the displacement variation has a fixed relationship with the magnitude of the input acceleration, which can be described as a two order spring damping vibration system with the single degree of freedom. And the mathematical model of the system is

$$ma = kx + c\dot{x} + m\ddot{x} \qquad (2\text{-}69)$$

where k is the equivalent elastic coefficient, c is the equivalent damping coefficient, m is the equivalent inertia mass, a is the input acceleration. According to equation (2-69), a formula can be find about the displacement and acceleration input:

$$x = ma/k + q_1 e^{(-C-\sqrt{c^2-4km})t/2m} + q_2 e^{(-C+\sqrt{c^2-4km})t/2m} \qquad (2\text{-}70)$$

where q_1 and q_2 are integral constants, depending on the boundary conditions of the system.

The precision of an accelerometer refers to its manufacturing accuracy and calibration accuracy. The manufacturing accuracy is determined by the design and the assembly accuracy, and the calibration accuracy is determined by scientific testing methods and data processing.

2.3.2 MEMS Accelerometer Error Model

The mathematical model of the dynamic accelerometer can be expressed as

$$\begin{bmatrix} A_x \\ A_y \\ A_z \end{bmatrix} = \begin{bmatrix} A_{x_0} \\ A_{y_0} \\ A_{z_0} \end{bmatrix} + \begin{bmatrix} \begin{bmatrix} k_x & s_{x1} & s_{x2} \\ s_{y1} & k_y & s_{y2} \\ s_{z1} & s_{z2} & k_z \end{bmatrix} \begin{bmatrix} a_x \\ a_y \\ a_z \end{bmatrix} + \begin{bmatrix} s_x & 0 & 0 \\ 0 & s_y & 0 \\ 0 & 0 & s_z \end{bmatrix} \begin{bmatrix} a_x^2 \\ a_y^2 \\ a_z^2 \end{bmatrix} \end{bmatrix} \qquad (2\text{-}71)$$

where A_x, A_y and A_z are the observations on the three axes of the dynamic accelerometer, A_{x_0}, A_{y_0} and A_{z_0} are the zero offset of the accelerometer, k_x,k_y and k_z are the scale factors, s_{x1},s_{x2},s_{y1},s_{y2},s_{z1},s_{z2} are the installation error coefficients, a_x,a_y and a_z are the force acceleration in the three directions. s_x,s_y and s_z are the two times error coefficients of the MEMS accelerometer. As the two times error has little influence on the precision of the accelerometer in the monitoring, it is not considered. So the error model of the output value of the MEMS accelerometer can be written as

$$\begin{bmatrix} A_x - A_{x_0} \\ A_y - A_{y_0} \\ A_z - A_{z_0} \end{bmatrix} = \begin{bmatrix} k_x & s_{x1} & s_{x2} \\ s_{y1} & k_y & s_{y2} \\ s_{z1} & s_{z2} & k_z \end{bmatrix} \begin{bmatrix} a_x \\ a_y \\ a_z \end{bmatrix} \qquad (2\text{-}72)$$

2.3.3 Six Position Calibration of the Dynamic Accelerometer

*Using the dynamic accelerometer to monitor the structure health, one needs to identify the acceleration observation model (2-72) (***Liu et al., 2016***). In other words, to determine the value of the coefficient matrix (2-72). In this study, the six position method is employed to determine the coefficient matrix of the MEMS accelerator. On the platform, the x, y, z axis each has two directions (up and down), so they have six directions together. Take the mean value of the output voltage of each position as the measurement of the accelerometer for later*

*calculations. Specifically, the six positions are the down-east-south, up-west-south, west-down-south, east-up- south, south-west- down, east-north-up (***Song et al., 2009***), as shown in table 2-1.*

*Table 2-1. Six position orientation and the gravity acceleration of each axis. (***Song ., 2009***)*

Position	Axis and Orientation			Gravity Acceleration (unit: g)		
	X axis	Y axis	Z axis	X axis	Y axis	Z axis
1	down	east	West	1	0	0
2	up	west	South	-1	0	0
3	west	down	South	0	1	0
4	east	up	South	0	-1	0
5	south	west	Down	0	0	1
6	east	north	Up	0	0	-1

The outputs of the MEMS accelerometer on the three axes are:

$$A_{i1} = A_{i0} + k_i, A_{i2} = A_{i0} - k_i, A_{i3} = A_{i0} + s_{i1}$$

$$A_{i4} = A_{i0} - s_{i1}, A_{i5} = A_{i0} + s_{i2}, A_{i6} = A_{i0} - s_{i2}$$

*Accordingly, the correlation coefficient of model (2-72) on the corresponding axes can be solved (***Liu et al., 2016***):*

$$A_{i0} = \frac{A_{i1} + A_{i2} + A_{i3} + A_{i4} + A_{i5} + A_{i6}}{6}$$

$$k_i = \frac{A_{i1} - A_{i2}}{2}$$

$$s_{i1} = \frac{A_{i3} - A_{i4}}{2}$$

$$s_{i2} = \frac{A_{i5} - A_{i6}}{2}$$

where,$i = x, y, z.$

2.3.4 Determination of Accelerometer Accuracy

***Meng et al.** (**2002**) proposed a simple but accurate approach to calibrate a triaxial accelerometer by an adapted theodolite. Models for calculating zero biases and scale factors were derived together with variance estimation of each estimated parameter (**Meng et al., 2002**). The output signal of the accelerometer is an analogous value such as the proportion between the output and input voltage. An analogue to digital (A-to-D) converter is usually necessary to digitize the outputs from the analogue seblensors.*

a

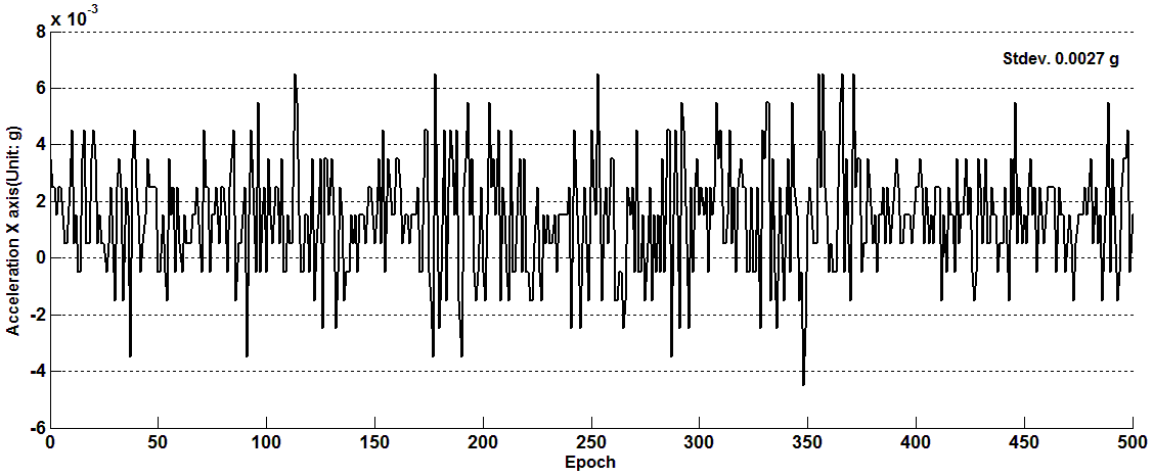

Fig. 2-13 Acceleration static observation of X axis

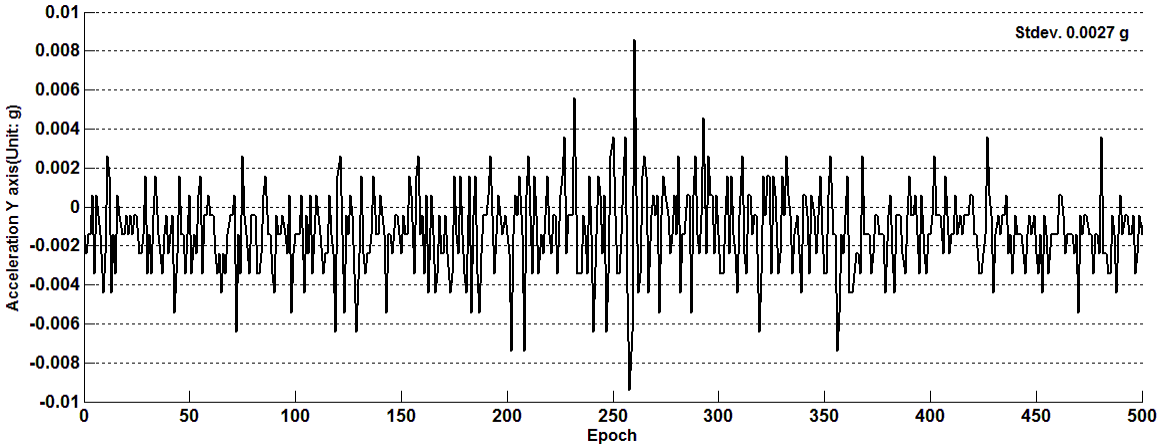

Fig. 2-14 Acceleration static observation of Y axis

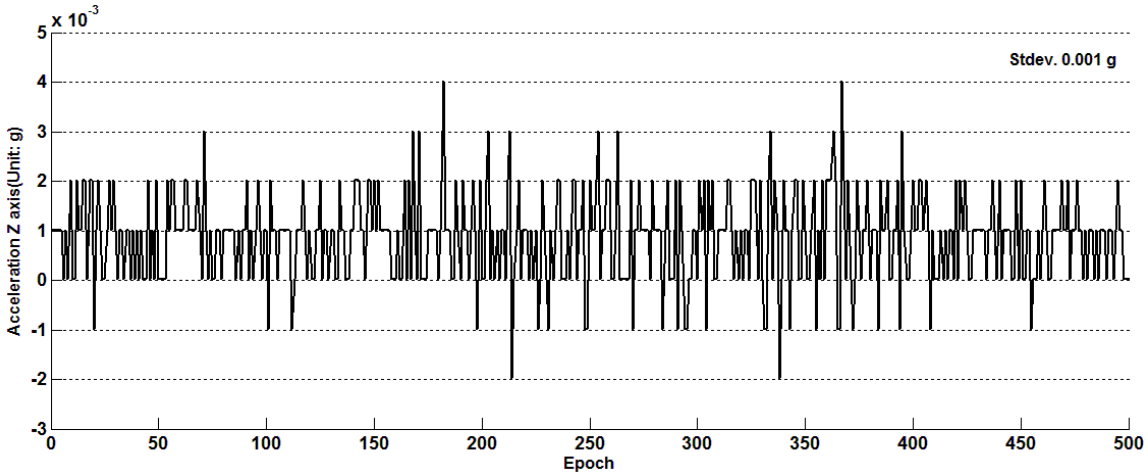

Fig. 2-15 Acceleration static observation of Z axis

The platform vibrates at a frequency of 10 Hz for 60 seconds, then vibrates at a low frequency of 0.2 Hz for 90 seconds. The obtained vibration data are given in figure 2-16, 2-17 *and* 2-18.

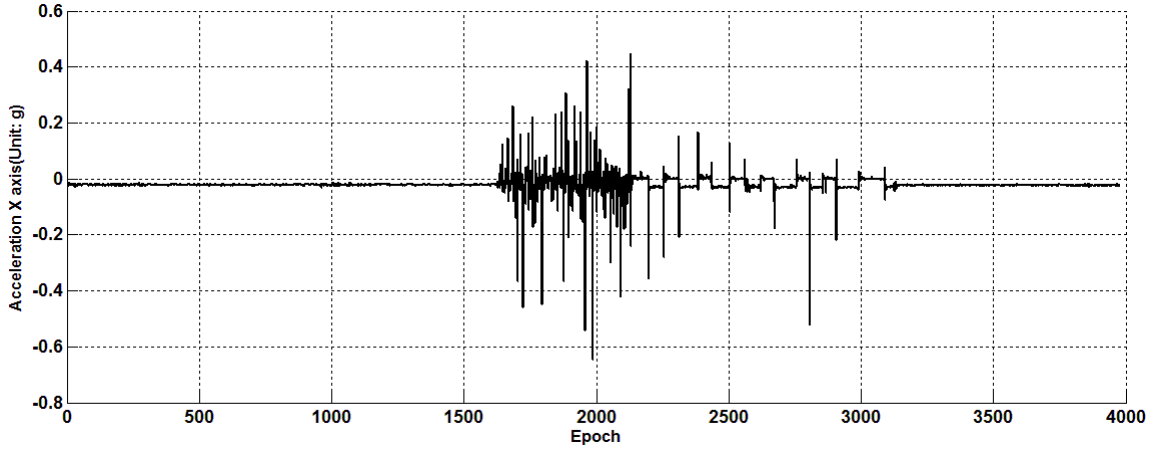

Fig. 2-16 Acceleration dynamic observation of X axis

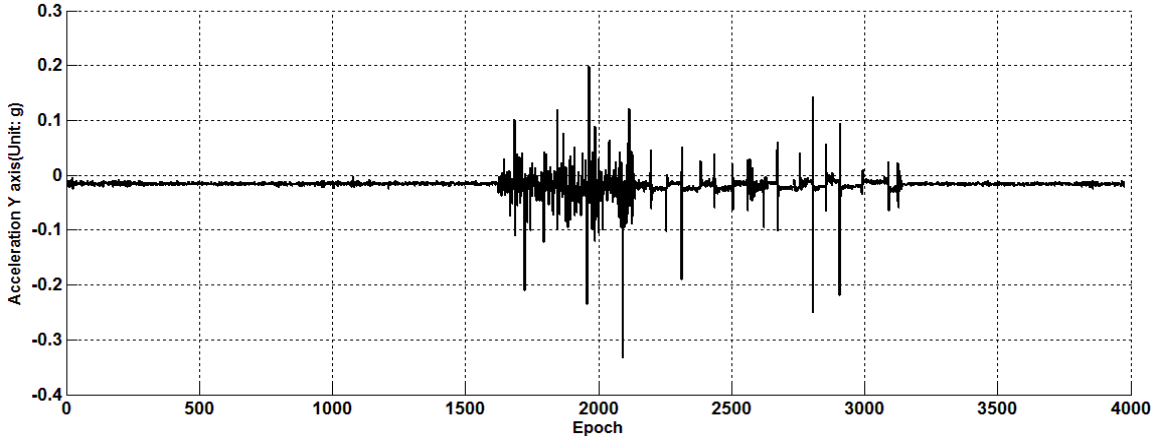

Fig. 2-17 Acceleration dynamic observation of Y axis

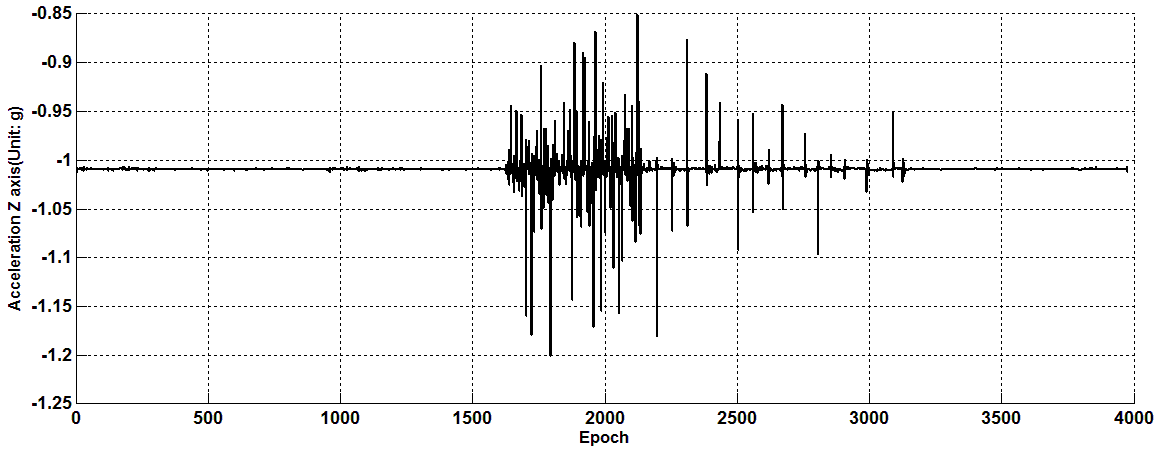

Fig. 2-18 Acceleration dynamic observation of Z axis

2.4 Other Sensors

In addition to the GPS, accelerometer and tilt-meter discussed in this study, significant amounts of other sensors may be used in deformation monitoring. **Dai et al.** *(***2009***) and* **Zhang et al.** *(***2012***) deployed the hydrostatic leveling system to analyze the temperature influence on the result. They advised the whole hydrostatic leveling system should be in an environment with the same temperature variation, so as to mitigate the system error.*

2.4.1 Hydrostatic Level

For large buildings, their displacements in the horizontal direction (X, Y) are small. But in the vertical direction (Z), buildings will have elevation changes due to gravity, which together with the uneven quality of components leads to uneven settlements. At present, high-rise building settlement monitoring generally adopts level for data collection, which has a heavy workload, low efficiency, and redundant errors. Adding to this, some feature points cannot meet the working space requirement, and the limited data collected are not sufficient for the time series of building settlement. The hydrostatic leveling system has many advantages, such as high precision, remote automation, and real-time measurement, so it has been used as an important method in the vertical displacement monitoring for large projects like subway tunnels. Hydrostatic leveling is based on the principle that fluid is always at the same level under gravity. The complete set of equipment mainly consists of 4 parts: the altimeter, the multi-purpose adjustable power supply, the connecting pipe

and the water tank. The system measures the difference of settlement points directly. For the absolute settlement of each measuring point, we need get the absolute elevation value of benchmarks by the optical leveling, and use it as the reference. Furthermore, we need to premeasure the benchmark elevation regularly.

Although the hydrostatic leveling system has been used in China for a long time, the technology has seen no major improvement. Its accuracy is affected by many factors, for example, the uneven pressure and temperature in the system, the accuracy of system calibration and gravity anomaly in the environment. In conclusion, there are still many problems need to be studied to obtain a stable and accurate hydrostatic leveling system.

2.4.2 Ultrasonic Flaw Detector

Ultrasonic flaw detector is a portable industrial nondestructive testing instrument which is fast, convenient, non-invasive and accurate in detecting, locating, assessing and diagnosing defects (cracks, porosity, incline) of the structure. Digital ultrasonic flaw detector is usually used to transmit ultrasound to the object and then obtain the internal information of the object by its reflection, Doppler effect, transmission, etc. The information will be processed to form an image. When the ultrasonic spreads into the test material, the material acoustic properties and internal organization changes will influence the propagation. The technology of understanding the material property and structure changes by the influence on and status of ultrasonic is called ultrasonic

detection. Ultrasonic detection methods include penetration method, pulse reflection method, tandem method, etc. The reflection method is based on the principle that the ultrasonic wave can be reflected in the interface with different acoustic impedance. When sound propagates from one medium to another medium, it will reflect at the interface. The greater the medium difference, the stronger the reflection. So we can emit an ultrasonic that has strong penetrability and can propagate in straight lines. Ultrasonic flaw detector receives this ultrasonic and determines the sizes, distributions and differences of structure mediums according to the reflection order and amplitude. The reflection order can tell the distance between the detector and the reflecting surface and the amplitude can indicate the size and differences of the mediums. This process involves ultrasonic generation, reception, signal conversion and processing, etc. As the ultrasonic flaw detector is very accurate, convenient, fast and causes no harm to the target object and operator, it has been widely used.

2.4.3 Electronic Total Station

The total station, also known as electronic total station, is developed from the optical theodolite. Different from the optical theodolite, the total station has a photoelectric scanning dial and automatic recording and displaying, which ease the angle measurement. By measuring the horizontal angle and vertical angle, distance (slant range, horizontal distance), height difference, the target point position measurement can be achieved. According to the angle measuring

precision, the total station can be divided into several types, 0.5 ", 1", 2 ", 3", 5 ", 7" and so on.

The electronic total station has new functions of automatic target recognition and aiming, which overcome the defects of artificial target aiming and make the total station smart. With the relating software, the intelligent total station can automatically achieve recognizing, aiming, and measuring of multiple targets. So the intelligent total station is also known as a measurement robot, such as the Leica TCA, TS total station.

The total station is widely used in precise engineering measurement and deformation monitoring, such as large scale building and underground tunnel construction. But, it requires inter-visibility between the target point and itself and its measuring distance is relatively short (less than 3 km). So the total station is limited and not applicable in some situations.

2.5 Summary

In this chapter, the basic principles and methods of GPS, accelerometer and tilt-meter instrument are introduced. The characteristics of GPS observation and data processing methods are also analyzed. This chapter gives a comprehensive introduction to the main error sources of GPS in SHM, tropospheric effects and multi-path effects, as well as their mitigation methods, which provides technology backgrounds for reducing these errors with multi-sensors in later chapters.

The commonly used sensor observation models are discussed, and the observation equation and error equation of tilt-meter and accelerometer are given. The observation matrix setting for tilt-meter and accelerometer are also presented. We test the equipment data stability of accelerometer and tilt-meter by inner average precision measurement. The accuracy is take as the prior information for the calculation in chapters 3, 4 and 5.

CHAPTER 3 MULTI-ANTENNA GPS AND SINGLE TILT-METER FUSION

GPS has become a reliable and useful technology for monitoring the deformation and dynamics of structures, such as bridges, dams and high-rise buildings. However, GPS positioning accuracy in such applications is highly sensitive to multipath effects. Additionally, for high-rise structure monitoring, the tropospheric effects cannot be effectively mitigated by the double-difference operations in GPS data processing.

*GPS multipath effects can be avoided or reduced by multipath-rejecting GPS antennas (e.g. advanced pinwheel compact controlled reception pattern antenna and choke-ring antenna) or multipath "resistant" receivers employing correlation techniques, such as the narrow correlation spacing, MET and MMW techniques (***Zhong et al., 2010***). Besides, some post-processing techniques are also used to eliminate multipath errors, such as weighting GPS observations based on SNR or C/No (***Rangwala et al., 1990; Chung et al., 2003; Cameron et al., 2002***). Nevertheless, none of these methods can completely mitigate multipath errors. It is also a very challenging task to model and mitigate the tropospheric effects in high-rise building monitoring. Thus, combining GPS receivers, accelerometers and displacement transducers can greatly increase the accuracy, reliability and productivity of the overall monitoring system.*

We will present in this section a structure monitoring system integrating a multi-antenna GPS system and a dual-axial tilt-meter, in order to effectively mitigate multipath errors in high-rise building monitoring.

3.1 Hardware Deployment

We set up a rigid steel platform (Figure 3-1) on which a dual-axial tilt-meter and three GPS antennas (A1, A2 and A3) were firmly attached. The distance between the antennas were 1 m and the tilt-meter was fixed at the center of the triangular platform. Single frequency GPS receivers (GPS 615) were used.

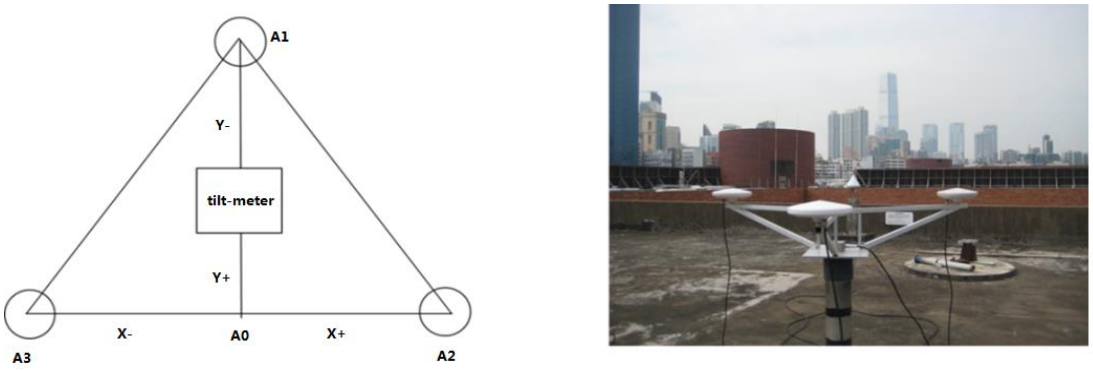

Fig. 3-1 Hardware of the integrated system

3.2 Observation Equations

3.2.1 Tilt-meter Observation Equations

As shown in Figure 3-1, tilt angles of device in figure 3-1 can be expressed as X_a *and* Y_a.

$$X_a = arcsin\left(\frac{H_2 - H_3}{\bar{L}_{23}}\right) \qquad (3\text{-}1)$$

$$Y_a = arcsin\left(\frac{H_0 - H_1}{\frac{\bar{L}_{12} + \bar{L}_{13}}{2} sin(\pi/3)}\right) \quad (3\text{-}2)$$

$H_i (i = 0,1,2,3)$ is the elevation of point A_i, and $\bar{L}_{12}$ and $\bar{L}_{13}$ are the known distances between antennas A_1 and A_2, and between A_1 and A_3, respectively.

The longitude (L), latitude (B) and elevation (H) of a point can be computed from the geocentric Cartesian coordinates X_i, Y_i, Z_i.

$$\begin{bmatrix} L \\ B \\ H \end{bmatrix} = \begin{bmatrix} arctan\left(\frac{Y}{X}\right) \\ arctan\left(\frac{Z(N+H)}{\sqrt{X^2+Y^2}[N(1-e^2)+H]}\right) \\ sin\left(\frac{Z}{B}\right) - N(1-e^2) \end{bmatrix} \quad (3\text{-}3)$$

Where:

$N = \frac{a}{\sqrt{1-e^2 sin^2 B}}$,

a is the semi-major axis and e is the eccentricity of the ellipsoid. Equations (3-1) and (3-2) can be rewritten as

$$X_a = arcsin\left(\frac{\frac{Z_2}{sinB_2} - \frac{Z_3}{sinB_3} - G}{\bar{L}_{23}}\right) \quad (3\text{-}4)$$

$$Y_a = arcsin\left(\frac{\frac{Z_3}{2sinB_3} + \frac{Z_2}{2sinB_2} - \frac{Z_1}{sinB_1} - F}{\frac{\bar{L}_{12} + \bar{L}_{13}}{2} sin(\pi/3)}\right) \quad (3\text{-}5)$$

where:

$$F = \left(\frac{a}{2\sqrt{1-e^2 sin^2 B_3}} + \frac{a}{2\sqrt{1-e^2 sin^2 B_2}} - \frac{a}{\sqrt{1-e^2 sin^2 B_1}}\right)(1-e^2)$$

$$G = \left(\frac{a}{\sqrt{1-e^2 sin^2 B_2}} - \frac{a}{\sqrt{1-e^2 sin^2 B_3}}\right)(1-e^2)$$

Linearizing the equation for the Y axis, we can get

$$Y_a^0 + V_y = \frac{\partial Y_a}{\partial Z_1} dZ_1 + \frac{\partial Y_a}{\partial Z_2} dZ_2 + \frac{\partial Y_a}{\partial Z_3} dZ_3 + \bar{Y}_a \qquad (3\text{-}6)$$

$$w_y + V_y = \frac{\frac{dZ_3}{2sinB_3} + \frac{dZ_2}{2sinB_2} - \frac{dZ_1}{sinB_1}}{\sqrt{K}} \qquad (3\text{-}7)$$

where:

$$K = \left(\frac{\bar{L}_{12} + \bar{L}_{13}}{2} sin(\pi/3)\right)^2 - \left(\frac{Z_3}{2sinB_3} + \frac{Z_2}{2sinB_2} - \frac{Z_1}{sinB_1} - F\right)^2$$

$$w_y = Y_a^0 - \bar{Y}_a$$

Y_a^0 is the measured tilt angle, and $\bar{Y}_a$ is the tilt angle calculated from the initial coordinates. The observation equation for the tilt angle along the X axis can be derived similarly

$$X_a^0 + V_x = \frac{\frac{dZ_2}{sinB_2} - \frac{dZ_3}{sinB_3}}{\sqrt{J}} + \bar{X}_a \qquad (3\text{-}8)$$

$$w_x + V_x = \frac{\frac{dZ_2}{sinB_2} - \frac{dZ_3}{sinB_3}}{\sqrt{J}} \tag{3-9}$$

where:

$$J = \bar{L}_{13}^2 - \left(\frac{Z_2}{sinB_2} - \frac{Z_3}{sinB_3} - G\right)^2$$

$$w_x = X_a^0 - \bar{X}_a$$

X_a^0 is the measured tilt angle; and $\bar{X}_a$ is the tilt angle calculated from the initial coordinates.

3.2.2 Constraint Equations

The observation equation of the distance between point A_1 and A_2 can be derived as follows.

$$L_{12} = \sqrt{(X_1 - X_2)^2 + (Y_1 - Y_2)^2 + (Z_1 - Z_2)^2}$$

$$L_{12}^0 + V_{L_{12}} = \frac{\partial L_{12}}{\partial X_1} dX_1 + \frac{\partial L_{12}}{\partial X_2} dX_2 + \frac{\partial L_{12}}{\partial Y_1} dY_1 + \frac{\partial L_{12}}{\partial Y_2} dY_2$$

$$+ \frac{\partial L_{12}}{\partial Z_1} dZ_1 + \frac{\partial L_{12}}{\partial Z_2} dZ_2 + \bar{L}_{12}$$

$$\begin{aligned} w_{L_{12}} + V_{L_{12}} = {} & \frac{(X_1 - X_2)}{\bar{L}_{12}} dX_1 - \frac{(X_1 - X_2)}{\bar{L}_{12}} dX_2 + \frac{(Y_1 - Y_2)}{\bar{L}_{12}} dY_1 \\ & - \frac{(Y_1 - Y_2)}{\bar{L}_{12}} dY_2 + \frac{(Z_1 - Z_2)}{\bar{L}_{12}} dZ_1 - \frac{(Z_1 - Z_2)}{\bar{L}_{12}} dZ_2 \end{aligned} \tag{3-10}$$

where:

$$\bar{L}_{12} = \sqrt{(\bar{X}_1 - \bar{X}_2)^2 + (\bar{Y}_1 - \bar{Y}_2)^2 + (\bar{Z}_1 - \bar{Z}_2)^2}$$

$$w_{L_{12}} = L_{12}^0 - \bar{L}_{12}$$

$\bar{L}_{12}$ is the distance calculated from the initial coordinate; and L_{12}^0 is the observed distance. We also can get

$$\begin{aligned} w_{L_{13}} + V_{L_{13}} = {} & \frac{(X_1 - X_3)}{\bar{L}_{13}} dX_1 - \frac{(X_1 - X_3)}{\bar{L}_{13}} dX_3 + \frac{(Y_1 - Y_3)}{\bar{L}_{13}} dX_1 \\ & - \frac{(Y_1 - Y_3)}{\bar{L}_{13}} dY_3 + \frac{(Z_1 - Z_3)}{\bar{L}_{13}} dZ_1 - \frac{(Z_1 - Z_3)}{\bar{L}_{12}} dZ_3 \end{aligned} \quad \textit{(3-11)}$$

$$\begin{aligned} w_{L_{23}} + V_{L_{23}} = {} & \frac{(X_2 - X_3)}{\bar{L}_{23}} dX_2 - \frac{(X_2 - X_3)}{\bar{L}_{23}} dX_3 + \frac{(Y_2 - Y_3)}{\bar{L}_{23}} dX_2 \\ & - \frac{(Y_2 - Y_3)}{\bar{L}_{23}} dY_3 + \frac{(Z_2 - Z_3)}{\bar{L}_{23}} dZ_2 - \frac{(Z_2 - Z_3)}{\bar{L}_{23}} dZ_3 \end{aligned} \quad \textit{(3-12)}$$

where:

$$\bar{L}_{13} = \sqrt{(\bar{X}_1 - \bar{X}_3)^2 + (\bar{Y}_1 - \bar{Y}_3)^2 + (\bar{Z}_1 - \bar{Z}_3)^2}$$

$$\bar{L}_{23} = \sqrt{(\bar{X}_2 - \bar{X}_3)^2 + (\bar{Y}_2 - \bar{Y}_3)^2 + (\bar{Z}_2 - \bar{Z}_3)^2}$$

$$w_{L_{13}} = L_{13}^0 - \bar{L}_{13}$$

$$w_{L_{23}} = L_{23}^0 - \bar{L}_{23}$$

Since three antennas are fixed to the platform and distance between each other is constant, we can assume that $w_{L_{11}}$, $w_{L_{12}}$ *and* $w_{L_{13}}$ *equal to zero during the observations.*

3.2.3 Combined Adjustment Model

If 4 satellites are involved in the observation process, the observation model of A_1, A_2 *and* A_3 *can be established as follows*

$$\boldsymbol{L} + \boldsymbol{v} = \boldsymbol{AX} \qquad (3\text{-}13)$$

where:

$$\boldsymbol{X} = [dX_1, dY_1, dZ_1, dX_2, dY_2, dZ_2, dX_3, dY_3, dZ_3]^T$$

$$\boldsymbol{L} = [\boldsymbol{L}_1^T, \boldsymbol{L}_2^T, \boldsymbol{L}_3^T]^T$$

$$\boldsymbol{A}_1 = \begin{bmatrix} \boldsymbol{E}_1 & 0 & 0 \\ 0 & \boldsymbol{E}_2 & 0 \\ 0 & 0 & \boldsymbol{E}_3 \end{bmatrix}$$

where $\boldsymbol{L}$, $\boldsymbol{E}_i$ *(i=1,2,3) have the same definitions with* $\boldsymbol{L}$, $\boldsymbol{E}$ *in (2-8). Based on (3-6) and (3-7) the following stochastic constraints can be established*

$$\boldsymbol{L}_2 + \boldsymbol{v}_2 = \boldsymbol{A}_2\boldsymbol{X} \qquad (3\text{-}14)$$

where:

$$\boldsymbol{L}_2 = [w_x, w_y]^T$$

$$\boldsymbol{X} = [dX_1, dY_1, dZ_1, dX_2, dY_2, dZ_2, dX_3, dY_3, dZ_3]^T$$

$$\boldsymbol{A}_2 = \begin{bmatrix} 0 & 0 & -\dfrac{1}{\sqrt{K}sinB_1} & 0 & 0 & \dfrac{1}{2\sqrt{K}sinB_2} & 0 & 0 & \dfrac{1}{2\sqrt{K}sinB_3} \\ 0 & 0 & 0 & 0 & 0 & -\dfrac{1}{\sqrt{J}sinB_2} & 0 & 0 & \dfrac{1}{\sqrt{J}sinB_3} \end{bmatrix}$$

Additionally, the following functional constraints can be established as the distance between A_i and A_j is a constant.

$$\sqrt{(X_i - X_j)^2 + (Y_i - Y_j)^2 + (Z_i - Z_j)^2} = L_{ij}$$

After the linearisation, it is written as

$$\boldsymbol{A}_3\boldsymbol{X} = \boldsymbol{L_3} \qquad (3\text{-}15)$$

where:

$$\boldsymbol{A}_3 = \begin{bmatrix} EX_{12} & EY_{12} & EZ_{12} & -EX_{12} & -EY_{12} & -EZ_{12} & 0 & 0 & 0 \\ EX_{13} & EY_{13} & EZ_{13} & 0 & 0 & 0 & -EX_{12} & -EY_{12} & -EZ_{12} \\ 0 & 0 & 0 & EX_{23} & EY_{23} & EZ_{23} & -EX_{23} & -EY_{23} & -EZ_{23} \end{bmatrix}$$

$$\boldsymbol{L_3} = [w_{L_{12}}, w_{L_{13}}, w_{L_{23}}]^T$$

$EX_{ij} = \frac{X_i - X_j}{\bar{L}_{ij}}$, $EY_{ij} = \frac{Y_i - Y_j}{\bar{L}_{ij}}$, $EZ_{ij} = \frac{Z_i - Z_j}{\bar{L}_{ij}}$

By the combined adjustment method, the constraint (3-15) is taken as the virtual observations, and the GPS and the tilt-meter observation equations are combined to form the main model. Then the solution can be obtained by weighted least squares.

$$\begin{bmatrix} L_1 \\ L_2 \\ L_3 \end{bmatrix} + \begin{bmatrix} v_1 \\ v_2 \\ 0 \end{bmatrix} = \begin{bmatrix} A_1 \\ A_2 \\ A_3 \end{bmatrix} X \qquad (3\text{-}16)$$

The weight matrix p of (3-16) can be written as

$$P = \begin{bmatrix} \frac{1}{\delta_{GPS}^2 cos^2(e)} & 0 & 0 \\ 0 & \frac{1}{\delta_T^2} & 0 \\ 0 & 0 & \frac{1}{10000^2} \end{bmatrix}$$

The weights of the GPS and tilt-meter in P are determined by (2.2.3) and (2.3.4). GPS observation precision $\boldsymbol{\delta_{GPS}}$ *is set as 2 mm and the tilt-meter precision* $\boldsymbol{\delta_T}$ *is set as 0.002 degrees in this study. e is the satellite observation elevate angle. The weight of distance constraint is set as 10,000 m.*

3.3 Simulation Experiment

To verify the algorithms, the following simulation experiments are designed. The simulation data are sampled by second for 1200 epochs.

The positions of satellites were calculated directly through satellite broadcast ephemeris from 10:00 to 15:00 on December 28, 2016. The WGS84 coordinates and plane coordinates of three known ground points are shown in table 3-1.

Table 3-1. WGS84 coordinates and plane coordinates of three known points (A1, A2, A3).

	North	East	Elevation	X(WGS84)	Y(WGS84)	Z(WGS84)
A1	2467346.949	518499.652	34.264	-2418209.734	5385904.753	2405486.1
A2	2467347.949	518499.652	34.264	-2418209.58	5385904.406	2405487.025

A3	2467347.449	518498.786	34.264	-2418208.867	5385904.934	2405486.563

As equation (3-17) shows, the distance between the satellite, the ground points and the random error are taken as the simulated GPS observations. Different observation errors are given in the experiment.

$$VL_{GPS} = sqrt((X_S - X_{A1}) * (X_S - X_{A1}) + (Y_S - Y_{A1}) * (Y_S - Y_{A1}) + (Z - Z_{A1}) * (Z_S - Z_{A1})) + N_{noise} \quad (3\text{-}17)$$

where VL_{GPS} is the simulated GPS observations, X_S, Y_S, Z_S is the satellite coordinates, X_{A1}, Y_{A1}, Z_{A1} is the coordinates of the station antenna A1, N_{noise} is the random error of normal distribution.

The simulation data are processed by three algorithms in each experiment.

Algorithm 1: obtain the solution by least squares with only GPS observations. This is referred to as the GPS Algorithm.

Algorithm 2: obtain the parameter solution with GPS observations and the distances among the three fixed GPS antennas. It is referred to as the GPS with Constrains Algorithm.

Algorithm 3: Add the tilt-meter measurements to method 2 and obtain the solution by the least squares algorithm with (3-16). This is referred to as the GPS/Tilt Algorithm.

To determine the influence of the tilt-meter accuracy, the number of GPS satellites and GPS observation precision on the algorithms, we designed three experiments in sections 3.3.1 to 3.3.3.

3.3.1 Influence of the Tilt-meter Accuracy on the Algorithms

Given the GPS observation accuracy 8 mm and all the visible satellites, we study the accuracy variation of the three algorithms when the precision of tilt-meter changes. Analysing the displacement sequence, we can obtain the standard deviation value shown in table 3-2.

The standard deviations of the GPS algorithm result are 2.6121 mm, 2.6463 mm and 3.7372 mm in the north, east and elevation directions. After adding the distance constraint (becoming the GPS algorithm with constrains), they are improved to 1.7523 mm, 1.8164 mm and 3.7048 mm in the three directions, respectively.

For the GPS/Tilt-meter algorithm, if the tilt-meter observation accuracy is 0.001 degree, the standard deviations are 1.7510 mm, 1.8051 mm and 2.5073 mm in the north, east and elevation directions, respectively. If the tilt-meter accuracy reduces to 0.005 degree, GPS/Tilt-meter algorithm cannot improve the calculation results.

Table 3-2. Standard deviations of three algorithms when the accuracy of the tilt-meter changes. (unit: mm) (precision: GPS, 8 mm; number of satellite, 9; Tilt-meter,0.001 to 0.015 degree)

Accuracy of the tilt-meter（degree）	GPS Algorithm			GPS with Constraints			GPS/Tilt-meter Algorithm		
	North	East	Elevation	North	East	Elevation	North	East	Elevation

0.001	2.6121	2.6463	3.7372	1.7523	1.8164	3.7048	1.7510	1.8051	2.5073
0.002							1.7518	1.8060	2.7683
0.003							1.7532	1.8158	3.1840
0.005							1.7594	1.8263	4.1968
0.010							1.7706	1.8593	7.1002
0.015							1.8049	1.9115	10.4007

Figures 3-2, 3-3, 3-4 compare the displacement sequences of the GPS/tilt-meter algorithm, when the tilt-meter accuracy is 0.001 degree, 0.005 degree and 0.01 degree, respectively. When the tilt-meter accuracy increases from 0.01 degree to 0.001 degree, the standard deviation decreases from 10.40 mm to 2.51 mm in the elevation direction, but there is no obvious change in the horizontal direction. The reason for this could be that the algorithm mainly constrains the correction effect in the elevation direction, which could be seen from equation (3-5) and equation (3-6).

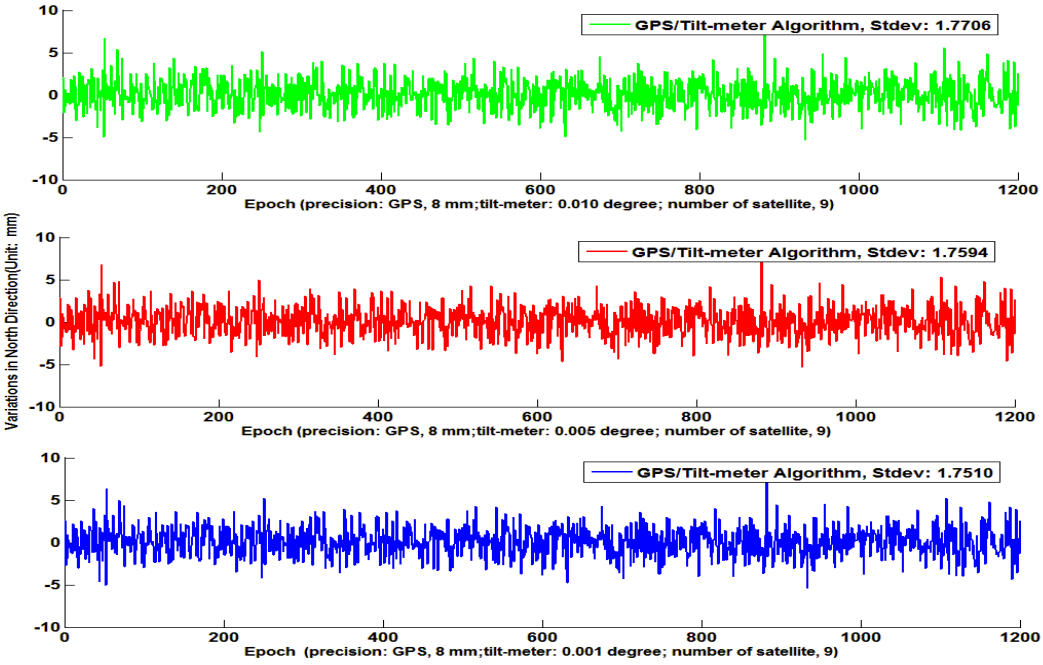

Fig. 3-2 Variations in the north direction with different tilt-meter accuracies (precision: GPS, 8 mm; number of satellite, 9; Tilt-meter, 0.001 to 0.01 degree)

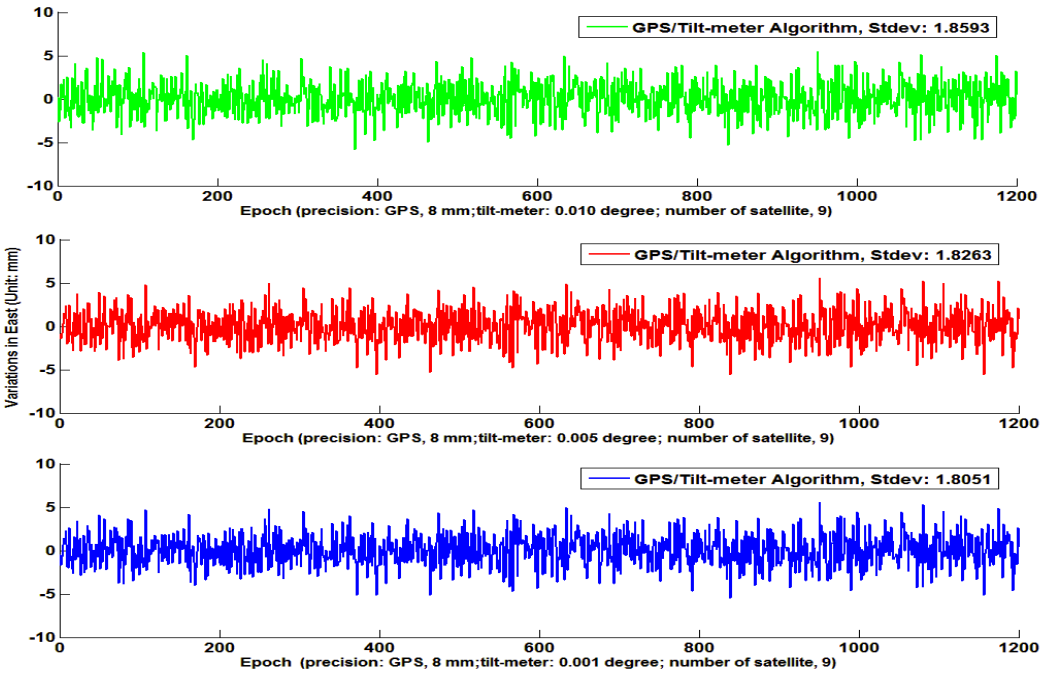

Fig. 3-3 Variations in the east direction with different tilt-meter accuracies (precision: GPS, 8 mm; number of satellite, 9; Tilt-meter, 0.001 to 0.01 degree)

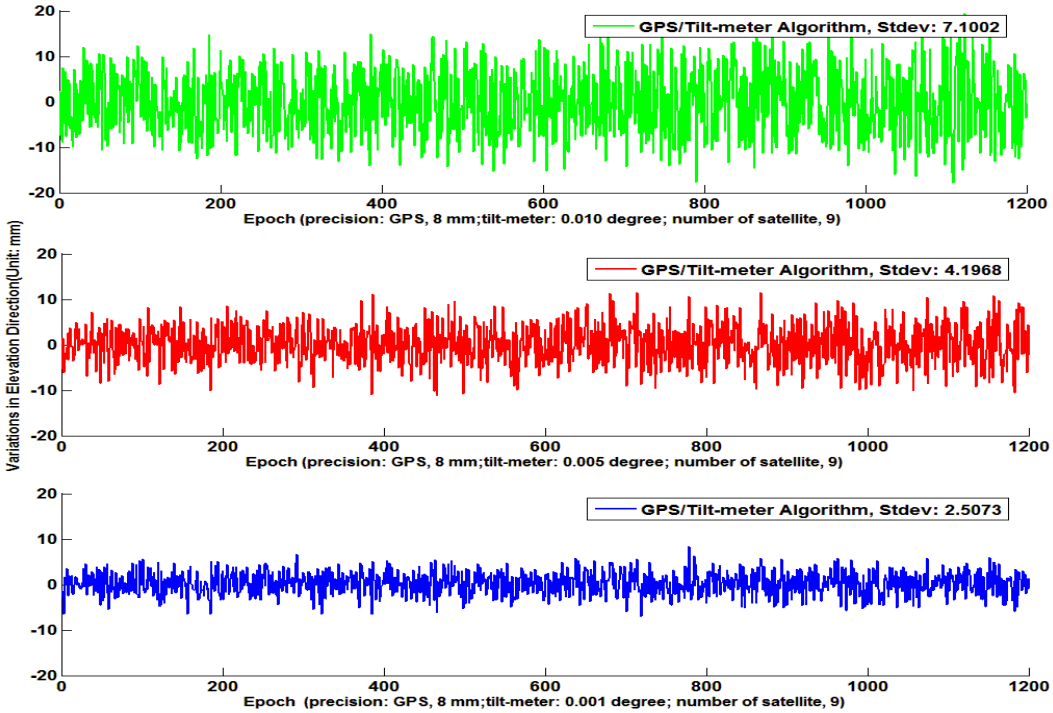

Fig. 3-4 Variations in the elevation direction with different tilt-meter accuracies (precision: GPS, 8 mm; number of satellite, 9; Tilt-meter, 0.001 to 0.01 degree)

3.3.2 The Effect of Number of Satellites on the Algorithms

Given the GPS observation accuracy of 8 mm and the tilt-meter observation precision equaling 0.003 degrees, we sort visible satellites according to their elevation angles (large to small) and obtain the results with different numbers of satellites. Standard deviations of the three algorithm are compared in table 3-3.

Table 3-3. Standard deviations of three algorithms when different numbers of satellites are used. (unit: mm) (precision: GPS, 8 mm; tilt-meter, 0.003 degree; number of satellites, 4 to 9)

Number of Visible Satellites	GPS Algorithm			GPS with Constrains			GPS/Tilt Algorithm		
	North	East	Elevation	North	East	Elevation	North	East	Elevation
4	4.0106	4.1487	5.9355	2.7597	2.8436	5.4780	2.7074	2.6363	4.1208
5	3.7344	3.4598	4.5191	2.5533	2.3536	4.3579	2.5427	2.3099	3.5889
6	3.1158	2.9738	4.1297	2.0966	2.0472	4.0896	2.0961	2.0278	3.3997
7	2.8953	2.7188	3.8937	1.9278	1.9013	3.8762	1.9247	1.8880	3.2857
8	2.6830	2.6592	3.7883	1.7839	1.8435	3.7688	1.7823	1.8330	3.2315
9	2.6121	2.6463	3.7372	1.7523	1.8164	3.7048	1.7532	1.8158	3.1840

As Table 3-3 shows, the accuracy of the GPS algorithm result is poor when only 4 satellites are used, with the standard deviations 4.01 mm, 4.15 mm, and 5.94 mm in the north, east and elevation directions, respectively. With more satellites, the standard deviations of GPS with constrains algorithm and the GPS/Tilt algorithm result decreases to about 1.5 mm in three directions, which means the geometric constraints can increase the observation information and improve the result reliability. Additionally, observation of the high precision tilt-meter can improve the solution accuracy.

Figures 3-5, 3-6, 3-7 *compare the displacement sequences of the first 200 epochs of the three algorithms, with 4 satellites, a GPS observation precision of 8 mm and the tilt-meter observation precision at 0.003 degree. The standard*

deviations of the GPS algorithm are 4.01 mm, 4.15 mm, and 5.94 mm in the north, east and elevation directions. The equivalents of GPS with constraints algorithm are 2.76 mm, 2.84 mm and 5.48 mm, and of the GPS/Tilt algorithm are 2.71 mm, 2.64 mm and 4.12 mm, respectively. The two latter algorithms have some improvement in deviations, because the geometric constraints between the three antennas and the tilt-meter observation are used to compensate for the insufficient GPS observation.

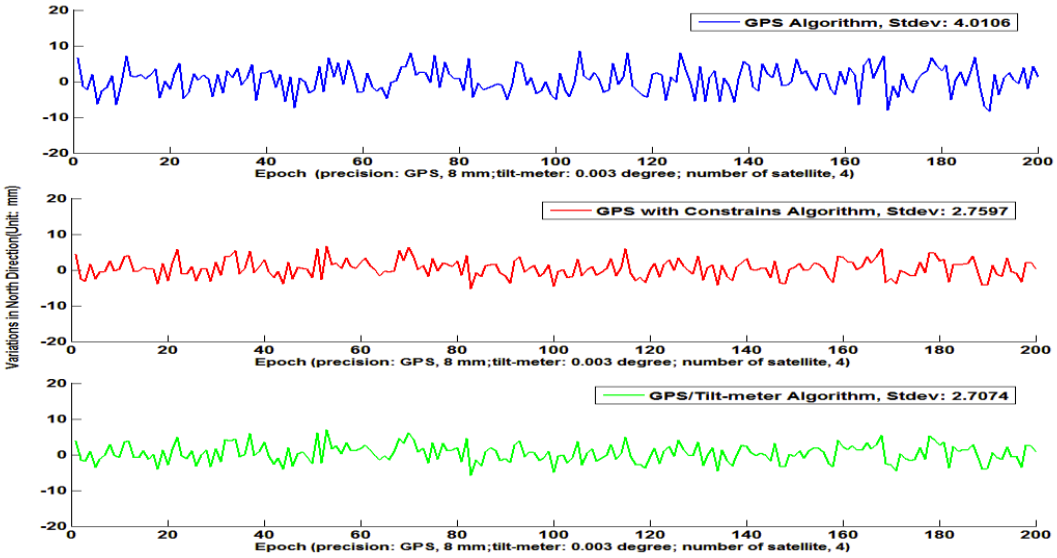

Fig. 3-5 Comparison of the algorithms in terms of the variation in the north direction (precision: GPS, 8 mm; tilt-meter, 0.003 degree; number of satellite, 4)

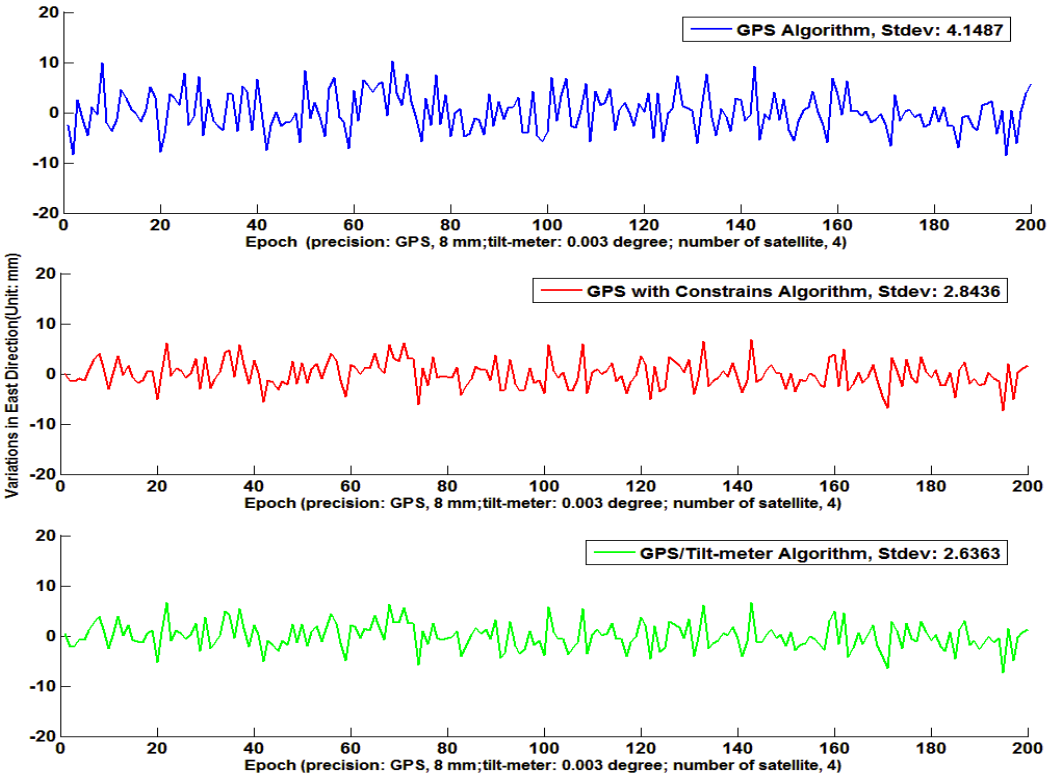

Fig. 3-6 Comparison of the algorithms in terms of the variation in the east direction (precision: GPS, 8 mm; tilt-meter, 0.003 degree; number of satellite, 4)

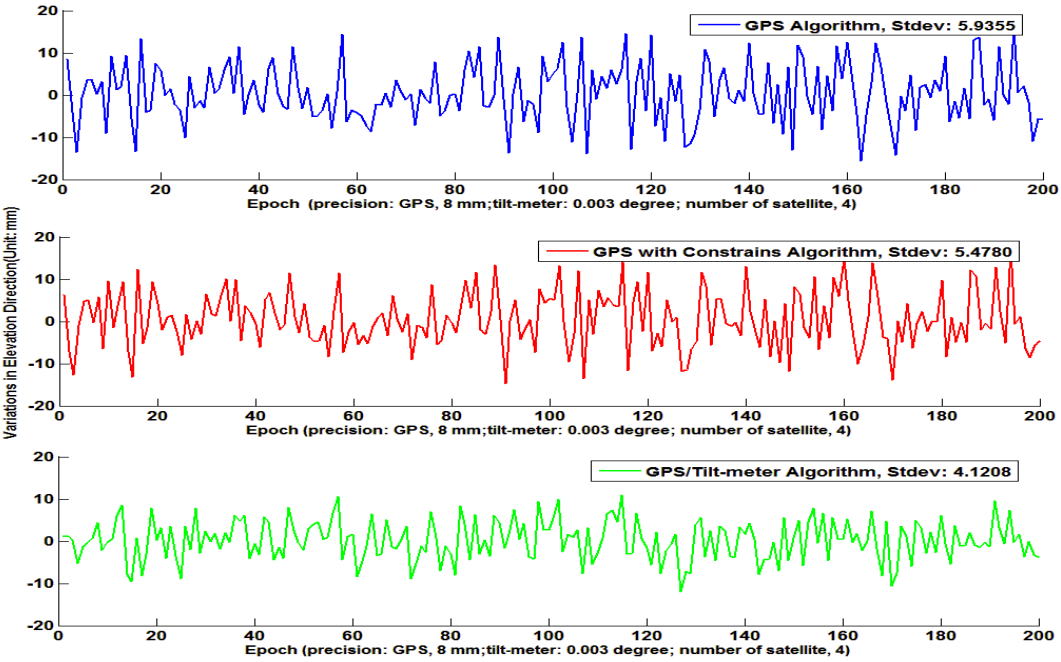

Fig. 3-7 Comparison of the algorithms in terms of the variation in the elevation direction (precision: GPS, 8 mm; tilt-meter, 0.003 degree; number of satellite, 4)

Figures 3-8, 3-9, 3-10 *compare the displacement sequences of the first 200 epochs of the three algorithms with 8 satellites, the GPS observation precision of 8 mm, and the tilt-meter accuracy of 0.003 degree. Clearly, as the number of satellites increases from 4 to 8, the standard deviations of the GPS algorithm results are decreased to 2.68 mm, 2.66 mm and 3.79 mm in the north, east and elevation directions, respectively. Similarly, the standard deviation values of the GPS with constraints algorithm results decrease to 1.78 mm, 1.84 mm and 3.77 mm, and to 1.78 mm, 1.83 mm and 3.23 mm for the GPS/Tilt algorithm, respectively.*

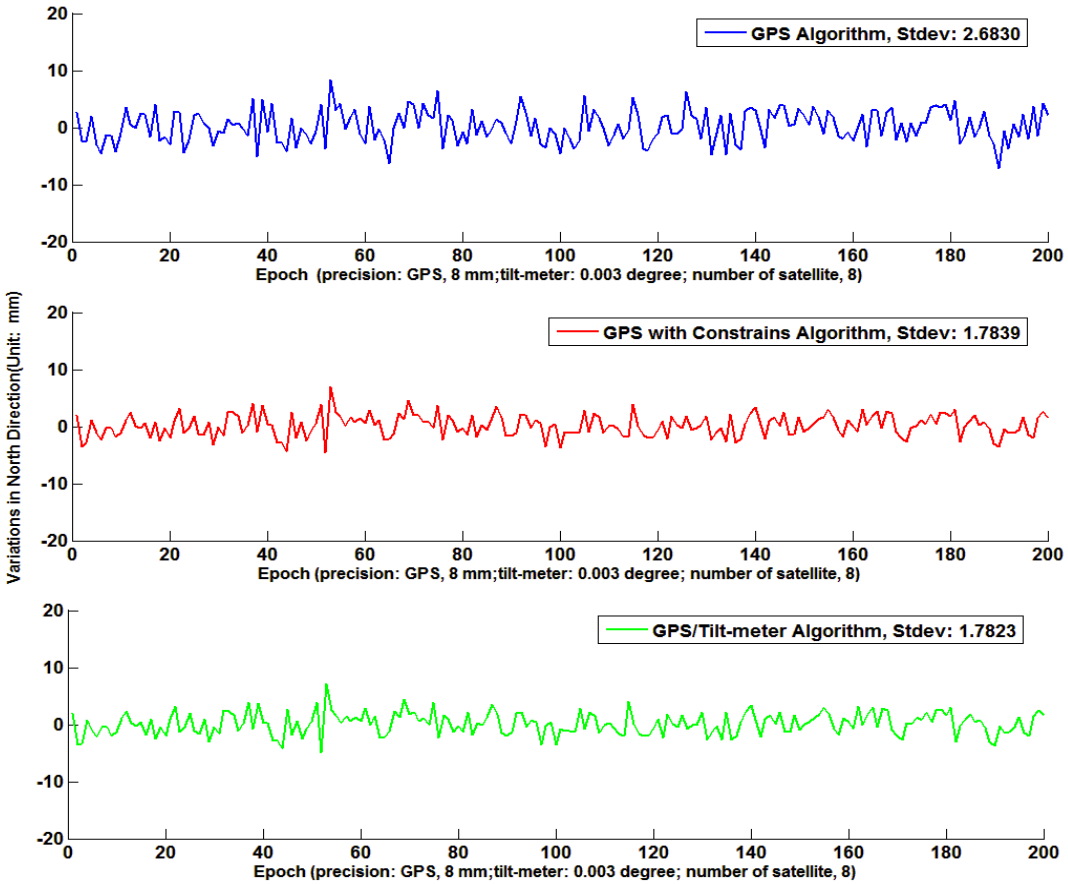

Fig. 3-8 Comparison of the algorithms in terms of the variation in the north direction (precision: GPS, 8mm, tilt-meter, 0.003 degree; number of Satellite, 8)

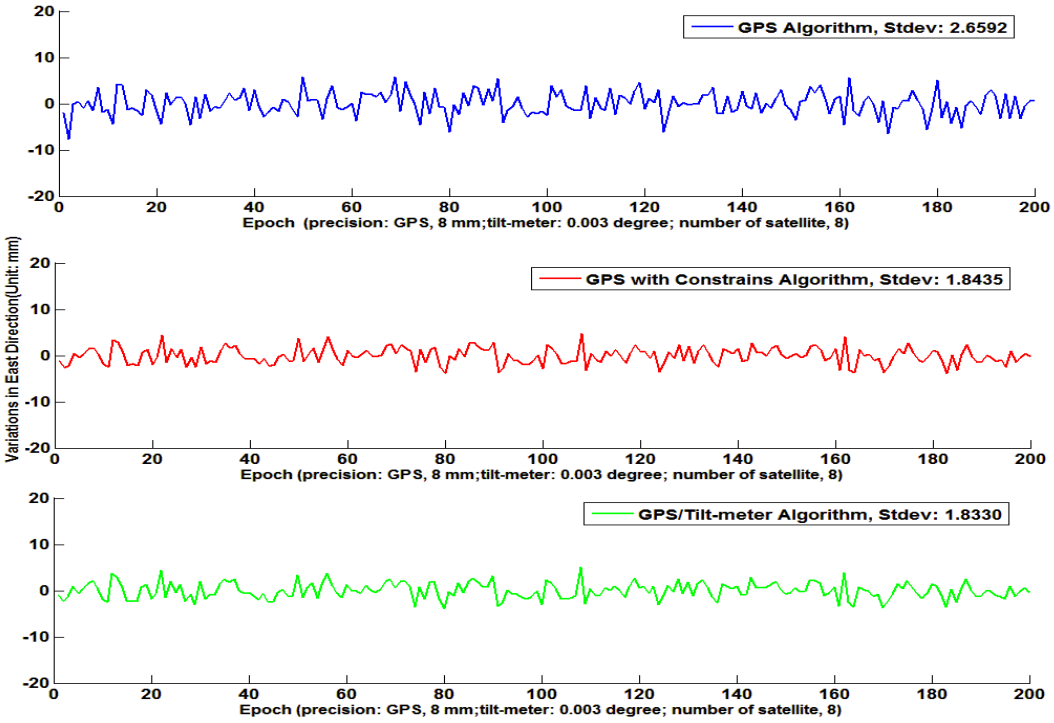

Fig. 3-9 Comparison of the algorithms in terms of the variation in the east direction (precision: GPS, 8 mm, tilt-meter, 0.003 degree; number of Satellite, 8)

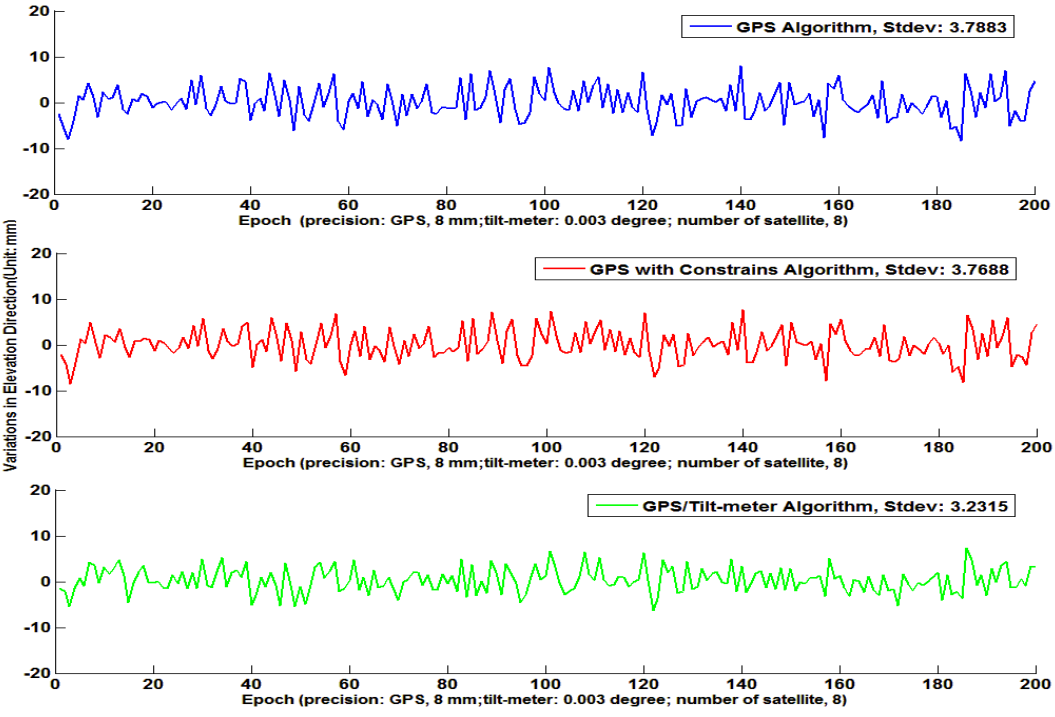

Fig. 3-10 Comparison of the algorithms in terms of the variation in the elevation direction (precision: GPS, 8 mm, tilt-meter, 0.003 degree; number of Satellite, 8)

3.3.3 Influence of GPS Data Accuracy on the Algorithms

Given the tilt-meter observation accuracy of 0.003 degree and 4 satellites, we calculated the results of the three algorithms when the precision of GPS observation changes. Analysing the displacement sequence of the results, we get the standard deviations shown in table 3-4.

Table 3-4. Standard deviations of the three algorithms with different GPS precisions. (unit: mm) (tilt-meter, 0.003 degree; number of satellite, 4; GPS, 5 to 15 mm)

GPS Accuracy (mm)	GPS Algorithm			GPS with Constrains			GPS/Tilt Algorithm		
	North	East	Elevation	North	East	Elevation	North	East	Elevation
5	2.5168	2.5431	3.7614	1.7219	1.7335	3.5760	1.7047	1.6544	3.5905
6	3.0281	3.1860	4.2744	2.0351	2.1175	3.9768	2.0361	2.0493	3.7235
8	4.0106	4.1487	5.9355	2.7597	2.8436	5.4780	2.7074	2.6363	4.1208
10	5.0358	5.0833	7.3752	3.4420	3.4030	6.8568	3.4250	3.2217	4.4660
15	7.6973	7.6729	10.7552	5.0916	5.1604	9.9704	5.0026	4.7489	5.5958

As table 3-4 shows, the accuracy of GPS measurements directly affects the result of the GPS algorithm. When the accuracy of GPS observation decreases from 5 mm to 15 mm, the deviations in the north, east, and elevation directions increase from 2.52 mm, 2.54 mm and 3.76 mm to 7.70 mm, 7.67 mm and 10.76 mm. Under the distance constraints, the result of GPS with constrains algorithm has some improvement in deviation. But this improvement is slight, because of the correlation between antennas A1, A2 and A3. The standard deviations of GPS/Tilt algorithm result have 35%, 38%, 48% improvement on the GPS algorithm in the north, east and elevation directions.

Figures 3-11, 3-12, 3-13 *compare the displacement sequences of the first 200 epochs of the three algorithms with 8 satellites. The GPS observation precision is set as 15 mm and the tilt-meter observation precision is set as 0.003 degree.*

Because of the low precision of satellite observation, the standard deviations of the GPS algorithm result are 7.70 mm, 7.67 mm and 10.76 mm in the north, east and elevation directions. But they are 5.09 mm, 5.16 mm and 9.97 mm for the GPS with constraints algorithm result and 5.00mm, 4.75 mm and 5.60 mm for the GPS/tilt-meter algorithm result because these two algorithms have the geometric constraints between three antennas and the tilt-meter observation data, which can compensate for of the insufficient GPS observation information.

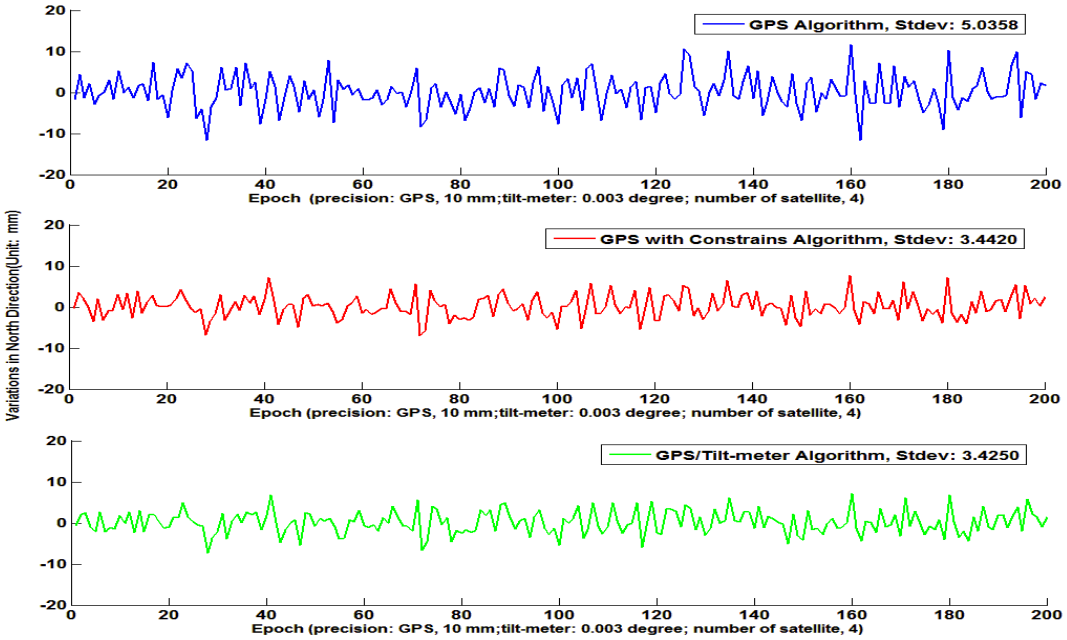

Fig. 3-11 Comparison of the algorithms in terms of the variation in the north direction (precision: GPS, 10 mm; tilt-meter, 0.003 degree; number of satellite, 4)

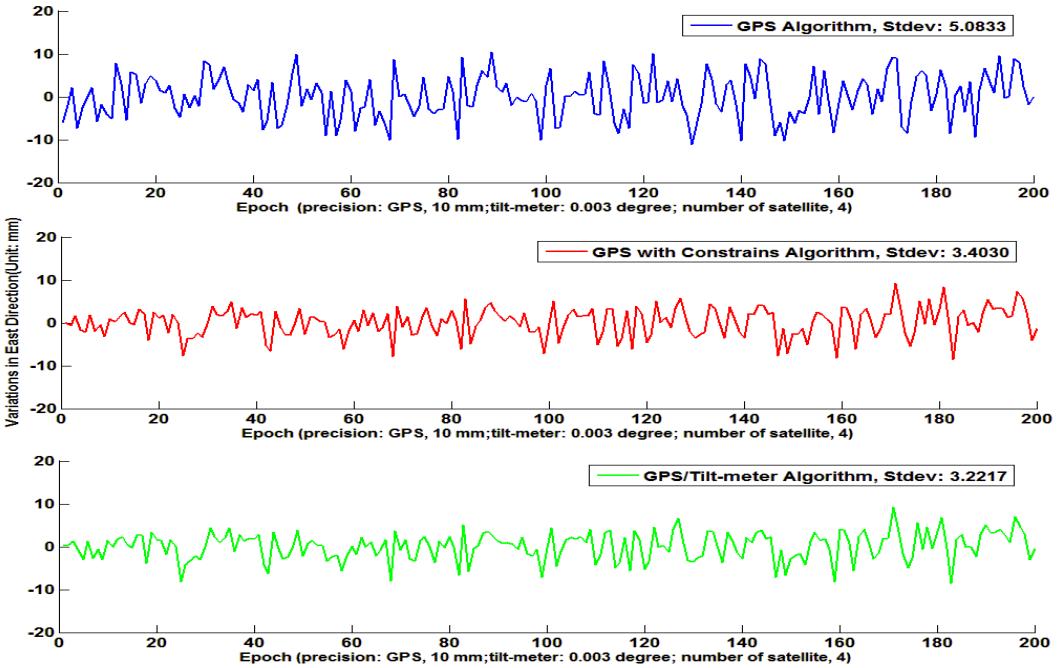

Fig. 3-12 Comparison of the algorithms in terms of the variation in the east direction (Precision: GPS, 10 mm; tilt-meter, 0.003 degree; number of satellite, 4)

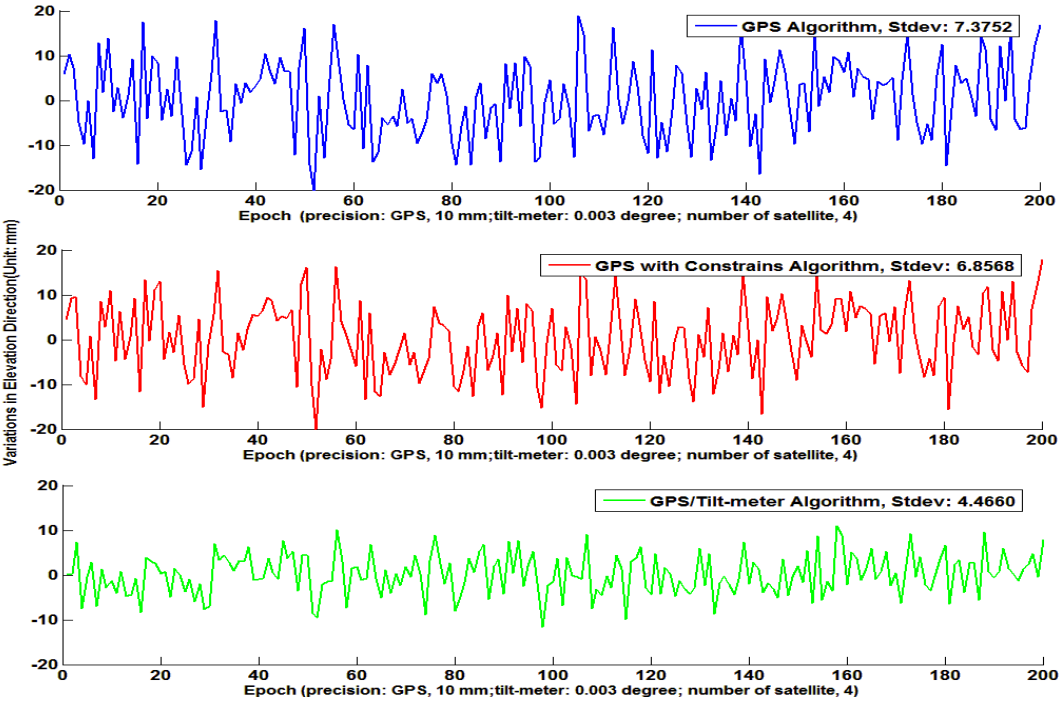

Fig. 3-13 Comparison of the algorithms in terms of the variation in the elevation direction (precision: GPS, 10 mm; tilt-meter, 0.003 degree; number of satellite, 4)

3.4 Case Study

We carried out a full week's observation with the integrated system, the F core, on the campus of the Polytechnic University. As figure 3-1 shows, the GPS system consists of four Novatel 615 receivers, among which three receivers are rover stations installed on the platform and the rest station is the reference station with a good sky view. A biaxial tilt-meter sensor (Rion HCA526T) was fixed on the centre of the platform. The data sampling rate was 1 Hz for both the GPS and the tilt-meter. The platform was kept stable during the experiment and the movement of the building (an 8-storey reinforced concrete building) was assumed to be insignificant. Comparison between the angles measured by the tilt-meter and those calculated from GPS observations shows that the tilt-meter measurements are much more accurate. Figure 3-14 shows one hour's results.

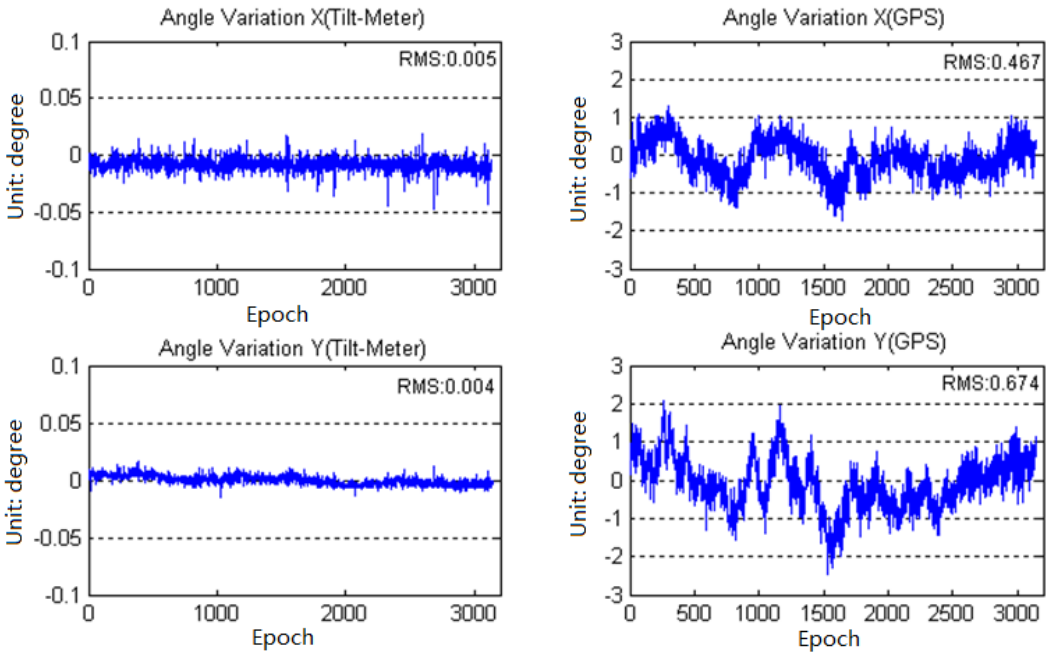

Fig. 3-14 Tilt angles from tilt-meter and GPS observations

The RMS values of the GPS measurements are 0.467 and 0.674 degrees on the X and Y axes, while those of the tilt-meter measurements are 0.005 and 0.004 degrees.

The distance variations calculated from the GPS observations are illustrated in Figure 3-15 where one-hour data was also used. The distance variation is within +10 mm.

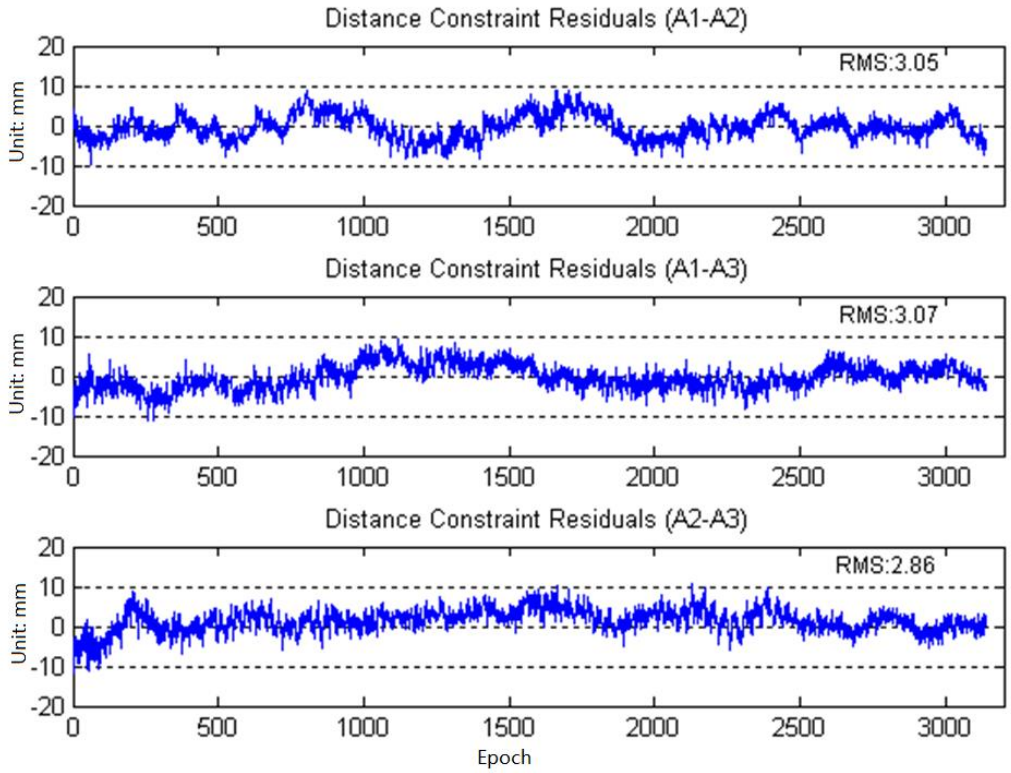

Fig. 3-15 Variations of distances calculated from GPS observations

Figures 3-16 and 3-17 compare the variations processed by GPS algorithm and by GPS/Tilt algorithm with two hours' observation. Clearly, the GPS/Tilt algorithm provides more accurate results.

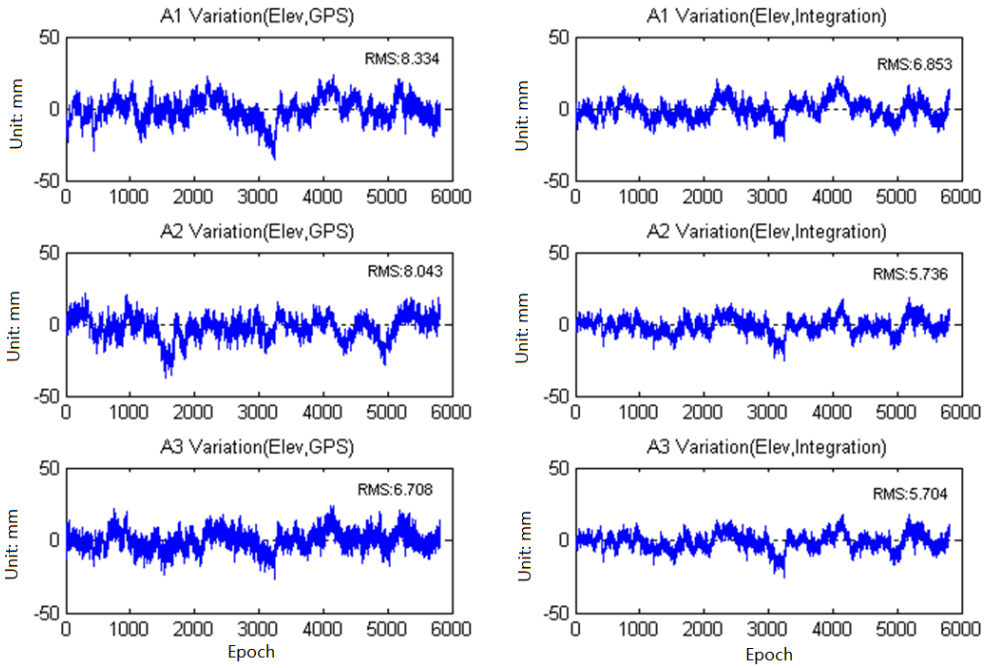

Fig. 3-16 Variations in the elevation direction obtained by GPS algorithm (left panels) and GPS/Tilt algorithm (right panels)

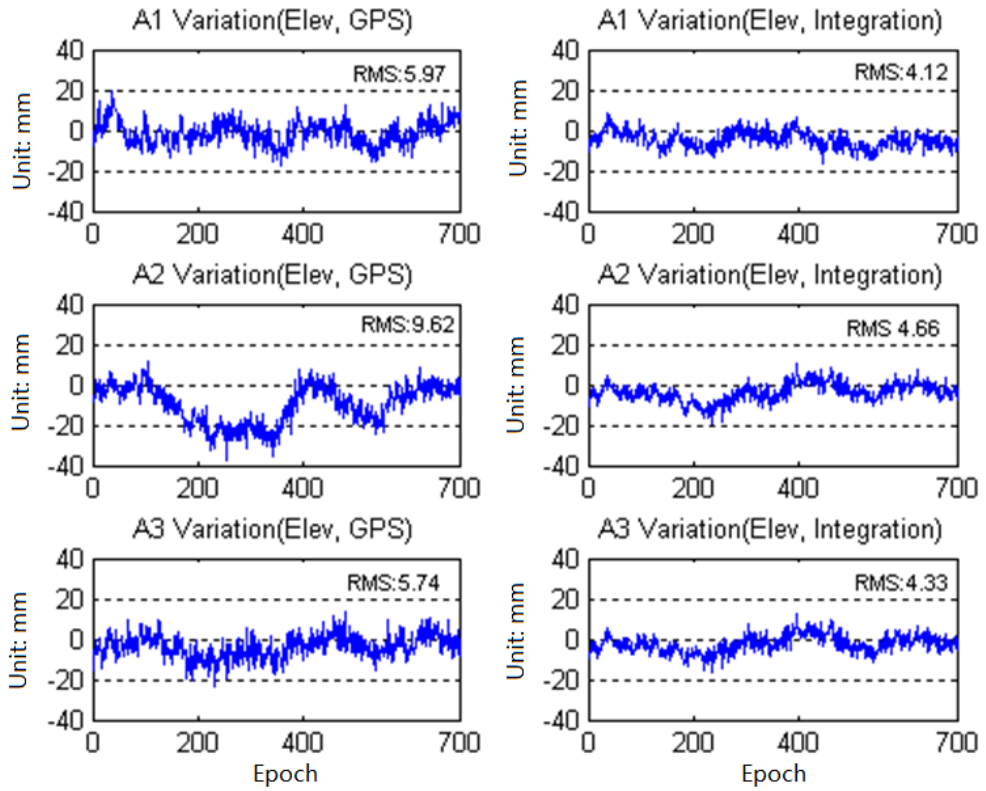

Fig. 3-17 Enlarged section of Fig. 3-16.

Table 3-5 shows the standard deviation based on the statistic results of the whole week, which shows the accuracy of the measurement was improved in all the three directions but especially in the elevation direction.

Table 3-5 Standard deviation of variations from GPS algorithm and from GPS/Tilt-meter algorithm

Point		North (mm)	East (mm)	Elevation (mm)
A1	GPS Algorithm	3.33	2.74	7.88
	GPS/Tilt-meter Algorithm	2.72	1.90	5.14
A2	GPS Algorithm	3.08	2.82	8.50
	GPS/Tilt-meter Algorithm	2.22	2.24	5.38
A3	GPS Algorithm	2.94	2.80	6.63
	GPS/Tilt-meter Algorithm	2.22	1.88	5.23

3.5 Discussions and Conclusions

This chapter studies an integrated structure monitoring system consisting of a multi-antenna GPS system and a dual-axial tilt-meter and presents the data processing model along with experimental results of the system. Two data fusion methods are given and several combination forms of multiple GPS antennas and tilt-meter are designed. We also analyse the influence of sensors with different accuracies on the algorithms. The experiments show that the GPS/Tilt algorithm can improve the accuracy by 37% over GPS algorithm when the GPS observation is abnormal (table 3-3).

CHAPTER 4 MULTI TILT-METER AND SINGLE GPS DATA FUSION

In the last chapter, we studied the methods of monitoring and data processing in a more severe multipath environment. In this chapter, we will study the environment monitoring technology of satellite being blocked seriously.

4.1 Principles of Data Fusion Method

*The accuracy of a GPS-derived position solution highly depends on the geometry of tracked satellites-receiver. However, when monitoring urban canyons, valley dams and deep open-cut mines, the number of visible satellites may not be sufficient to reliably determine the precise position (***Dai et al., 2001***).*

A tilt-meter is an instrument designed to measure very small horizontal tilts. With high precision, easy installation and environment adaptive ability, it has been used extensively in monitoring volcanoes, responses of dams to filling, small movements of potential landslides and responses of structures to various influences such as loading and foundation settlement. **Yigit et al.** *(***2008***) measured a tall building named RIXOS with a tilt-meter that experienced hurricane weather and compared the results with GPS results in both time and frequency domains. If a high-rise building does not keep its linear features under the wind loading, the displacements derived by the tilt-meter would be incorrect.*

*Pseudo-satellite, a kind of ground-based instrument transmitting GPS-like signals, can improve the "open air" signal availability for applications when the GPS signal is unavailable and geometry of visible satellites is not sufficient (***Lee**

et al., 2002). When the GPS signals are blocked, the pseudo-satellite system can significantly improve the accuracy, reliability, availability and integrity of the monitoring solution (**Choi, 2000**). However, utilizing pseudo-satellite brings some new problems, such as the near-far effect, multi-path effect, time synchronisation and elevation problems. Solving these problems is the premise to achieve high precision positioning.

In this chapter, tilt-meter and GPS sensors are combined based on the pseudo-satellite technology. The tilt angle is converted to virtual-satellite observations to improve satellite geometric structure and reduce the effect of multi-path error.

4.2 Observations Equations

4.2.1 Deformation Linearisation

Under external forces such as wind-loading, earthquake and temperature variation, buildings would deviate from their original positions with some inclined angles. As figure 4-1 shows, the displacement can be obtained from the inclined angle and deflection radius (**Yigit, 2008**). However, the relationship between the building height and displacement is complex and not completely linear. As shown in Figure 4-2, we installed a number of tilt-meters on different floors to obtain the displacement section by section. Equation 4-1 summed the displacement of each storey as a general offset d.

$$d = \sum_{i=1}^{n} h_i sin\alpha_i + \varepsilon_{inc} \qquad (4\text{-}1)$$

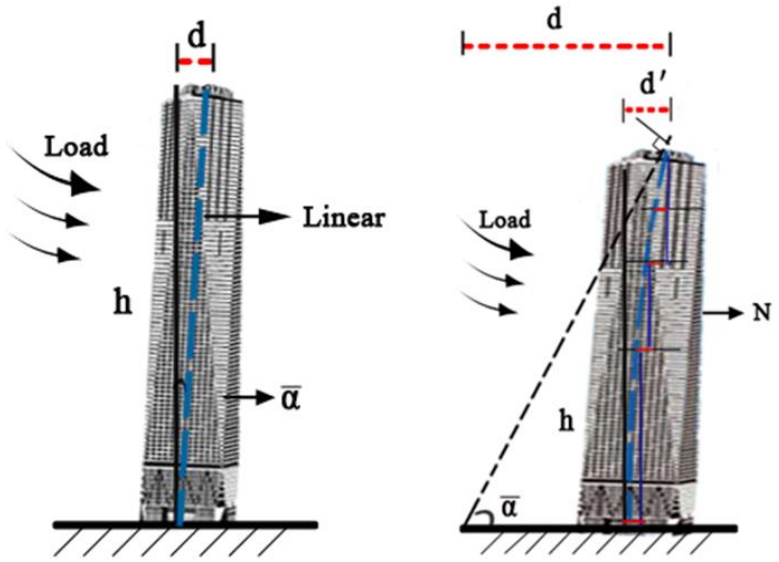

Fig. 4-1 Diagram of Linear displacement & tortuosity displacement (Yigit, 2008)

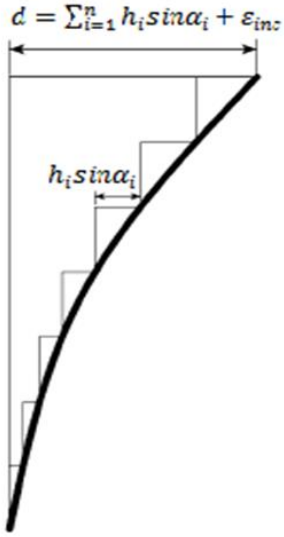

Fig. 4-2 Linear displacement in each section

4.2.2 Torsion Correction

*Building deformation usually occurs along with torsion and shift (***Llera et al., 1995***). Torsion makes the tilt-meter rotate a small angle and the axes will deviate from the original coordinate system. So it is necessary to correct the*

rotation angle by using a compass. Equation 4-2 shows the basic formula transition.

$$\alpha = cos(\chi)\,\alpha' + sin(\chi)\,\beta' \qquad (4\text{-}2)$$
$$\beta = -sin(\chi)\,\alpha' + cos(\chi)\,\beta'$$

χ is the measurement of the rotate angle, α is tilt in the north direction, β is tilt in east direction, α' and β' are the measurement of the tilt-meter.

4.2.3 Displacement Conversion

To unify GPS and tilt-meter observation, we installed a GPS antenna, a tilt-meter and an electronic compass on a platform. As figure 4-3 shows, the compass centre, the tilt-meter and the GPS antenna phase are on the same plumb line. The X- tilt direction is directed to the north and the Y-tilt direction is directed to the east. Making the compass point to the north direction and setting the initial measured value as 0, we measured the distance between the tilt-meter center and GPS antenna phase center and the GPS antenna height.

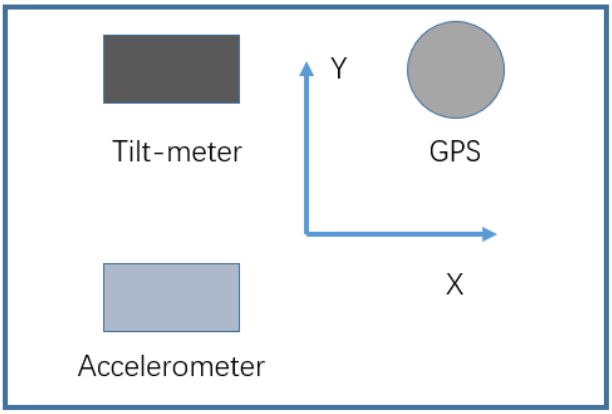

Fig. 4-3 Integration platform diagram

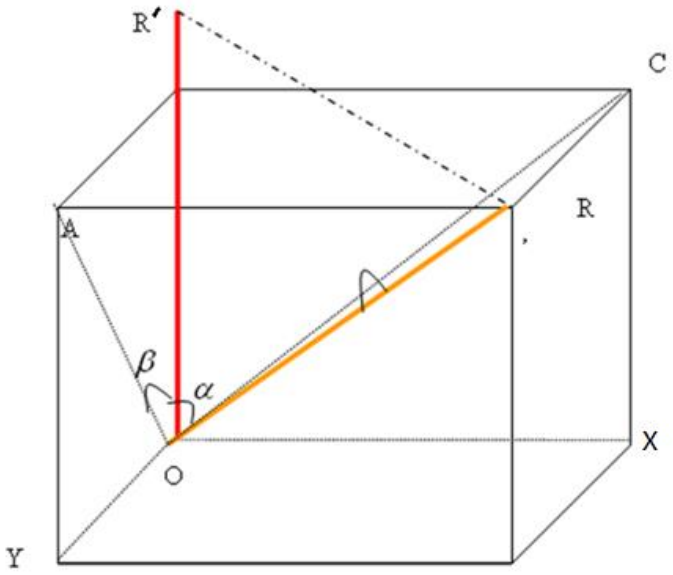

Fig. 4-4 Diagram of the conversion from tilt variation to displacement variation

As Figure 4-4 shows, axis X is in the north direction and Y is in the east direction. Point O is the supporting point when the device tilts. Assume point O is relatively stable. When deformation occurs, the point R moves to position R'. The tilt-meter can measure tilt angles in the X (north) and Y (east) directions. Since point O is stable and the distance between O and R is known, the movement can be calculated by tilt angle.

$$(OR')^2 = BC^2 + OB^2 + AB^2 = x^2 + y^2 + h^2$$

$$tan(\alpha) = \frac{BC}{OB} = x/h$$

$$tan(\beta) = \frac{BC}{OB} = y/h$$

As Figure 4-4 shows

(4-3-a)

$$dx = tan(\alpha)\, h - x_0$$

$$dy = tan(\beta)\, h - y_0 \qquad (4\text{-}3\text{-}b)$$

$$dh = \sqrt{\frac{OR^2}{1 + tan^2(\alpha) + tan^2(\beta)}} - z_0 \qquad (4\text{-}3\text{-}c)$$

where (dx, dy, dh) *is the displacement of point O' from O in the plane coordinate system and* (x_0, y_0, h_0) *is the coordinate of the stable point O.*

The observations in (4-3) are in the plane coordinate system which should be converted to WGS-84 Cartesian coordinate system. By (4-4), the NEU can be directly converted to the XYZ direction.

$$\bar{X} = \begin{bmatrix} \Delta X \\ \Delta Y \\ \Delta Z \end{bmatrix}_{Earth} = H_2 \begin{bmatrix} \Delta N \\ \Delta E \\ \Delta U \end{bmatrix}_{Site} \qquad (4\text{-}4)$$

where:

$$H_2 = \begin{bmatrix} -\sin B_0 \cos L_0 & -\sin L_0 & \cos B_0 \cos L_0 \\ -\sin B_0 \sin L_0 & \cos L_0 & \cos B_0 \sin L_0 \\ \cos B_0 & 0 & \sin B_0 \end{bmatrix}$$

where B_0 *and* L_0 *are the longitude and latitude of the measurement station. Thus, we can establish the GPS observation model and m tilt-meter observation models based on (2-8):*

$$\boldsymbol{L + e = EX} \qquad (4\text{-}5\text{-}a)$$

$$\boldsymbol{X} = \bar{\boldsymbol{X}} + \boldsymbol{\varepsilon} \qquad (4\text{-}5\text{-}b)$$

where $\boldsymbol{X} = [\boldsymbol{dx}, \boldsymbol{dy}, \boldsymbol{dz}]^{\boldsymbol{T}}$ *is the displacement of the observation point and* $\boldsymbol{e}$, $\boldsymbol{L}$ *and* $\boldsymbol{E}$ *have the same definition with those in (2-8). (4-5-b) is the tilt-meter equation and its observation values have been considered in the coordinate system of GPS.*

$$\bar{\boldsymbol{X}} = \left[\sum_{i=1}^{m} dx_i \quad \sum_{i=1}^{m} dy_i \quad \sum_{i=1}^{m} dh_i\right]^{\boldsymbol{T}} \qquad (4\text{-}5\text{-}c)$$

Establish the following adjustment criteria

$$min\{(\boldsymbol{L} - \boldsymbol{EX})^T \boldsymbol{P}_{GPS}(\boldsymbol{L} - \boldsymbol{EX}) + (\boldsymbol{X} - \bar{\boldsymbol{X}})^T \boldsymbol{P}_{\bar{\boldsymbol{X}}}(\boldsymbol{X} - \bar{\boldsymbol{X}}) \qquad (4\text{-}6)$$

where $\boldsymbol{P}_{\bar{\boldsymbol{X}}}$ *is the weight matrix of the observation equation of tilt-meter, which is set according to the importance of m tilt-meters in the displacement measurement. If these tilt-meter observations have the same importance, they will be given the same weight, i.e., set* $\boldsymbol{P}_{\bar{\boldsymbol{X}}}$ *as a unit matrix. The objective function is*

$$f(\boldsymbol{X}) = (\boldsymbol{L} - \boldsymbol{EX})^T \boldsymbol{P}_{GPS}(\boldsymbol{L} - \boldsymbol{EX}) + (\boldsymbol{X} - \bar{\boldsymbol{X}})^T \boldsymbol{P}_{\bar{\boldsymbol{X}}}(\boldsymbol{X} - \bar{\boldsymbol{X}})$$

Let

$$\frac{\partial f(\boldsymbol{X})}{\partial \boldsymbol{X}} = -2\boldsymbol{E}^T \boldsymbol{P}_{GPS}(\boldsymbol{L} - \boldsymbol{EX}) + 2\boldsymbol{P}_{\bar{\boldsymbol{X}}}(\boldsymbol{X} - \bar{\boldsymbol{X}}) = \boldsymbol{0}$$

we can get

$$\widehat{\boldsymbol{X}} = (\boldsymbol{E}^T \boldsymbol{P}_{GPS} \boldsymbol{E} + \boldsymbol{P}_{\overline{X}})^{-1} (\boldsymbol{E}^T \boldsymbol{P}_{GPS} \boldsymbol{L} + \boldsymbol{P}_{\overline{X}} \overline{\boldsymbol{X}}) \quad (4\text{-}7)$$

GPS observation and tilt-meter observation are usually considered with equal importance. In the actual deformation monitoring data analysis or prediction, we can add an adjustment coefficient $\boldsymbol{\alpha}$ *to the tilt-meter, which is similar to adding a weight coefficient* $\boldsymbol{\alpha}$ *to the adjustment criterion (4-6) to get a new adjustment criterion*

$$min\{(\boldsymbol{L} - \boldsymbol{EX})^T \boldsymbol{P}_{GPS} (\boldsymbol{L} - \boldsymbol{EX}) + \alpha (\boldsymbol{X} - \overline{\boldsymbol{X}})^T \boldsymbol{P}_{\overline{X}} (\boldsymbol{X} - \overline{\boldsymbol{X}})\} \quad (4\text{-}8)$$

The parameter vector value can also be estimated with (4-8).

where:

$$\widehat{\boldsymbol{X}} = (\boldsymbol{E}^T \boldsymbol{P}_{GPS} \boldsymbol{E} + \alpha \boldsymbol{P}_{\overline{X}})^{-1} (\boldsymbol{E} \boldsymbol{P}_{GPS} \boldsymbol{L} + \alpha \boldsymbol{P}_{\overline{X}} \overline{\boldsymbol{X}}) \quad (4\text{-}9)$$

According to (4-8) and (4-9), when $\boldsymbol{\alpha} = \boldsymbol{0}$*, only the GPS observation has contribution to the solution:*

$$\widehat{\boldsymbol{X}}_{GPS} = (\boldsymbol{E}^T \boldsymbol{P}_{GPS} \boldsymbol{E})^{-1} \boldsymbol{E} \boldsymbol{P}_{GPS} \boldsymbol{L} \quad (4\text{-}10)$$

Obviously, $\widehat{\boldsymbol{X}}$ *and* $\widehat{\boldsymbol{X}}_{GPS}$ *are unbiased estimates, and their covariance matrix are*

$$cov(\widehat{\boldsymbol{X}}_{GPS}) = \boldsymbol{\sigma}^{\boldsymbol{2}} (\boldsymbol{E}^T \boldsymbol{P}_{GPS} \boldsymbol{E})^{-1} \quad (4\text{-}11)$$

$$cov(\widehat{\boldsymbol{X}}) = \boldsymbol{\sigma}^{\boldsymbol{2}} (\boldsymbol{E}^T \boldsymbol{P}_{GPS} \boldsymbol{E} + k \boldsymbol{P}_{\overline{X}})^{-1} (\boldsymbol{E}^T \boldsymbol{P}_{GPS} \boldsymbol{E} + k^{\boldsymbol{2}} \boldsymbol{P}_{\overline{X}}) (\boldsymbol{E}^T \boldsymbol{P}_{GPS} \boldsymbol{E} + k \boldsymbol{P}_{\overline{X}})^{-1} \quad (4\text{-}12)$$

Based on the Gauss-Markov theorem, we get

$$cov(\widehat{\boldsymbol{X}}) < cov(\widehat{\boldsymbol{X}}_{GPS}) \tag{4-13}$$

This suggests that the estimates obtained based on the measurements of GPS and tilt-meter is better than that collected only by the measurement of GPS.

4.2.4 Selection of Adaptive Factors

Adding a weight coefficient $\boldsymbol{\alpha}$ *to (4-8) can adjust the weight of tilt-meter observation and balance the contribution of the GPS observation and tilt-meter observation to the fusion estimation. In practical monitoring, how to determine the adaptive factor needs further study, but it is related to the observation of GPS and tilt-meter. According to the Bayes estimation, when the accuracy of the observation and the corresponding weight matrix is high enough, the adaptive factor value should be 1. Below is a method to solve the adaptive factor.*

Assume $\boldsymbol{P_{GPS} = \sigma^2 \Sigma_e^{-1}}$*, let*

$$\Delta\widehat{\boldsymbol{X}} = \widehat{\boldsymbol{X}}_{GPS} - \overline{\boldsymbol{X}} \tag{4-14}$$

$$\left\|\Delta\widehat{\boldsymbol{X}}\right\| = \left(\Delta\widehat{\boldsymbol{X}}\right)^T \boldsymbol{P}_{\overline{\boldsymbol{X}}} \Delta\widehat{\boldsymbol{X}} \tag{4-15}$$

So we have

$$\sigma_{\overline{X}}^2 \approx \frac{\left(\Delta\widehat{\boldsymbol{X}}\right)^T \boldsymbol{P}_{\overline{\boldsymbol{X}}} \Delta\widehat{\boldsymbol{X}}}{m} \tag{4-16}$$

And

$$\left\| \frac{\Delta \widehat{\boldsymbol{X}}}{m\sigma^2} \right\| \approx \frac{\sigma_{\overline{\boldsymbol{X}}}^2}{\hat{\sigma}^2} \tag{4-17}$$

where m is the quantity of the tilt-meter. If $\left\| \frac{\Delta \widehat{\boldsymbol{X}}}{\boldsymbol{m\sigma^2}} \right\| > 1$, *we can get* $\boldsymbol{\sigma_{\overline{X}}^2 > \hat{\sigma}^2}$, *which means the effect of tilt-meter observation is too large and then its weight should be reduced. Assuming* $\boldsymbol{\sigma_{\overline{X}}^2 < \hat{\sigma}^2}$, *GPS observations contribute more to the solution.*

From the view of variance component estimation, $\sigma_{\overline{\boldsymbol{X}}}^2$ *should approach* $\hat{\sigma}^2$. *If the GPS observation equation is ill-conditioned, we make the tilt-meter observation equation to enable the GPS equation get stable solutions. Therefore, we have*

$$\frac{\left(\Delta \widehat{\boldsymbol{X}}\right)^T \boldsymbol{P}_{\overline{\boldsymbol{X}}} \Delta \widehat{\boldsymbol{X}}}{m} \leq \hat{\sigma}^2 \tag{4-18}$$

That means $\boldsymbol{\alpha} < 1$. *We can construct a method to calculate the adaptive factor* α.

$$\alpha = \begin{cases} 1, & \left\| \frac{\Delta \widehat{\boldsymbol{X}}}{m\sigma^2} \right\| \leq c \\ \frac{c}{\left\| \frac{\Delta \widehat{\boldsymbol{X}}}{m\sigma^2} \right\|}, & \left\| \frac{\Delta \widehat{\boldsymbol{X}}}{m\sigma^2} \right\| > c \end{cases} \tag{4-19}$$

where c is a constant with a value between 1.0 and 1.5.

4.3 Simulation Experiment

We designed the following simulation experiments to verify these algorithms. Simulation data is sampled by second for one hour. The satellite position is determined by the ephemeris directly. According to equation (3-17), the

simulated GPS observation is the distance between the satellite and the known ground point plus random errors, the error changes with experiments.

In the simulated tilt-meter observation, the tilt angle error changes with the experiment.

Three algorithms are designed for data processing.

Algorithm 1: calculate the solution by least squares with only GPS observations.

Algorithm 2: Estimate the parameter based on GPS and tilt-meter observations by (4-7)

Algorithm 3: Estimate the parameter based on GPS and tilt-meter observations by (4-9)

We designed three experiments based on the observation precision of the tilt-meter and GPS.

4.3.1 Impacts of Tilt-meter Precision on the Algorithms

Setting the GPS observation precision as 8 mm, we used all satellites to test the impact of tilt-meter observation precision on the algorithms. The results are shown in table 4-1. Both the GPS/tilt-meter algorithm and the adaptive fusion algorithm contain tilt-meter measurements, but the latter uses the adaptive adjustment factor to adjust the weights of GPS and tilt-meter observations.

Table 4-1. Standard deviations of the three algorithms with different accuracies. (unit: mm) (precision: GPS, 8 mm; tilt-meter, 0.001 degree; Tilt-meter, 0.001 to 0.015 degree)

Precision of Tilt-meter (degree)	GPS Algorithm			GPS/Tilt-meter Algorithm			Adaptive Fusion Algorithm		
	North	East	Up	North	East	Up	North	East	Up
0.001	2.60	2.60	3.64	0.87	0.82	0.76	0.78	0.74	0.69
0.002				1.34	1.31	1.32	1.24	1.21	1.22
0.003				1.64	1.62	1.69	1.56	1.54	1.60
0.005				1.98	1.97	2.24	1.93	1.93	2.18
0.010				2.32	2.32	3.07	2.35	2.34	3.09
0.015				2.58	2.51	3.51	2.51	2.64	3.37

Figures 4-5, 4-6 and 4-7 show the sequence diagrams of the three algorithms, when the GPS observation precision is 8 mm and the tilt-meter observation precision is 0.001 degree. Clearly, the accuracy of GPS/Tilt-meter algorithm is improved 66%, 68% and 79% in the three directions, compared with that of the GPS algorithm. The accuracy of adaptive fusion algorithm are improved about 71%, 70% and 79%.

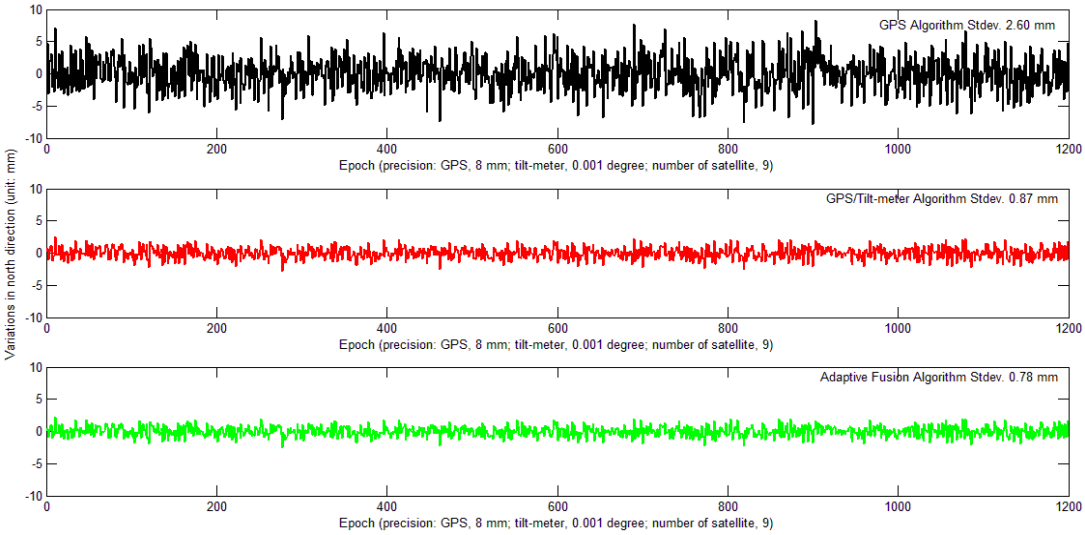

Fig.4-5 Comparison of the algorithms in terms of the variation in the north direction (precision: GPS, 8 mm; tilt-meter, 0.001 degree; number of satellite, 9)

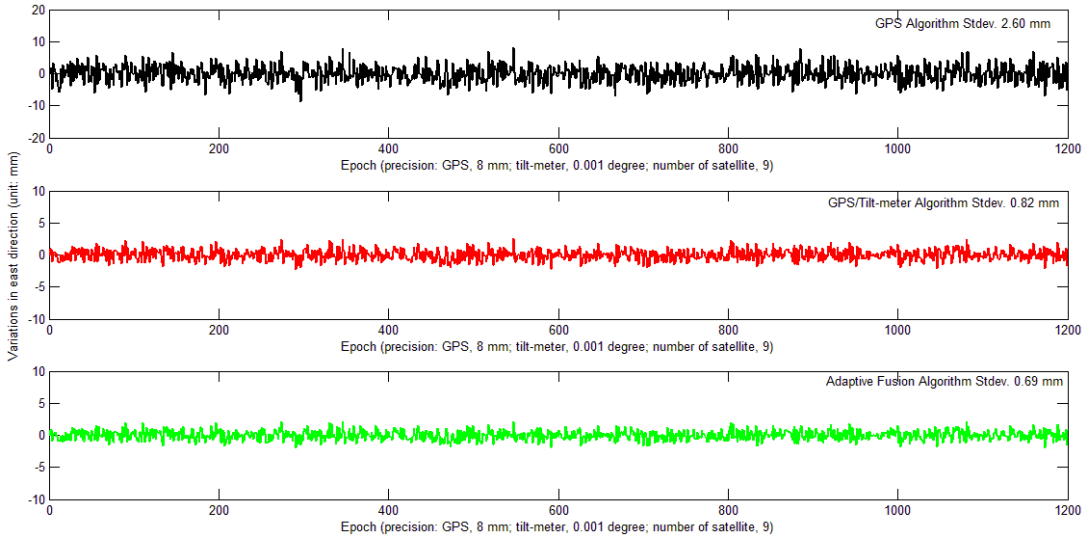

Fig. 4-6 Comparison of the algorithms in terms of the variation in the east direction (precision: GPS, 8 mm; tilt-meter, 0.001 degree; number of satellite, 9)

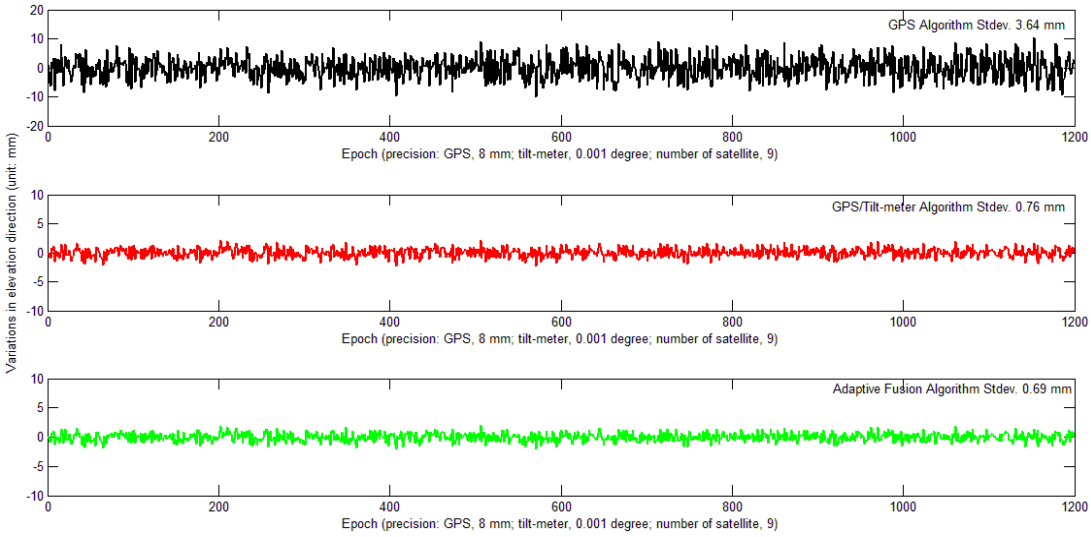

Fig. 4-7 Comparison of the algorithms in terms of the variation in the elevation direction (precision: GPS, 8 mm; tilt-meter, 0.001 degree; number of satellite, 9)

Figures 4-8, 4-9 and 4-10 are the sequence diagrams of the three algorithms, when the GPS precision is 8 mm and the tilt-meter accuracy is 0.01 degree. The standard deviation of GPS/Tilt-meter algorithm and the adaptive fusion algorithm in the three direction are close to that of the GPS algorithm.

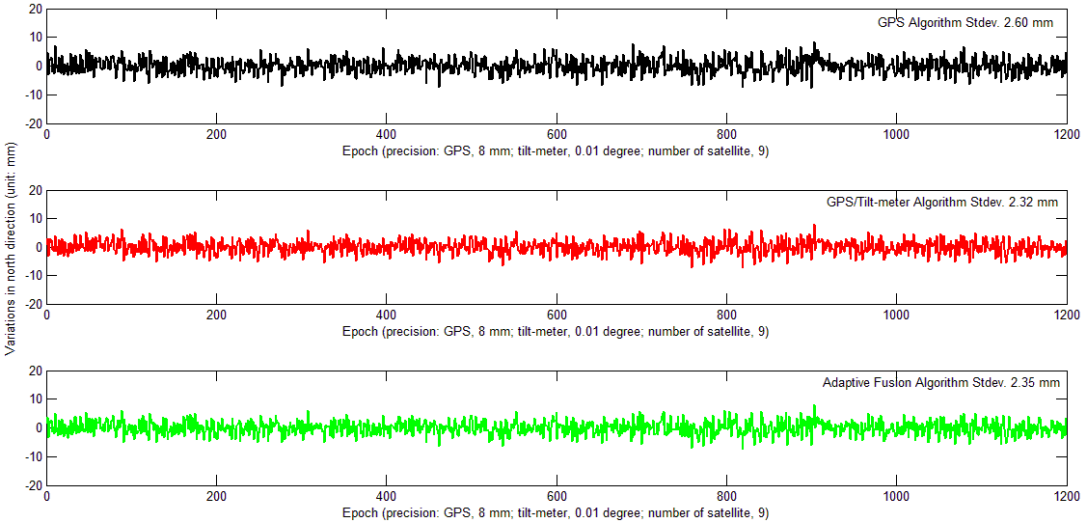

Fig. 4-8 Comparison of the algorithms in terms of the variation in the north direction (precision: GPS, 8 mm; tilt-meter, 0.01 degree; number of satellite, 9)

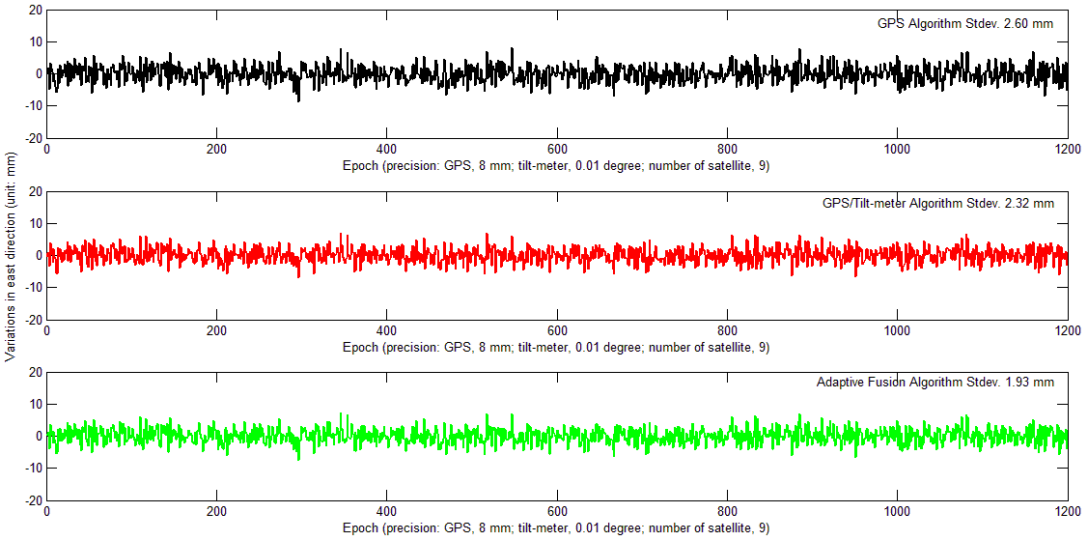

Fig. 4-9 Comparison of the algorithms in terms of the variation in the east direction (precision: GPS, 8 mm; tilt-meter, 0.01 degree; number of satellite, 9)

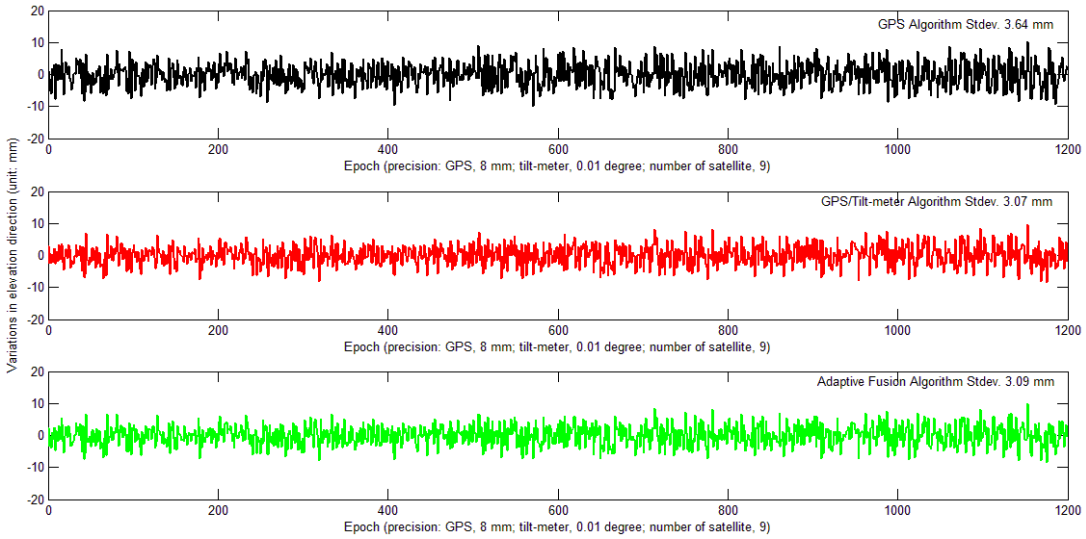

Fig. 4-10 Comparison of the algorithms in terms of the variation in the elevation direction (precision: GPS, 8 mm; tilt-meter, 0.01 degree; number of satellite, 9)

So the accuracies of GPS/Tilt-meter algorithm and the adaptive algorithm gradually increase when the tilt-meter accuracy is improved from 0.015 degree to 0.001degree and they increase significantly when the observation precision of the tilt-meter reaches 0.003 degrees. But if the observation accuracy is lower than GPS, the GPS/Tilt algorithm and adaptive fusion algorithm will not work.

4.3.2 Influence of Number of Satellite on Algorithm

To test the number of visible satellites influence on the algorithms, we set the GPS observation precision as 5 mm, and the tilt-meter observation accuracy as 0.003 degree. As shown in table 4-2, the standard deviations of GPS algorithm result in the elevation direction is improved from 4.40 mm to 2.33 mm when the number of satellites increases from 4 to 9. The standard deviation of the GPS/Tilt-meter algorithm result and the adaptive fusion algorithm result have significantly improvement on that of the GPS algorithm.

Table 4-2. Standard deviations of the three algorithms with different visible satellite number. (unit: mm) (precision: tilt-meter, 0.01 degree; GPS, 8 mm; number of satellites, 4 to 9)

Number of Visible Satellite	GPS Algorithm			GPS/Tilt Algorithm			Adaptive Algorithm		
	North	East	Elevation	North	East	Elevation	North	East	Elevation
4	3.21	3.11	4.40	1.49	1.46	1.55	1.49	1.47	1.55
5	2.53	2.53	3.62	1.41	1.40	1.52	1.42	1.41	1.53
6	2.31	2.05	2.85	1.36	1.28	1.44	1.37	1.29	1.45
7	1.94	1.81	2.60	1.29	1.23	1.45	1.30	1.24	1.45
8	1.83	1.65	2.43	1.23	1.18	1.42	1.24	1.19	1.42
9	1.63	1.59	2.33	1.20	1.14	1.40	1.21	1.16	1.41

As figures 4-11, 4-12 and 4-13 show, the standard deviations of the GPS algorithm result are 3.21 mm in the north, 3.11 mm in the east and 4.4 mm in the elevation when only 4 satellites are available. As the GPS/Tilt-meter algorithm and the adaptive fusion algorithm consider extra observations, the standard deviations are improved by 54%, 53%, 65% and 51%, 52%, 67%, respectively.

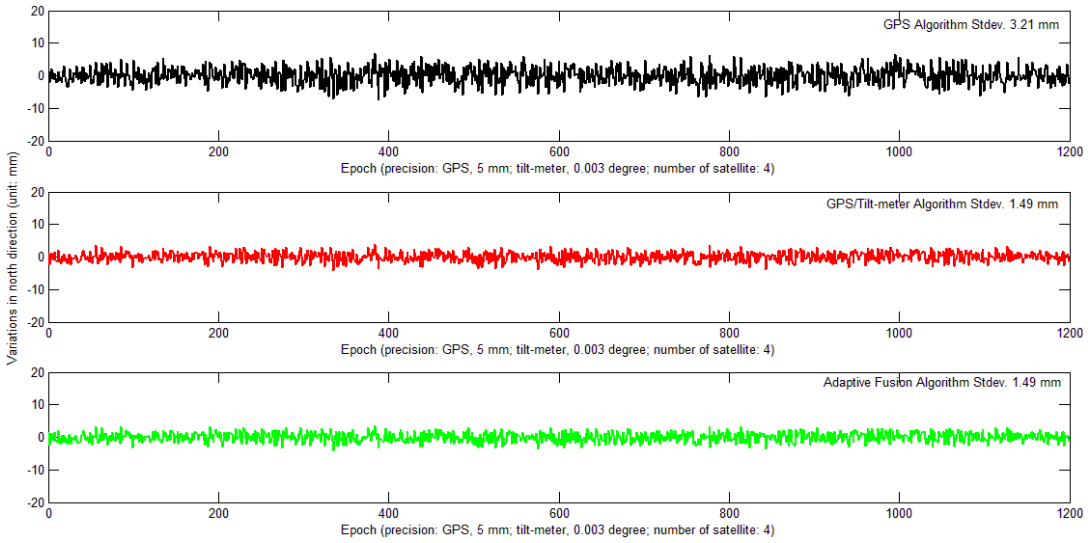

Fig. 4-11 Comparison of the algorithms in terms of the variation in the north direction (precision: GPS, 5 mm; tilt-meter, 0.003 degree; number of satellite: 4)

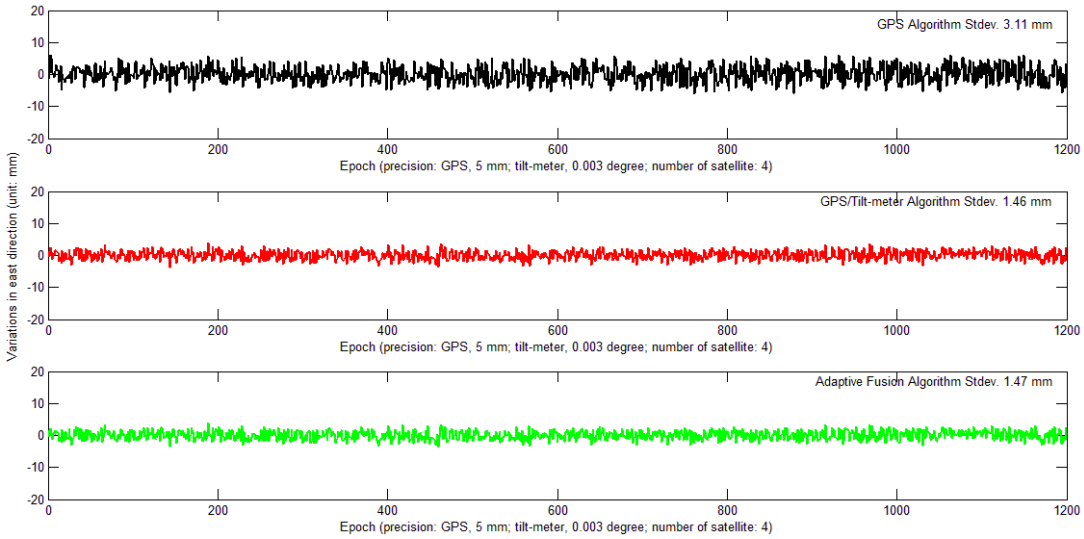

Fig. 4-12 Comparison of the algorithms in terms of the variation in the east direction (precision: GPS, 5 mm; tilt-meter, 0.003 degree; number of satellite: 4)

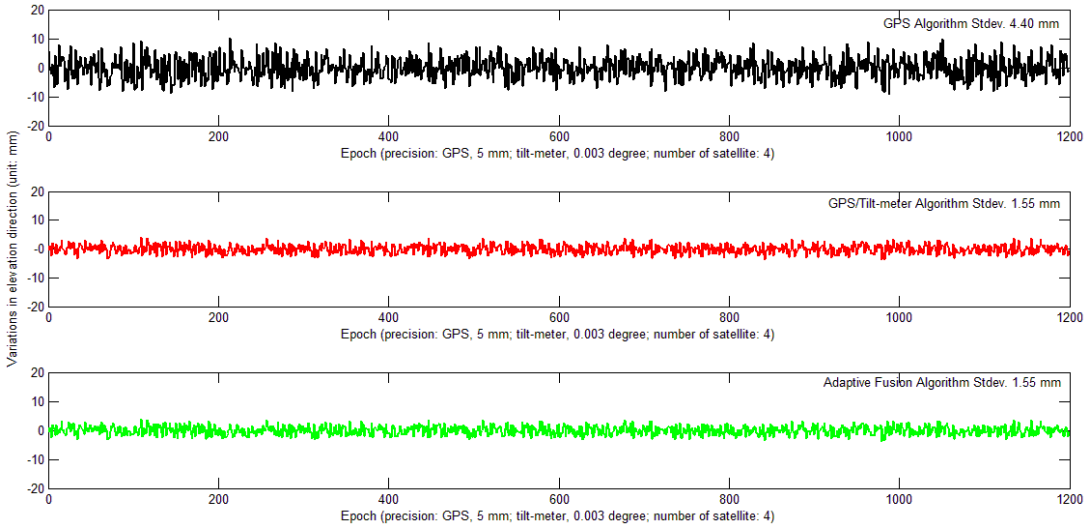

Fig. 4-13 Comparison of the algorithms in terms of the variation in the elevation direction (precision: GPS, 5 mm; tilt-meter, 0.003 degree; number of satellite: 4)

As figures 4-14, 4-15 and 4-16 show when 9 GPS visible satellites are available, the standard deviations of the GPS algorithm result are increased to 1.61 mm, 1.59 mm and 2.33 mm in the three directions. And the accuracy is improved by 26%, 28%, 39% in the GPS/Tilt-meter algorithm and by 14%, 23%, 48% in the adaptive fusion algorithm.

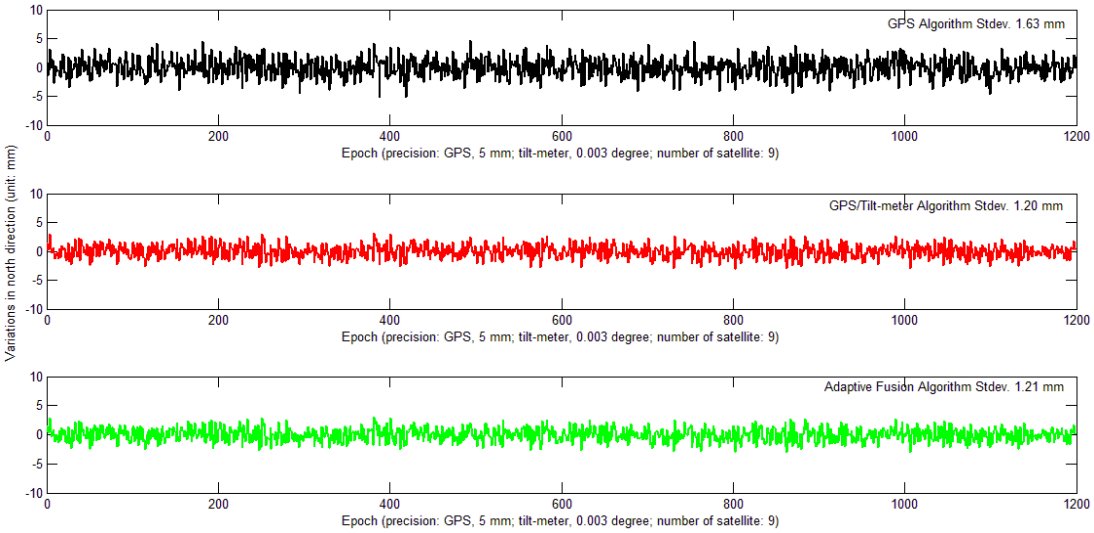

Fig. 4-14 Comparison of the algorithms in terms of the variation in the north direction (precision: GPS, 5 mm; tilt-meter, 0.003 degree; number of satellite: 9)

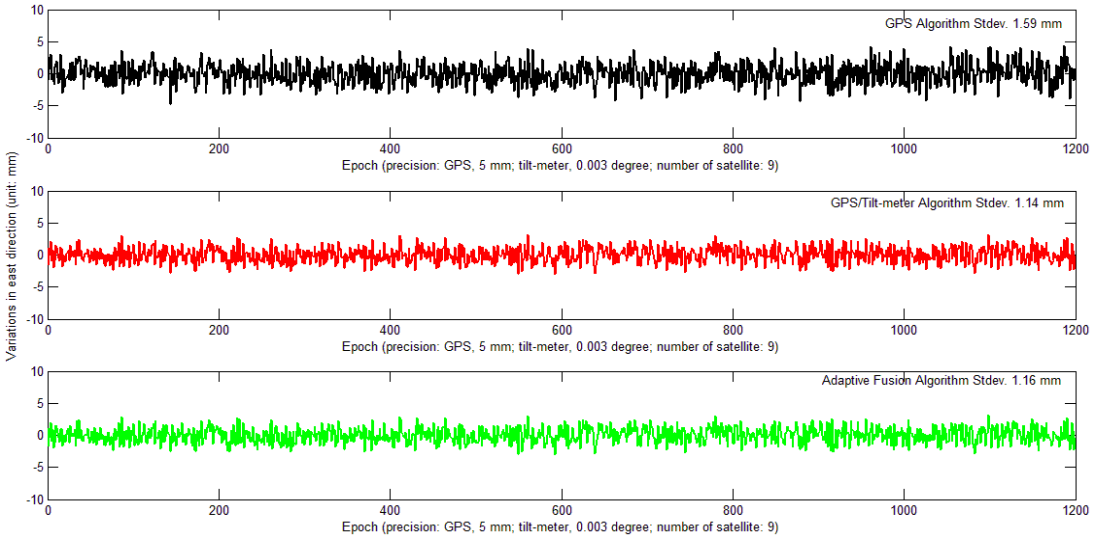

Fig. 4-15 Comparison of the algorithms in terms of the variation in the east direction (precision: GPS, 5 mm; tilt-meter, 0.003 degree; number of satellite: 9)

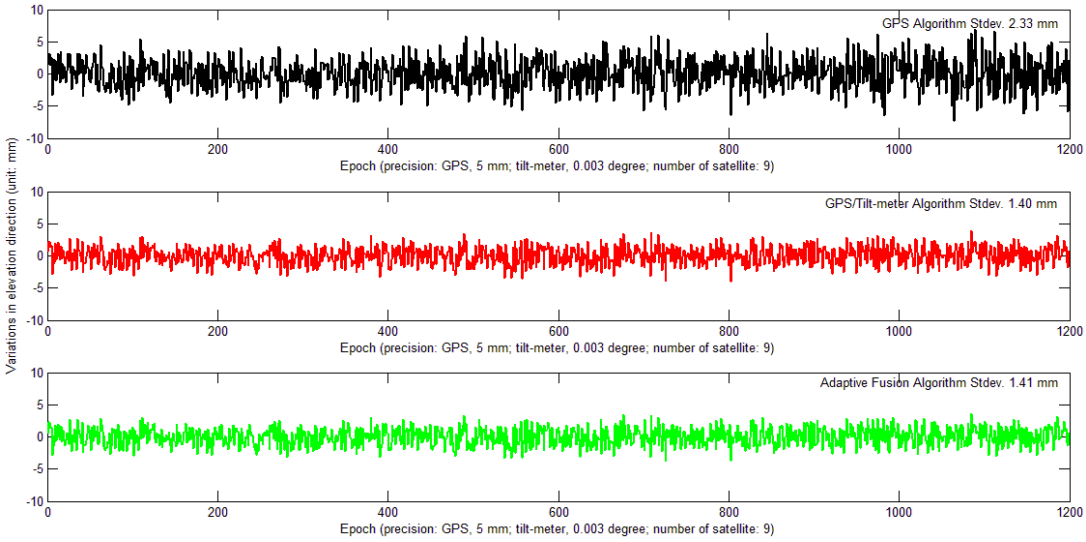

Fig. 4-16 Comparison of the algorithms in terms of the variation in the elevation direction (precision: GPS, 5 mm; tilt-meter, 0.003 degree; number of satellite: 9)

So, if available GPS observation satellites are not enough, considering extra observations can effectively improve the algorithm effect and the monitoring system precision.

4.4 Case Study

To verify the effectiveness of the algorithm, an experiment was done on the campus of the Hong Kong Polytechnic University. As Figure 4-17 shows, GPS and tilt-meter were installed on the roof of Z core building. In this study, the GPS system consists of two Novatel 615 receivers. One was the rover station installed on the platform of the sixth floor, and the other was the reference station installed on a pillar at the top of building with a good sky view. A biaxial tilt-meter sensor (RION HCA 526T), one GPS antenna of rover station and one 360-degree prism were fixed on a tripod. The length of one leg of the tripod can be adjusted to make a tilt angle and make GPS antenna shifted. A robotic total

station (model: TS15) was used to measure the displacement when the tripod tilts at an angle. Its measurements are treated as the true value to evaluate the accuracy of this algorithm. Reference stations are installed beside the integrated device.

Fig. 4-17 Experiment instrument platform

The tilt-meter and GPS measurements were collected with a sampling rate of one second for 2 hours. Then the measurements were processed by (4-7) and (4-9) and the results are shown in Figures 4-18, 4-19 and 4-20. The GPS algorithm, the GPS/Tilt-meter algorithm and the adaptive fusion algorithm are able to track any movement in time. The adaptive fusion algorithm can automatically adjust the weight of two observations and make full use of the tilt-meter to correct abnormal observations of GPS, so its efficiency is significantly improvement on

that of the GPS algorithm. The precision of the GPS/Tilt-meter algorithm in the three directions have been improved obviously with adaptive factors, which is 46.4%(5.6 mm to 3.0 mm) in the north direction, 29.4%(1.7 mm to 1.2 mm) in the east direction and 27.3%(2.2 mm to 1.6 mm) in the elevation.

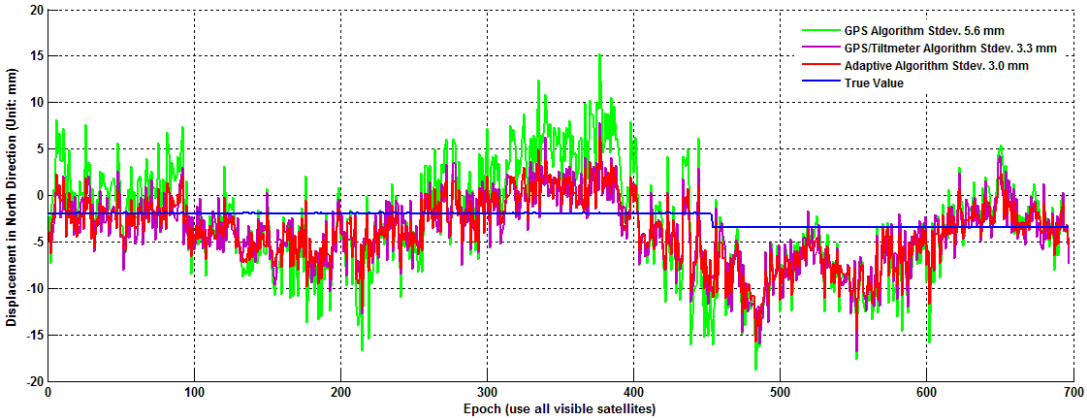

Fig. 4-18 Comparison of the algorithms in terms of the movement in the north direction (Use all the visible satellites)

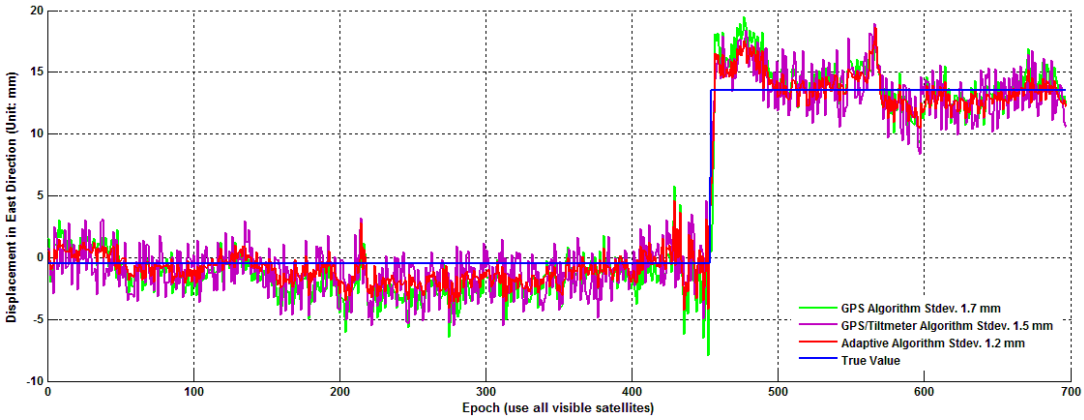

Fig. 4-19 Comparison of the algorithms in terms of the movement in the east direction (Use all the visible satellites)

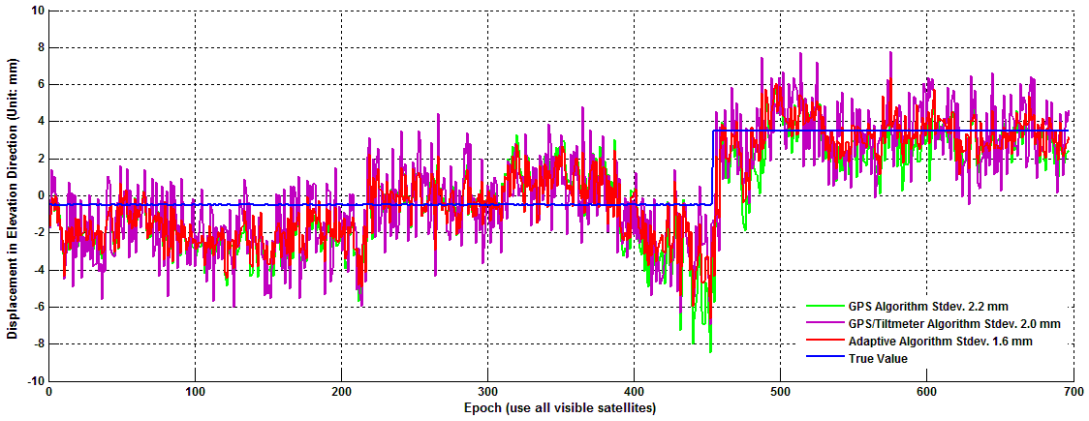

Fig. 4-20 Comparison of the algorithms in terms of the movement in the elevation direction (Use all the visible satellites)

In fact, when GPS technology is used to monitor building deformations, satellite signals are often blocked by surrounding structures. Figure 4-21-a *shows 9 satellites can be observed in the sky and figure* 4-21-b *shows that only 4 satellites are observed when half of the sky view is blocked.*

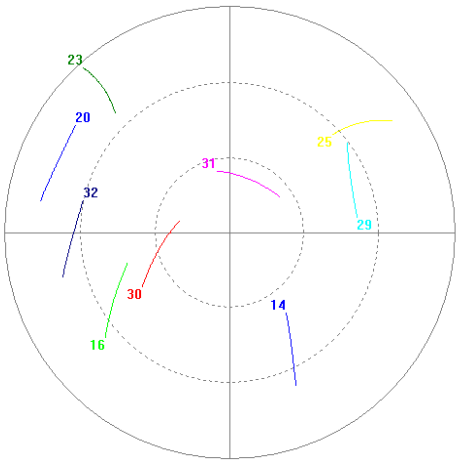

Fig. 4-21-a Sky view of satellites

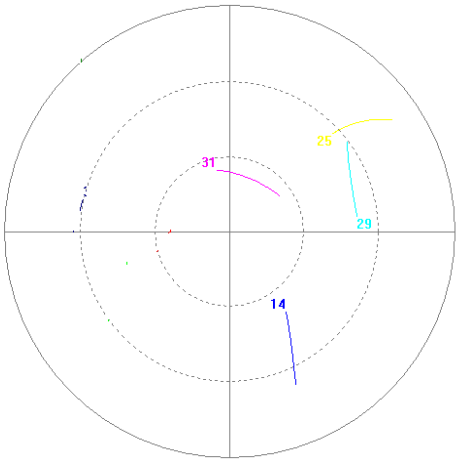

Fig. 4-21-b Satellites observed after mask

In order to compare the effectiveness of the virtual observation satellites, this study masked some satellites between the 90th to 240th epochs and only kept 4

satellites with the highest elevation angle to simulate the satellite occlusion in the urban environment with high buildings.

The results are shown in table 4-3, figures 4-22, 4-23 and 4-24. Since the satellites geometry structure became weak, the standard deviation increases from 5.6 mm to 16.9 mm in the north direction, from 1.7 mm to 3.0 mm in the east direction and from 2.2 mm to 2.7 mm in elevation direction. The standard deviation with adaptive factors improved by 83%, 36% and 51% in the north, east and elevation directions, respectively. This means the algorithm is significantly improved even with abnormal GPS observations.

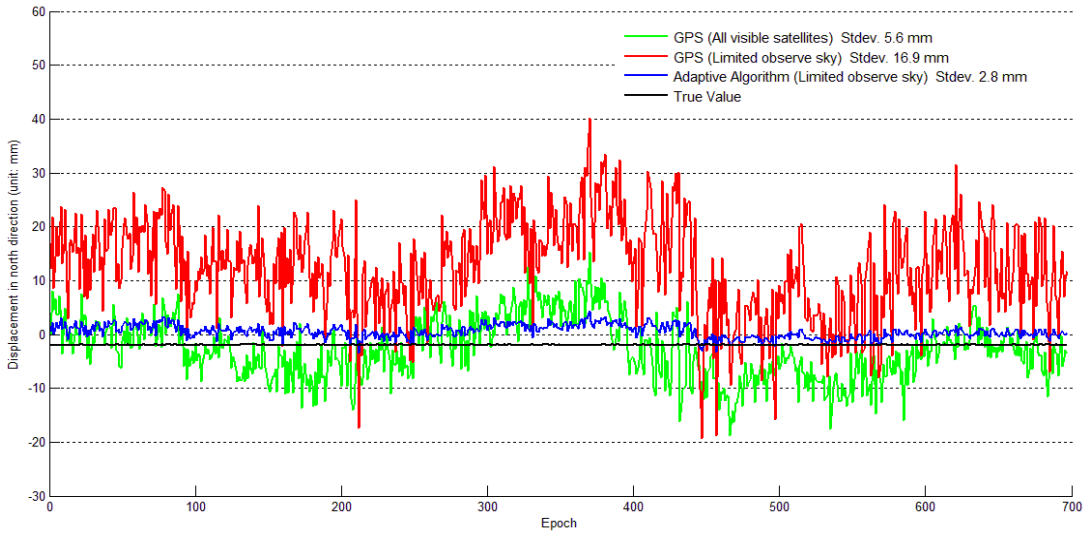

Fig. 4-22 Comparison of the algorithms in terms of the variation in the north direction

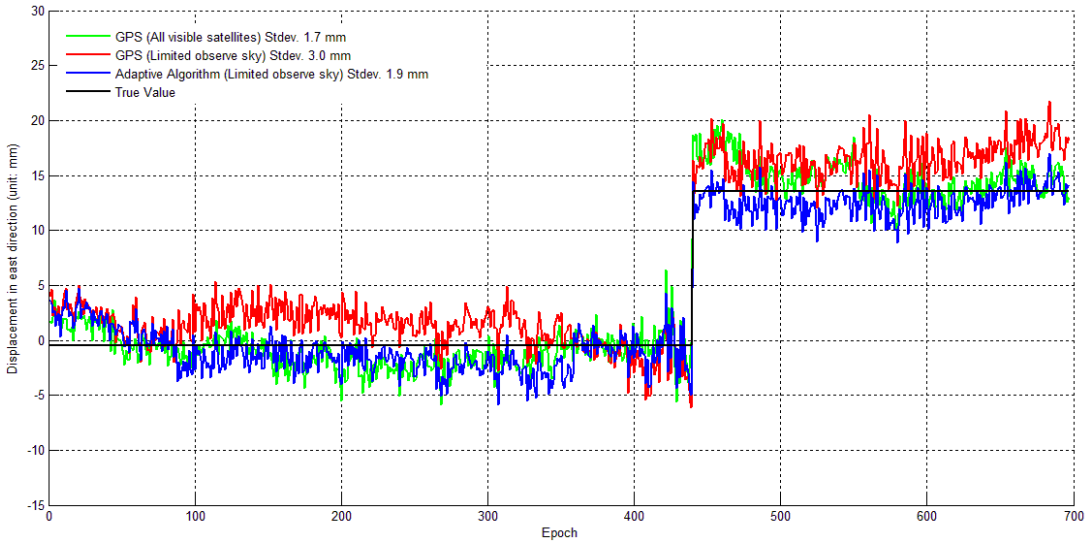

Fig. 4-23 Comparison of the algorithms in terms of the variation in the east direction

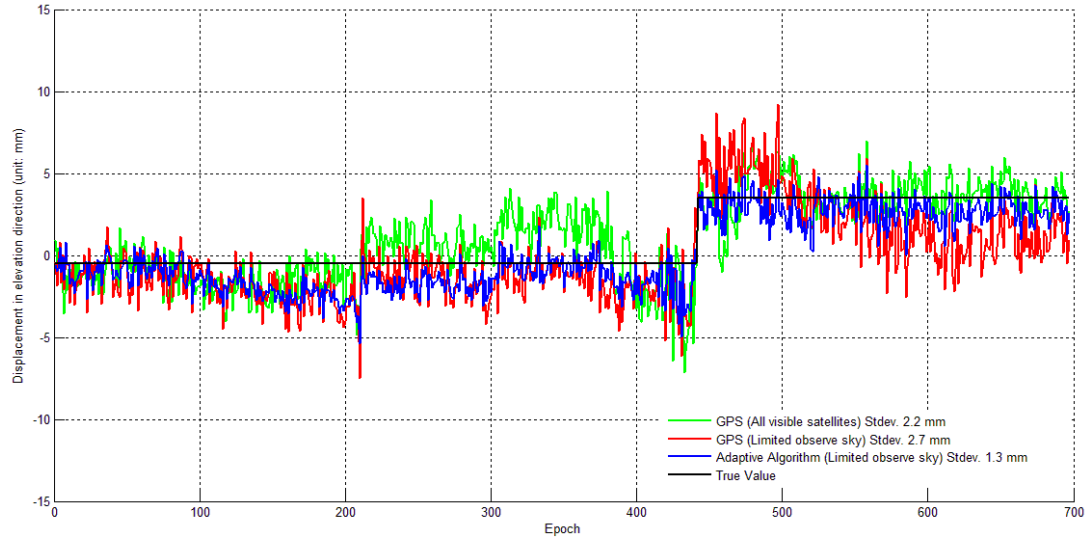

Fig. 4-24 Comparison of the algorithms in terms of the variation in the elevation direction

Table 4-3 Standard deviation of variations from GPS/Tilt algorithm and from adaptive algorithm

	Accuracy Improve on Algorithm (Standard Deviation, Unit: mm)								
	GPS Algorithm			GPS/Tilt Algorithm			Adaptive Algorithm		
	North	East	Elevation	North	East	Elevation	North	East	Elevation
Use all the visible satellites	5.6	1.7	2.2	3.3	1.5	2	3	1.2	1.6
Limited observe sky	16.9	3	2.7	3.5	2.2	2.6	2.8	1.9	1.3

4.5 Discussions and Conclusions

This chapter constructs several least squares algorithms with constraint, and proposes to use an adaptive factor to adjust the contribution of the GPS observation and tilt-meter observation to the parameter estimation. In the case study, by the adaptive fusion algorithm, the RMS was improved by 84%, 37.4% and 35.9% in the north, east and elevation directions, respectively, when the GPS observation is abnormal. This is because the adaptive fusion algorithm can improve the system reliability. When GPS observation is abnormal, reduce the weight of the GPS observation and improve the weight of the tilt-meter and reduce the influence of outliers on the estimation results.

CHAPTER 5 MULTI SENSOR DATA FUSION METHOD

In the third chapter and the fourth chapter, we study the different circumstances of the SHM monitoring technology and data processing methods, these methods are generally only suitable for static monitoring of the situation, but they are not suitable for monitoring high dynamic structures, such as building vibration under the hurricane. In this chapter, we study the fusion of GPS, tilt-meter and accelerometer in the dynamic observation model. We establish the observation equation of the accelerometer and integrate the displacement obtained by the tilt-meter into the filter model with stochastic constraints, which provides a new method of data fusion for SHM.

5.1 Multi Sensor Data Fusion

*SHM uses sensors to detect the situation of structure's important parts or components. With the development of GPS receiver technology, especially the improvement of GPS satellite signal solution accuracy and the emerge of ambiguity solution, the real-time, high dynamic and precision displacement measurement can be achieved, which makes the real-time safety monitoring of large structures feasible. The accelerometer can obtain the structure acceleration under the vibration caused by external loads and its sampling rate can be as high as 1000Hz (**Roberts, 2004**). It is very light (0.5 g) and compact*

(diameter 5 mm), so it can be installed at many locations of a structure and has little effect on the properties of the vibrating system.

Combining GPS surveying with tilt-meters and accelerometers is a way to reduce multi-path errors and increase the positioning accuracy. As GPS and accelerometer can compensate for each other, integrating GPS measurements with accelerometer measurements can enhance the accuracy of the total displacement response (static plus dynamic) of a structure (*Chan et al., 2006***). However, available GPS-Accelerometer integration models are very simple. Some of them only add acceleration components to the equation of state, without giving the observation equation of the acceleration. Some do not consider the accelerometer characteristics (***Dai et al., 2011; Lin et al., 2016***). Li fuses aerospace inertial navigation model and petroleum logging parameters, including two optical fiber gyroscopes and three accelerometers to form inertial measurement unit(IMU), and achieved an attitude heading reference system. (***Ren et al., 2010. Li et al., 2016***). This study focus on the integration of accelerometer and tilt-meter, to achieve more applicable, cheaper and easier technology system in engineering. 5.2 Kalman Filtering Model**

The kinematic (or dynamic) method is written as

$$\boldsymbol{X}_k = \boldsymbol{\Phi}_k \boldsymbol{X}_{k-1} + \boldsymbol{G}_k \boldsymbol{W}_k \qquad (5\text{-}1)$$

where $\boldsymbol{X}_{k-1}$ *and* $\boldsymbol{X}_k$ *are the state vectors at epochs* t_{k-1} *and* t_k *respectively;* $\boldsymbol{W}_k$ *is a kinematic model noise vector;* $\boldsymbol{\Phi}_k$ *is the design matrix of the observational equation.*

$$\boldsymbol{X}_k = [\boldsymbol{x}_k, \dot{\boldsymbol{x}}_k, \ddot{\boldsymbol{x}}_k]^T . \boldsymbol{X}_k = [\boldsymbol{s}_k, \boldsymbol{v}_k, \boldsymbol{a}_k]^T$$

$$\boldsymbol{\Phi}_k = \begin{bmatrix} \boldsymbol{I}_3 & \Delta t \boldsymbol{I}_3 & 0.5(\Delta t)^2 \boldsymbol{I}_3 \\ \boldsymbol{0} & \boldsymbol{I}_3 & \Delta t \boldsymbol{I}_3 \\ \boldsymbol{0} & \boldsymbol{0} & \boldsymbol{I}_3 \end{bmatrix}, \quad \boldsymbol{G}_k = \begin{bmatrix} \frac{1}{6}(\Delta t)^3 \boldsymbol{I}_3 \\ \frac{1}{2}(\Delta t)^2 \boldsymbol{I}_3 \\ \Delta t \boldsymbol{I}_3 \end{bmatrix}$$

where, $\boldsymbol{s}_k = [\Delta x_k, \Delta y_k, \Delta z_k]^T$, $\boldsymbol{v}_k = [v_{xk}, v_{yk}, v_{zk}]^T$, $\boldsymbol{a}_k = [a_{xk}, a_{yk}, a_{zk}]^T$, $\Delta \boldsymbol{x_k}, \Delta \boldsymbol{y_k}, \Delta \boldsymbol{z_k}$ *are the displacements of monitoring points in x, y, z directions,* $\boldsymbol{v_{xk}}, \boldsymbol{v_{yk}}, \boldsymbol{v_{zk}}$ *are the speed in x, y, z directions and* $\boldsymbol{a_{xk}}, \boldsymbol{a_{yk}}, \boldsymbol{a_{zk}}$ *are the acceleration in x, y, z directions.* $\Delta \boldsymbol{t}$ *is the observation interval.* $\boldsymbol{I_3}$ *is the three order unit matrix and* $\boldsymbol{0}$ *is the three order zero matrix. Assume* $\boldsymbol{W_k}$ *is a stationary white noise sequence and the disturbance of acceleration is a stochastic process with the Gauss white noise, whose expectation is 0 and covariance matrix is* $\boldsymbol{\delta^2 I_3}$ *.The unit of* $\boldsymbol{\delta^2}$ *is* $\boldsymbol{m^2 s^{-4}}$*. According to the covariance propagation law, we can calculate the covariance matrix of* $\boldsymbol{W_k}$*.*

$$\boldsymbol{\Sigma}_{\boldsymbol{W}_k} = \boldsymbol{G}_k^T \begin{bmatrix} \boldsymbol{I}_3 & 0 & 0 \\ 0 & \boldsymbol{I}_3 & 0 \\ 0 & 0 & \delta^2 \boldsymbol{I}_3 \end{bmatrix} \boldsymbol{G}_k \qquad (5\text{-}2)$$

From (2-8), we can get

$$\boldsymbol{L}_{GPS}(t) = -l_B^k \Delta x + l_B^j \Delta x - m_B^k \Delta y + m_B^j \Delta y - n_B^k \Delta z + n_B^j \Delta z + \nabla \Delta \varepsilon \qquad (5\text{-}3)$$

where

$$\boldsymbol{L}_{GPS} = \nabla \Delta \Phi_{AC}^{jk} - \nabla \Delta R_{AB}^{jk} + \nabla \Delta N_{AC}^{jk} - \nabla \Delta_{12,T}^{jk} - \nabla \Delta_{AC,M}^{jk} \qquad (5\text{-}4)$$

or

$$\boldsymbol{L}_{kGPS} = \boldsymbol{E}_{kGPS} \begin{bmatrix} \Delta x_k \\ \Delta y_k \\ \Delta z_k \end{bmatrix} + \boldsymbol{v}_{1k} \qquad (5\text{-}5)$$

where

$$\boldsymbol{E}_{kGPS} = \begin{bmatrix} l_B^2 - l_B^1 & m_B^2 - m_B^1 & n_B^2 - n_B^1 \\ l_B^3 - l_B^1 & m_B^3 - m_B^1 & n_B^3 - n_B^1 \\ \cdots & \cdots & \cdots \\ l_B^n - l_B^1 & m_B^n - m_B^1 & n_B^n - n_B^1 \end{bmatrix} \tag{5-6}$$

and the observation equation of the accelerometer is

$$\boldsymbol{L}_{ACC} = \begin{bmatrix} F_x - F_{x0} \\ F_y - F_{y0} \\ F_z - F_{z0} \end{bmatrix} = \begin{bmatrix} S_{kx} & K_{xy} & K_{xz} \\ K_{yx} & S_{ky} & K_{yz} \\ K_{zx} & K_{zy} & S_{kz} \end{bmatrix} \begin{bmatrix} a_{xk} \\ a_{yk} \\ a_{zk} \end{bmatrix} + \boldsymbol{v}_{1k} = \boldsymbol{K} \begin{bmatrix} a_{xk} \\ a_{yk} \\ a_{zk} \end{bmatrix} + \boldsymbol{v}_{2k} \tag{5-7}$$

where F_x, F_y, F_z *are the accelerometer observations in x, y, z directions,* $\boldsymbol{S_{kx}}$, $\boldsymbol{S_{ky}}$, $\boldsymbol{S_{kz}}$ *are the scale factors of the accelerometer,* $\boldsymbol{K_{xy}}$, $\boldsymbol{K_{xz}}$, $\boldsymbol{K_{yx}}$, $\boldsymbol{K_{yz}}$, $\boldsymbol{K_{zx}}$, $\boldsymbol{K_{zy}}$ *are the installation error coefficients of the accelerometer. In calibration, the component of the Coriolis acceleration on the sensitive axis is ignored.*

The observation model integrating GPS and acceleration is

$$\boldsymbol{L}_k = \begin{bmatrix} \boldsymbol{L}_{GPS} \\ \boldsymbol{L}_{ACC} \end{bmatrix} = \boldsymbol{H}_k \boldsymbol{X}_k + \boldsymbol{v}_k \tag{5-8}$$

where

$$\boldsymbol{H}_k = \begin{bmatrix} \boldsymbol{E}_{GPS} & \boldsymbol{0} & \boldsymbol{0} \\ \boldsymbol{0} & \boldsymbol{0} & \boldsymbol{K} \end{bmatrix}, \quad \boldsymbol{v}_k = \begin{bmatrix} \boldsymbol{v}_{1k} \\ \boldsymbol{v}_{2k} \end{bmatrix}$$

The predicted state vector $\overline{\boldsymbol{X}}_k$ *is written as*

$$\overline{\boldsymbol{X}}_k = \boldsymbol{\Phi}_k \widehat{\boldsymbol{X}}_{k-1} \tag{5-9}$$

and

$$\boldsymbol{\Sigma}_{\overline{\boldsymbol{X}}_k} = \boldsymbol{\Phi}_k \boldsymbol{\Sigma}_{\widehat{\boldsymbol{X}}_{k-1}} \boldsymbol{\Phi}_k^T + \boldsymbol{\Sigma}_{\boldsymbol{W}_k} \tag{5-10}$$

The state estimation in Kalman filter is

$$\widehat{\boldsymbol{X}}_k = \overline{\boldsymbol{X}}_k + \boldsymbol{K}_k(\boldsymbol{L}_k - \boldsymbol{H}_k \overline{\boldsymbol{X}}_k) \tag{5-11}$$

$$\boldsymbol{K}_k = \boldsymbol{\Sigma}_{\overline{\boldsymbol{X}}_k} \boldsymbol{H}_k^T (\boldsymbol{H}_k \boldsymbol{\Sigma}_{\overline{\boldsymbol{X}}_k} \boldsymbol{H}_k^T + \boldsymbol{R}_k)^{-1} \tag{5-12}$$

$$\boldsymbol{\Sigma}_{\widehat{\boldsymbol{X}}_k} = (\boldsymbol{I} - \boldsymbol{K}_k \boldsymbol{H}_k) \boldsymbol{\Sigma}_{\overline{\boldsymbol{X}}_k} \tag{5-13}$$

From the observation equation (4-1), we get

$$\boldsymbol{B}_k \boldsymbol{X}_k = \boldsymbol{d}_k \tag{5-14}$$

where $\boldsymbol{B}_k$ *is a known* $s \times n$ *matrix* ($s < n$) *and* $\boldsymbol{d}_k$ *can be written as*

$$\boldsymbol{d}_k = \begin{bmatrix} \sum_{i=1}^{n} dx_i \\ \sum_{i=1}^{n} dy_i \\ \sum_{i=1}^{n} dh_i \end{bmatrix}$$

dx_i， dy_i *and* dh_i *have the same definition with those in (4-5-b)*

From （4-5-c）, *we get* $\boldsymbol{X}_k = \boldsymbol{d}_k$, *which is the same as* $\boldsymbol{B}_k = \boldsymbol{I}$

5.3 The Solution Methods for Constrained Filtering

We can get the Kalman model

$$\boldsymbol{X}_k = \boldsymbol{\Phi}_k \boldsymbol{X}_{k-1} + \boldsymbol{W}_k$$

$$\boldsymbol{L'}_k = \begin{bmatrix} \boldsymbol{L}_k \\ \boldsymbol{d}_k \end{bmatrix} = \begin{bmatrix} \boldsymbol{H}_k \\ \boldsymbol{B}_k \end{bmatrix} \boldsymbol{X}_k + \begin{bmatrix} \boldsymbol{v}_k \\ \boldsymbol{v}_{3k} \end{bmatrix} \tag{5-15}$$

With (5-15), the measurement equation has been augmented without changing the state equation.

The constrained filtering approach begins with the standard unconstrained estimate $\widehat{\boldsymbol{X}}_k$ *by (5-11) to (5-13), which is then projected onto the constraint surface. This can be written as*

$$\widehat{\boldsymbol{X}}_{STk} = \min_{\boldsymbol{X}} (\boldsymbol{X}_k - \widehat{\boldsymbol{X}}_k)^T \boldsymbol{P}_k \left(\boldsymbol{X}_k - \widehat{\boldsymbol{X}}_k\right), \boldsymbol{B}_k \boldsymbol{X}_k = \boldsymbol{d}_k \tag{5-16}$$

where

$$\boldsymbol{P}_k = \boldsymbol{\Sigma}_{\widehat{\boldsymbol{X}}_k}^{-1}$$

So (5-16) can be rewritten as

$$\widehat{\boldsymbol{X}}_{STk} = \widehat{\boldsymbol{X}}_k - \boldsymbol{\Sigma}_{\widehat{\boldsymbol{X}}_k} \boldsymbol{B}_k^T (\boldsymbol{B}_k \boldsymbol{\Sigma}_{\widehat{\boldsymbol{X}}_k} \boldsymbol{B}_k^T)^{-1} (\boldsymbol{B}_k \widehat{\boldsymbol{X}}_k - \boldsymbol{d}_k) \tag{5-17}$$

Let

$$\boldsymbol{M}_k = \boldsymbol{\Sigma}_{\widehat{\boldsymbol{X}}_k} \boldsymbol{B}_k^T (\boldsymbol{B}_k \boldsymbol{\Sigma}_{\widehat{\boldsymbol{X}}_k} \boldsymbol{B}_k^T)^{-1}$$

(5-17) can be written as

$$\widehat{\boldsymbol{X}}_{STk} = \widehat{\boldsymbol{X}}_k - \boldsymbol{M}_k (\boldsymbol{B}_k \widehat{\boldsymbol{X}}_k - \boldsymbol{d}_k)$$

So, we have

$$\boldsymbol{X}_k - \widehat{\boldsymbol{X}}_{STk} = \boldsymbol{X}_k - \widehat{\boldsymbol{X}}_k + \boldsymbol{M}_k[(\boldsymbol{B}_k\widehat{\boldsymbol{X}}_k - \boldsymbol{d}_k) - (\boldsymbol{B}_k\boldsymbol{X}_k - \boldsymbol{d}_k)]$$

$$= \boldsymbol{X}_k - \widehat{\boldsymbol{X}}_k + \boldsymbol{M}_k\boldsymbol{B}_k(\widehat{\boldsymbol{X}}_k - \boldsymbol{X}_k)$$

$$= -(\boldsymbol{I} - \boldsymbol{M}_k\boldsymbol{B}_k)(\widehat{\boldsymbol{X}}_k - \boldsymbol{X}_k)$$

Therefore

$$\boldsymbol{\Sigma}_{\widehat{\boldsymbol{X}}_{STk}} = E[(\boldsymbol{X}_k - \widehat{\boldsymbol{X}}_{STk})(\boldsymbol{X}_k - \widehat{\boldsymbol{X}}_{STk}]^T]$$

$$= (\boldsymbol{I} - \boldsymbol{M}_k\boldsymbol{B}_k)E[(\widehat{\boldsymbol{X}}_k - \boldsymbol{X}_k)(\widehat{\boldsymbol{X}}_k - \boldsymbol{X}_k)^T](\boldsymbol{I} - \boldsymbol{M}_k\boldsymbol{B}_k)^T$$

$$= (\boldsymbol{I} - \boldsymbol{M}_k\boldsymbol{B}_k)\boldsymbol{\Sigma}_{\widehat{\boldsymbol{X}}_k}(\boldsymbol{I} - \boldsymbol{M}_k\boldsymbol{B}_k)^T = (\boldsymbol{I} - \boldsymbol{M}_k\boldsymbol{B}_k)\boldsymbol{\Sigma}_{\widehat{\boldsymbol{X}}_k}$$

We calculate $\widehat{\boldsymbol{X}}_{\boldsymbol{k}}$ *and* $\boldsymbol{\Sigma}_{\widehat{\boldsymbol{X}}_{\boldsymbol{k}}}$ *by iterative filtering formulas (5-11) and (5-13), then calculate the filtering solution with constraints* $\widehat{\boldsymbol{X}}_{\boldsymbol{STk}}$, $\boldsymbol{\Sigma}_{\widehat{\boldsymbol{X}}_{\boldsymbol{STk}}}$ *by (5-17). The iterative process is as follows*

$$\overline{\boldsymbol{X}}_k = \boldsymbol{\Phi}_k\widehat{\boldsymbol{X}}_{k-1}$$

$$\boldsymbol{\Sigma}_{\overline{\boldsymbol{X}}_k} = \boldsymbol{\Phi}_k\boldsymbol{\Sigma}_{\widehat{\boldsymbol{X}}_{k-1}}\boldsymbol{\Phi}_k^T + \boldsymbol{\Sigma}_{\boldsymbol{W}_k}$$

$$\widehat{\boldsymbol{X}}_{k1} = \overline{\boldsymbol{X}}_k + \boldsymbol{K}_k(\boldsymbol{L}_k - \boldsymbol{H}_k\overline{\boldsymbol{X}}_k)$$

$$\boldsymbol{K}_k = \boldsymbol{\Sigma}_{\overline{\boldsymbol{X}}_k}\boldsymbol{H}_k^T(\boldsymbol{H}_k\boldsymbol{\Sigma}_{\overline{\boldsymbol{X}}_k}\boldsymbol{H}_k^T + \boldsymbol{R}_k)^{-1}$$

$$\boldsymbol{\Sigma}_{\widehat{\boldsymbol{X}}_{k1}} = (\boldsymbol{I} - \boldsymbol{K}_k\boldsymbol{H}_k)\boldsymbol{\Sigma}_{\overline{\boldsymbol{X}}_k}$$

$$\boldsymbol{M}_k = \boldsymbol{\Sigma}_{\widehat{\boldsymbol{X}}_{k1}}\boldsymbol{B}_k^T(\boldsymbol{B}_k\boldsymbol{\Sigma}_{\widehat{\boldsymbol{X}}_{k1}}\boldsymbol{B}_k^T)^{-1}$$

$$\widehat{\boldsymbol{X}}_k = \widehat{\boldsymbol{X}}_{k1} - \boldsymbol{M}_k(\boldsymbol{B}_k\widehat{\boldsymbol{X}}_{k1} - \boldsymbol{d}_k)$$

$$\boldsymbol{\Sigma}_{\widehat{\boldsymbol{X}}_k} = (\boldsymbol{I} - \boldsymbol{M}_k\boldsymbol{B}_k)\boldsymbol{\Sigma}_{\widehat{\boldsymbol{X}}_{k1}}$$

5.4 Adaptive Filter Method for Constrained Filtering

In section 5.3, we got the solution of state parameters $\widehat{\boldsymbol{X}}_k$ *by (5-17).*

$$\widehat{\boldsymbol{X}}_k = \widehat{\boldsymbol{X}}_{k1} - \boldsymbol{M}_k(\boldsymbol{B}_k\widehat{\boldsymbol{X}}_{k1} - \boldsymbol{d}_k)$$

where $\widehat{\boldsymbol{X}}_{k1}$ *is the fusion results of GPS/accelerator filtering, and* $\boldsymbol{M}_k$ *is the item obtained from tilt-meter measurements. In this section, we use a factor to adjust the observation weight.*

Let $\boldsymbol{V}_k$ *be the residual of the observational vector* $\boldsymbol{L}_k$*, and* $\overline{\boldsymbol{V}}_k$ *is written as*

$$\overline{\boldsymbol{V}}_k = \boldsymbol{L}_k - \boldsymbol{H}_k\overline{\boldsymbol{X}}_k\,,\ \ \boldsymbol{V}_k = \boldsymbol{L}_k - \boldsymbol{H}_k\widehat{\boldsymbol{X}}_k$$

The Lagrangian optimisation problem can be solved by

$$min\, F_k = \boldsymbol{V}_k^T\boldsymbol{P}_{\widehat{X}_k}\boldsymbol{V}_k + \alpha_k\widehat{\boldsymbol{X}}_k^T\boldsymbol{P}_{\overline{X}_k}\widehat{\boldsymbol{X}}_k + 2\boldsymbol{\beta}_k^T(\boldsymbol{B}_k\widehat{\boldsymbol{X}}_k - \boldsymbol{d}_k) \qquad (5\text{-}18\text{-}a)$$

where

$$\boldsymbol{P}_{\overline{X}_k} = \boldsymbol{\Sigma}_{\overline{X}_k}^{-1}, \boldsymbol{P}_{\widehat{X}_k} = \boldsymbol{\Sigma}_{\overline{X}_k}^{-1} \qquad (5\text{-}18\text{-}b)$$

α_k *is the adaptive factor,* $\boldsymbol{\beta}_k$ *is a Lagrangian multiple vector.*

$$\frac{\partial F_k}{\partial \widehat{\boldsymbol{X}}_k} = -2\boldsymbol{H}_k^T\boldsymbol{R}_k\left(\boldsymbol{L}_k - \boldsymbol{H}_k\widehat{\boldsymbol{X}}_k\right) + 2\alpha_k\boldsymbol{P}_{\overline{X}_k}\widehat{\boldsymbol{X}}_k + 2\boldsymbol{B}_k^T\boldsymbol{\beta}_k = 0 \qquad (5\text{-}19)$$

Considering the observational error equation (5-8), we get

$$\widehat{\boldsymbol{X}}_k = (\boldsymbol{H}_k^T \boldsymbol{P}_{\widehat{\boldsymbol{X}}_k} \boldsymbol{H}_k + \alpha_k \boldsymbol{P}_{\overline{\boldsymbol{X}}_k})^{-1} \boldsymbol{H}_k^T \boldsymbol{P}_{\widehat{\boldsymbol{X}}_k} \boldsymbol{L}_k - (\boldsymbol{H}_k^T \boldsymbol{P}_{\widehat{\boldsymbol{X}}_k} \boldsymbol{H}_k + \alpha_k \boldsymbol{P}_{\overline{\boldsymbol{X}}_k})^{-1} \boldsymbol{B}_k^T \boldsymbol{\beta}_k \tag{5-20}$$

*In (5-20), the first term is an adaptive Kalman filter estimator (***Yang et al., 2001***).*

Let

$$\widehat{\boldsymbol{X}}_k^0 = (\boldsymbol{H}_k^T \boldsymbol{P}_{\hat{X}_k} \boldsymbol{H}_k + \alpha_k \boldsymbol{P}_{\overline{\boldsymbol{X}}_k})^{-1} \boldsymbol{H}_k^T \boldsymbol{P}_k \boldsymbol{L}_k \tag{5-21}$$

and

$$\boldsymbol{\Sigma}_{\widehat{\boldsymbol{X}}_k^0} = (\boldsymbol{H}_k^T \boldsymbol{P}_{\hat{X}_k} \boldsymbol{H}_k + \alpha_k \boldsymbol{P}_{\overline{\boldsymbol{X}}_k})^{-1} = \frac{1}{\alpha_k} (\frac{1}{\alpha_k} \boldsymbol{H}_k^T \boldsymbol{P}_{\hat{X}_k} \boldsymbol{H}_k + \boldsymbol{P}_{\overline{\boldsymbol{X}}_k})^{-1} \tag{5-22}$$

then we have

$$\widehat{\boldsymbol{X}}_k = \widehat{\boldsymbol{X}}_k^0 - \boldsymbol{\Sigma}_{\widehat{\boldsymbol{X}}_k^0} \boldsymbol{B}_k^T \boldsymbol{\beta}_k \tag{5-23}$$

Considering the constraint equation (5-14), we get

$$\boldsymbol{B}_k \widehat{\boldsymbol{X}}_k - \boldsymbol{d}_k = \boldsymbol{B}_k \widehat{\boldsymbol{X}}_k^0 - \boldsymbol{B}_k \boldsymbol{\Sigma}_{\widehat{\boldsymbol{X}}_k^0} \boldsymbol{B}_k^T \boldsymbol{\beta}_k - \boldsymbol{d}_k = 0 \tag{5-24}$$

where

$$\widehat{\boldsymbol{\beta}}_k = (\boldsymbol{B}_k \boldsymbol{\Sigma}_{\widehat{\boldsymbol{X}}_k^0} \boldsymbol{B}_k^T)^{-1} (\boldsymbol{B}_k \widehat{\boldsymbol{X}}_k^0 - \boldsymbol{d}_k) \quad (5\text{-}25)$$

From (5-23) and (5-25) we get

$$\begin{aligned} \widehat{\boldsymbol{X}}_k &= \widehat{\boldsymbol{X}}_k^0 - \boldsymbol{\Sigma}_{\widehat{\boldsymbol{X}}_k^0} \boldsymbol{B}_k^T (\boldsymbol{B}_k \boldsymbol{\Sigma}_{\widehat{\boldsymbol{X}}_k^0} \boldsymbol{B}_k^T)^{-1} (\boldsymbol{B}_k \widehat{\boldsymbol{X}}_k^0 - \boldsymbol{d}_k) \\ &= \widehat{\boldsymbol{X}}_k^0 - \frac{1}{\alpha_k} \left(\frac{1}{\alpha_k} \boldsymbol{H}_k^T \boldsymbol{P}_{\hat{X}_k} \boldsymbol{H}_k \right. \\ &\left. + \boldsymbol{P}_{\overline{X}_k}\right)^{-1} \boldsymbol{B}_k^T (\boldsymbol{B}_k \boldsymbol{\Sigma}_{\widehat{\boldsymbol{X}}_k^0} \boldsymbol{B}_k^T)^{-1} (\boldsymbol{B}_k \widehat{\boldsymbol{X}}_k^0 - \boldsymbol{d}_k) \end{aligned} \quad (5\text{-}26)$$

Different from (5-17), (5-26) has a weight factor $\frac{1}{\alpha_k}$ *in the second item, called the adaptive factor, which is used for adjusting the weight of tilt-meter measurements in fusion.*

$\widehat{\boldsymbol{X}}_k^0$ *is the key item in (5-26),* α_k *is the adaptive factor, which can be defined as*

$$\alpha_k = \begin{cases} 1 & tr(\overline{\boldsymbol{V}}_k \overline{\boldsymbol{V}}_k^T) \le tr(\boldsymbol{\Sigma}_{\overline{\boldsymbol{V}}_k}) \\ \dfrac{tr(\boldsymbol{\Sigma}_{\overline{\boldsymbol{V}}_k})}{tr(\overline{\boldsymbol{V}}_k \overline{\boldsymbol{V}}_k^T)} & otherwise \end{cases} \quad (5\text{-}27)$$

where

$$\overline{\boldsymbol{V}}_k = \boldsymbol{H}_k \overline{\boldsymbol{X}}_k - \boldsymbol{L}_k \quad (5\text{-}28\text{-}a)$$

$$\boldsymbol{\Sigma}_{\overline{\boldsymbol{V}}_k} = \boldsymbol{H}_k^T \boldsymbol{P}_{\overline{X}_k} \boldsymbol{H}_k + \boldsymbol{R}_k \quad (5\text{-}28\text{-}b)$$

*Formulas (5-28a) and (5-28b) show the kinematic model error when the measurement vector is reliable (***Yang et al., 2006***). Now, we have the adaptive*

filtering algorithm with constrains as follows for fusing GPS, accelerometer and tilt-meter:

Step1: calculate the standard Kalman filter

$$\overline{\boldsymbol{X}}_k = \boldsymbol{\Phi}_k \widehat{\boldsymbol{X}}_{k-1}$$

$$\boldsymbol{\Sigma}_{\overline{\boldsymbol{X}}_k} = \boldsymbol{\Phi}_k \boldsymbol{\Sigma}_{\widehat{\boldsymbol{X}}_{k-1}} \boldsymbol{\Phi}_k^T + \boldsymbol{\Sigma}_{\boldsymbol{W}_k}$$

$$\widehat{\boldsymbol{X}}_k = \overline{\boldsymbol{X}}_k + \boldsymbol{K}_k(\boldsymbol{L}_k - \boldsymbol{H}_k \overline{\boldsymbol{X}}_k)$$

$$\boldsymbol{K}_k = \boldsymbol{\Sigma}_{\overline{\boldsymbol{X}}_k} \boldsymbol{H}_k^T (\boldsymbol{H}_k \boldsymbol{\Sigma}_{\overline{\boldsymbol{X}}_k} \boldsymbol{H}_k^T + \boldsymbol{R}_k)^{-1}$$

$$\boldsymbol{\Sigma}_{\widehat{\boldsymbol{X}}_k} = (\boldsymbol{I} - \boldsymbol{K}_k \boldsymbol{H}_k) \boldsymbol{\Sigma}_{\overline{\boldsymbol{X}}_k}$$

Step2: calculate adaptive factor by (5-18b)

$$\boldsymbol{P}_k = \boldsymbol{\Sigma}_{\widehat{\boldsymbol{X}}_k}^{-1}, \quad \boldsymbol{P}_{\overline{\boldsymbol{X}}_k} = \boldsymbol{\Sigma}_{\overline{\boldsymbol{X}}_k}^{-1}$$

$$\widetilde{\boldsymbol{X}}_k = (\boldsymbol{H}_k^T \boldsymbol{P}_k \boldsymbol{H}_k)^{-1} \boldsymbol{H}_k^T \boldsymbol{P}_k \boldsymbol{L}_k$$

$$\alpha_k = \begin{cases} \dfrac{1}{tr(\boldsymbol{\Sigma}_{\overline{\boldsymbol{X}}_k})} & tr(\widetilde{\boldsymbol{X}}_k \widetilde{\boldsymbol{X}}_k^T) \le tr(\boldsymbol{\Sigma}_{\overline{\boldsymbol{X}}_k}) \\ \dfrac{}{tr(\widetilde{\boldsymbol{X}}_k \widetilde{\boldsymbol{X}}_k^T)} & otherwise \end{cases}$$

Step3: calculate adaptive filtering estimation with constraints

$$\widehat{\boldsymbol{X}}_k^0 = (\boldsymbol{H}_k^T \boldsymbol{P}_k \boldsymbol{H}_k + \alpha_k \boldsymbol{P}_{\overline{\boldsymbol{X}}_k})^{-1} \boldsymbol{H}_k^T \boldsymbol{P}_k \boldsymbol{e}_k$$

$$\boldsymbol{\Sigma}_{\widehat{\boldsymbol{X}}_k^0} = (\boldsymbol{H}_k^T \boldsymbol{P}_k \boldsymbol{H}_k + \alpha_k \boldsymbol{P}_{\overline{\boldsymbol{X}}_k})^{-1}$$

$$\widehat{\boldsymbol{X}}_k = \widehat{\boldsymbol{X}}_k^0 - \boldsymbol{\Sigma}_{\widehat{\boldsymbol{X}}_k^0}\boldsymbol{B}_k^T(\boldsymbol{B}_k\boldsymbol{\Sigma}_{\widehat{\boldsymbol{X}}_k^0}\boldsymbol{B}_k^T)^{-1}(\boldsymbol{B}_k\widehat{\boldsymbol{X}}_k^0 - d_k)$$

$$= \widehat{\boldsymbol{X}}_k^0 - \frac{1}{\alpha_k}(\frac{1}{\alpha_k}\boldsymbol{H}_k^T\boldsymbol{P}_{\hat{X}_k}\boldsymbol{H}_k + \boldsymbol{P}_{\bar{X}_k})^{-1}\boldsymbol{B}_k^T(\boldsymbol{B}_k\boldsymbol{\Sigma}_{\widehat{\boldsymbol{X}}_k^0}\boldsymbol{B}_k^T)^{-1}(\boldsymbol{B}_k\widehat{\boldsymbol{X}}_k^0 - \boldsymbol{d}_k)$$

5.5 Simulation Study and Analysis

To verify the algorithms, we designed the following simulation experiments.

The data are sampled by second for 1200 epochs. Satellite positions are determined directly through the satellite broadcast ephemeris from 10:00 to 15:00 on December 28, 2016. Set a known ground point with WGS84 coordinates (-2418209.734, 5385904.753, 2405486.1) and plane coordinates (2467346.949, 518499.652, 34.264). According to (3-17), the distance between the satellite and the ground point plus the random error are taken as the simulated GPS observations. In the simulation data, the observation errors of GPS, tilt-meter and accelerometer are set separately according to the experiments.

In order to verify the dynamic performance of the algorithm, we bring the vibration displacement into the simulated data, in which vibration is generated by the following simulation function:

$$Offset_N = Dis_N * sin\left(\frac{\pi r_t}{30}\right)$$

$$Offset_E = Dis_E * sin\left(\frac{\pi r_t}{30}\right) \quad (5\text{-}29)$$

$$Offset_U = Dis_U * sin(\frac{\pi r_t}{8})$$

where r_t is the epoch number, Dis_N, Dis_E and Dis_U are the vibration amplitudes in the north, east and elevation directions. In this test, they are 12 mm, 15 mm and 20 mm. The vibration cycle is 30 epochs. Similarly, the tilt measurement was obtained by (3-1) and (3-2). The acceleration value is obtained by using the two order difference to the displacement.

In the experiment, four data processing programs are designed:

Algorithm 1: Solve the displacement by the Kalman filter with only the GPS observation. This is referred to as GPS filtering.

Algorithm 2: Solve the displacement by combining GPS observation and accelerometer observation with standard kalman. This is referred to as the GPS/ Accelerometer filtering.

Algorithm 3: Solve the displacement by the GPS observation, accelerometer observation and tilt-meter observation with formula 5-17. This is referred to as the GPS/Accelerometer/Tilt filtering.

Algorithm 4: Solve the displacement by the GPS observation, accelerometer observation and tilt-meter observation with formula 5-20. This is referred to as GPS/ Accelerometer /tilt-meter adaptive filtering.

*The first two algorithms have been introduced in chapter 1 (**Dai et al., 2011; Yu et al., 2014**). The GPS/Acc/Tilt filtering takes the tilt-meter observation into consideration and solves the displacement by the new filtering method described in section 5.3. The GPS/Accelerometer/Tilt-meter adaptive filtering is based on the filtering model introduced in section 5.4.*

5.5.1 Influence of GPS Data Accuracy on the Algorithms

Set the tilt-meter observation precision as 0.02 degree, the accelerometer observation precision as 0.002g and the GPS observation precision is 2 mm, 5mm, 10 mm and 15 mm, respectively. Subtracting the simulated truth value from the calculated results, we can get the standard deviations (Table 5-1).

Table 5-1. Standard deviations of the four algorithms with different GPS precisions. (unit: mm) (Precision: GPS, 2 to 15 mm; tilt-meter, 0.02 degree; accelerometer, 0.002g, available GPS satellite number:4)

GPS Precision (Unit: mm)	GPS Filtering			GPS/Acc Filtering			GPS/Acc/Tilt Filtering			GPS/Acc/Tilt adaptive Filtering		
	North	East	UP	North	East	UP	North	East	UP	North	East	UP
2	0.97	1.03	1.41	0.88	0.91	1.23	1.94	2.11	2.37	1.83	1.89	2.00
5	2.50	2.63	3.47	2.23	2.34	2.99	1.92	2.12	2.45	1.83	1.94	1.99
10	4.97	5.22	7.12	4.48	4.67	6.15	1.91	2.06	2.39	1.88	1.89	1.96
15	7.47	7.60	10.76	6.67	6.77	9.29	1.96	2.07	2.35	1.85	1.92	1.99

As Table 5-1 shows, with the improvement of GPS observation precision, the standard deviations of the four algorithms gradually decrease. Although, the accelerometer observation is considered by the GPS/Acc/Tilt filtering, its effect is not obvious because of the slow and small displacement. The GPS/Acc/Tilt filtering algorithm and GPS/Accelerometer/Tilt-meter adaptive filtering algorithm both take the observation of the accelerometer and tilt-meter into consideration, which improves the reliability of the whole observation system

and reduces the influence of the poor GPS observation accuracy on the results. The results show that bringing in high precision sensors can improve the accuracy of the solution of the deformation parameters in the multi-sensor fusion based on GPS observation.

Figure 5-1 shows the displacement sequence of the four algorithms in the north direction with a GPS observation precision of 10 mm. The precisions of GPS filtering and GPS/Acc filtering are poor, with the standard deviation 4.97 mm and 4.48 mm, respectively. However, GPS/Acc/Tilt filtering and GPS/Acc/Tilt adapter filtering standard deviations are 1.91 mm and 1.89mm, respectively, about 60% improvement on the precisions of other two algorithms.

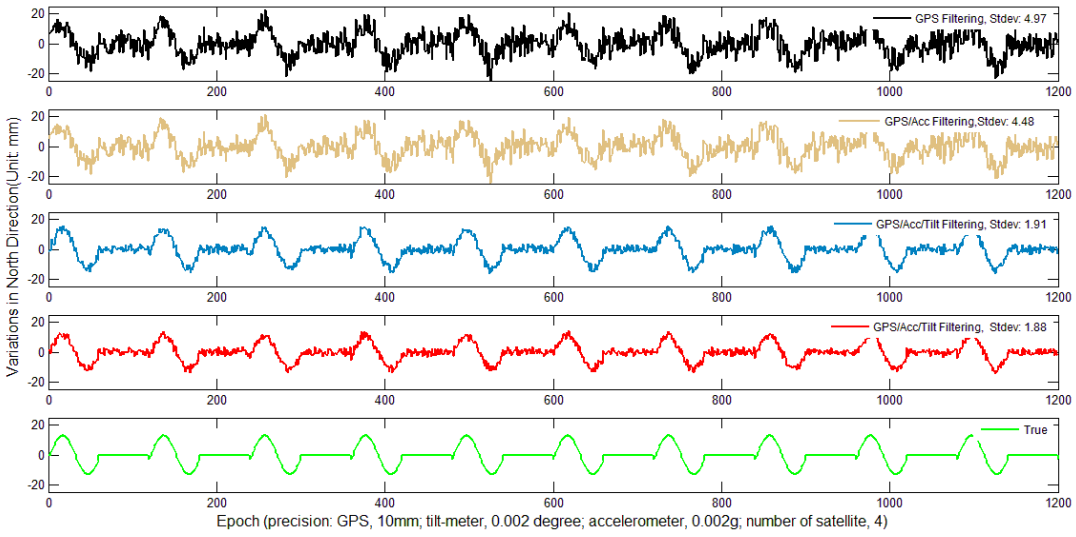

Fig. 5-1 Comparison of the algorithms in terms of the variations in the north direction (precision: GPS, 10mm; tilt-meter, 0.02 degree; accelerometer, 0.002g; number of satellite, 4)

Figure 5-2 shows the displacement sequence of the four algorithms in the east direction, with a GPS observation accuracy of 10 mm. The precisions of GPS

filtering and GPS/Acc filtering are poor, with standard deviations 5.22 mm and 4.67 mm. The standard deviations of GPS/Acc/Tilt filtering and GPS/Acc/Tilt adapter filtering are 2.06 mm and 1.89 mm, which have about 60% improvement on the precisions of other two algorithms.

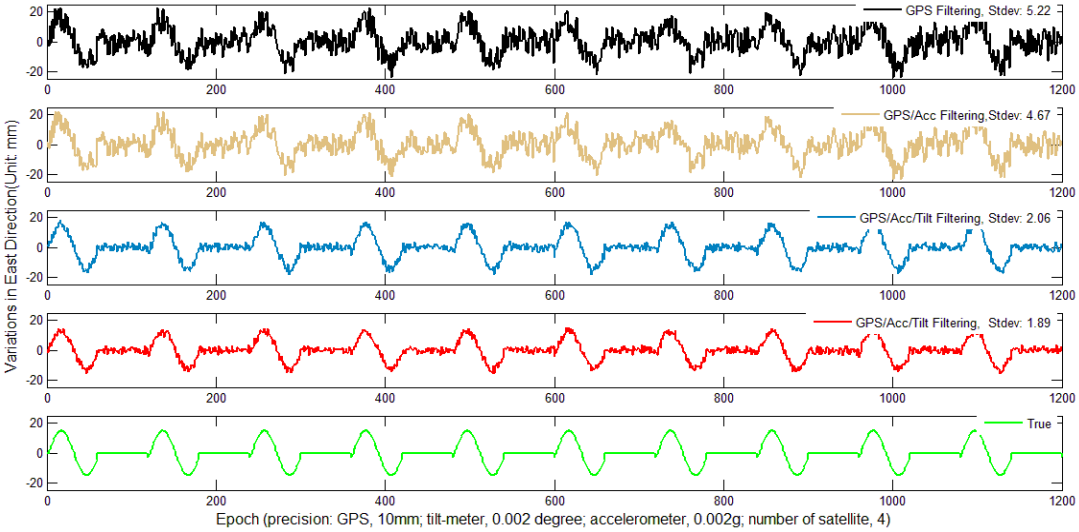

Fig. 5-2 Comparison of the algorithms in terms of the variations in the east direction (precision: GPS, 10mm; tilt-meter, 0.02 degree; accelerometer, 0.002g; number of satellite, 4)

Figure 5-3 *show the displacement sequence of the four algorithms in the elevation, with the GPS observation accuracy of 10 mm. The precision of GPS filtering and GPS/Acc filtering are poor, with standard deviations 7.12 mm and 6.15mm. GPS/Acc/Tilt filtering and GPS/Acc/Tilt adapter filtering have accuracies 68% improvement on the former two algorithms, with standard deviations as 2.39mm and 1.96 mm, respectively.*

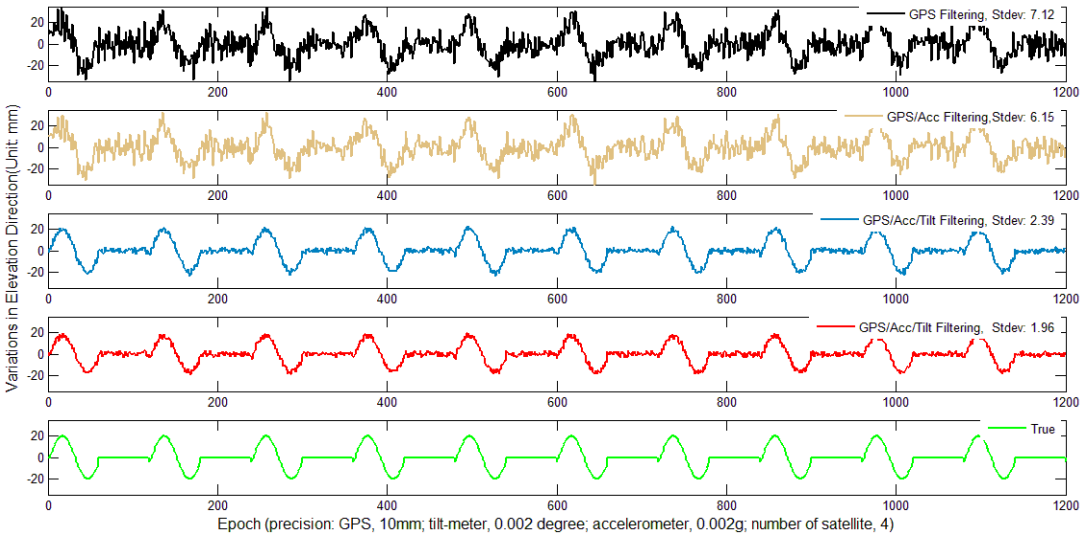

Fig. 5-3 Comparison of the algorithms in terms of the variations in the elevation direction (precision: GPS, 10mm; tilt-meter, 0.02 degree; accelerometer, 0.002g; number of satellite, 4)

5.5.2 Influence of number of Satellites on the Algorithms

Setting the tilt-meter observation precision as 0.02 degree, the accelerometer observation precision as 0.002 g and the GPS observation precision as 10 mm, we calculate the displacement with 4, 6, 8 and 9 satellites, respectively. The standard deviation is obtained after subtracting the simulated truth value from the results, see table 5-2.

Table 5-2. Standard deviations of the four algorithms with different numbers of satellites. (unit: mm) (Precision, GPS, 5 mm; tilt-meter 0.02 degree; accelerometer, 0.003g; number of satellites, 4 to 9)

Number of GPS Satellites	GPS Filtering			GPS/Acc Filtering			GPS/Acc/Tilt Filtering			GPS/Acc/Tilt Adaptive Filtering		
	North	East	UP	North	East	UP	North	East	UP	North	East	UP
4	2.50	2.63	3.47	2.23	2.34	2.99	1.95	2.13	2.38	1.84	1.92	2.00
6	1.86	1.90	2.51	1.71	1.77	2.27	1.93	2.06	2.40	1.88	1.89	2.01
8	1.62	1.63	2.28	1.51	1.53	2.08	1.92	2.10	2.38	1.87	1.93	2.04
9	1.57	1.62	2.26	1.47	1.52	2.06	1.95	2.08	2.40	1.83	1.88	2.02

As table 5-2 shows, with the increase of the number of visible satellites, the standard deviation of the 4 algorithms gradually decrease. Because of the satellite insufficiency, the standard deviation of GPS filtering is as high as 2.50mm. Although the GPS/Acc filtering considers the accelerometer observation, no obvious effect is found in this kind of slow and small displacement. GPS/Acc/Tilt filtering and GPS/Acc/Tilt adaptive filtering takes the observation of accelerometer and tilt-meter into consideration, which can significantly improve the accuracy of the solution. So it can been found that, GPS/Acc/Tilt filtering and GPS/Acc/Tilt adaptive filtering with only 4 GPS satellites available can work better than that of using only GPS data with 9 satellites observed.

Figure 5-4 *show the displacement sequence of the four algorithms in the north direction when 4 GPS satellites are used. The precisions of GPS filtering and GPS/Acc filtering are poor, with standard deviations 2.50 mm and 2.23mm, respectively. However, GPS/Acc/Tilt filtering and GPS/Acc/Tilt adapter filtering have improvement on precisions with standard deviations 1.95mm and 1.84mm, respectively.*

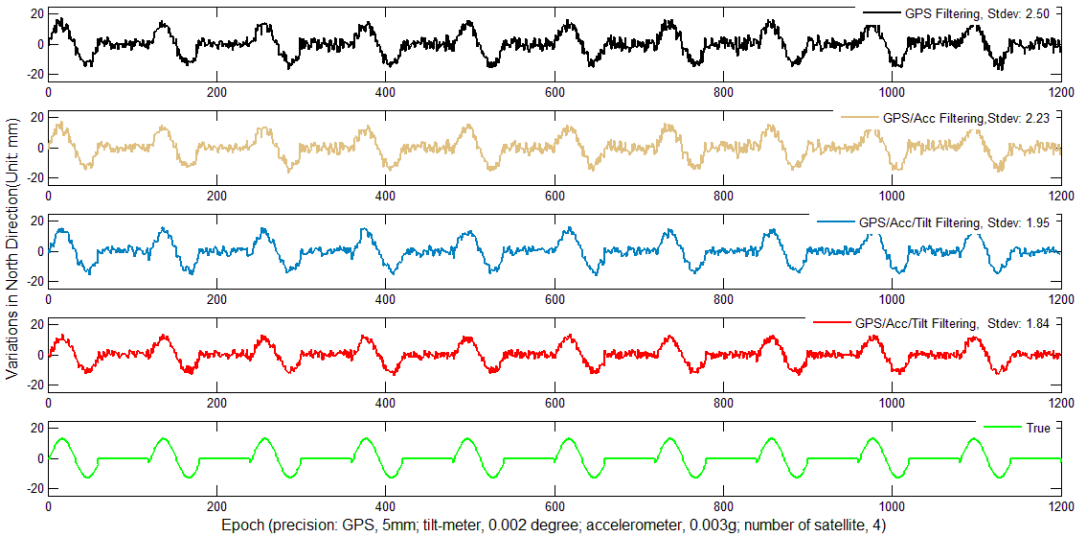

Fig. 5-4 Comparison of the algorithms in terms of the variations in the north direction (precision: GPS, 5mm; tilt-meter, 0.02 degree; accelerometer, 0.003 g; number of satellite, 4)

Figure 5-5 shows the displacement sequence of the four algorithms in the east direction, when 4 GPS satellites are used. The precisions of GPS filtering and GPS/Acc filtering are poor, with standard deviations 2.63 mm and 2.34mm. However, the standard deviations of GPS/Acc/Tilt filtering and GPS/Acc/Tilt adapter filtering are 2.13mm and 1.92mm, respectively.

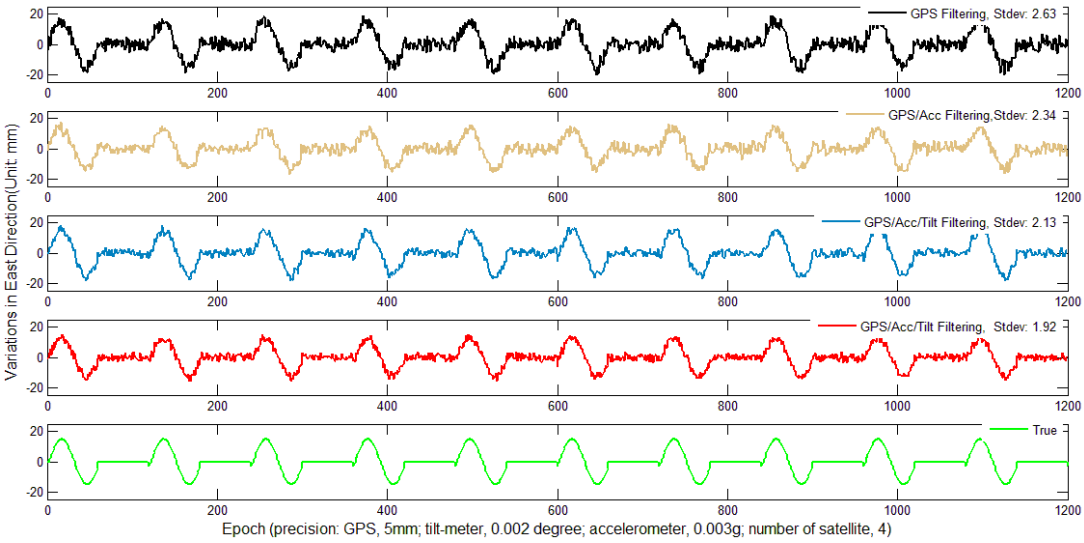

Fig. 5-5 Comparison of the algorithms in terms of the variations in the east direction (precision: GPS, 10mm; tilt-meter, 0.02 degree; accelerometer, 0.002 g; number of satellite, 4)

Figure 5-6 shows the displacement sequence of the four algorithms in the elevation direction, when 4 GPS satellites are used. The precisions of GPS filtering and GPS/Acc filtering are poor, with standard deviations 3.47 mm and 2.99 mm. The standard deviations of GPS/Acc/Tilt filtering and GPS/Acc/Tilt adapter filtering significantly are 2.38 mm and 2.00 mm, respectively.

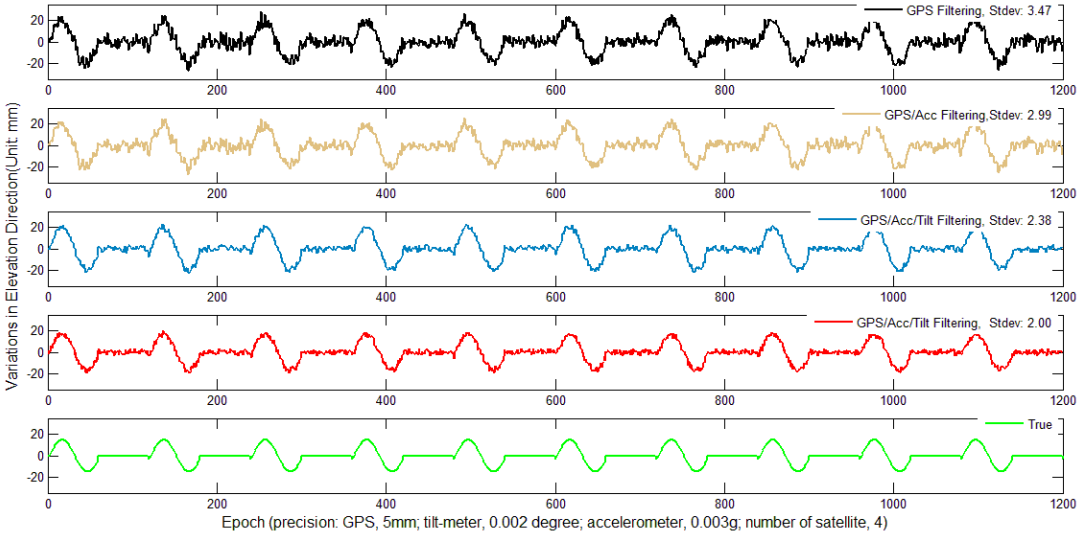

Fig. 5-6 Comparison of the algorithms in terms of the variations in the elevation direction (precision: GPS, 5mm; tilt-meter, 0.02 degree; accelerometer, 0.003 g; number of satellite, 4)

Comparing it with figures 5-1 to 5-6, we can say the fusion of multi-sensors can significantly improve the reliability of the observation system and reduce the influence of the abnormal situation on the results, if the GPS observation precision is poor or the satellites are insufficient.

Table 5-3. Standard deviations of the four algorithms with different numbers of satellites. (unit: mm) (Precision, GPS, 10 mm; tilt-meter 0.005 degree; accelerometer, 0.002g; number of satellites, 4 to 9)

Number of GPS Satellites	GPS Filtering			GPS/Acc Filtering			GPS/Tilt Filtering			GPS/Acc/Tilt Filtering		
	North	East	UP	North	East	UP	North	East	UP	North	East	UP
4	4.97	5.22	7.12	4.48	4.67	6.15	2.92	3.03	5.99	3.04	3.09	3.22
6	3.78	3.81	4.91	3.48	3.53	4.44	2.67	2.74	4.64	3.01	3.05	3.18
8	3.20	3.43	4.52	2.98	3.21	4.10	2.42	2.60	4.28	2.99	3.05	3.18
9	3.13	3.41	4.44	2.92	3.19	4.03	2.40	2.60	4.21	2.97	3.03	3.17

5.6 Case Study

To verify the effectiveness of these algorithms, an experiment was carried out on the campus of the Hong Kong Polytechnic University. GPS, an accelerometer and tilt-meter were installed on the roof of Z core building. In this study, the GPS system consisted of two Novatel 615 receivers. One was set as a rover station on the platform near the sixth floor and the other was the reference station installed on a pillar with a good sky view. The data sampling of GPS receiver was set as 10 Hz. During the experiment, x-direction of the biaxial tilt-meter sensor (Rion HCA526T) pointed to the due north and the y-direction pointed to the due east. The sampling rate is 10Hz. One 360-degree prism was fixed on a tripod. The length of one knighthead of the tripod can be adjusted to make a tilt angle and GPS antenna movement. A robotic total station (model: TS15) was used to measure the displacement when the tripod tilted at an angle. The result was taken as the true value to evaluate the accuracy of the algorithms. Reference stations were installed near the integrated device.

Fig. 5-7 Instruments and experiment environment

The device was fixed on a stable tripod. If the tripod tilts around the bottom support points during the displacement and the tilt angle and radius are known, we can convert tilt-meter measurements into the displacements in the east and north directions by formula (4-1). In order to verify the effectiveness of these algorithms, we firstly collected the static observation data. Then we stretched the tripod leg in the east/west direction to make the device tilt a little and moved the antenna correspondingly. At the end, we added continuous vibration to the device and tracked the continuous dynamic displacement by the total station.

Processing the collected data with the four algorithms, we got the results shown in figures 5-8, 5-9 *and* 5-10*. After a static observation for 6 minutes, the*

displacement changes at the 385th epoch. At that epoch, the displacement is -1 mm, 8 mm and 5 mm in the north, east and elevation directions. From epoch 645, the platform started to display irregular vibration, whose displacement sequence was tracked by the total station. We take this measurement as the true value.

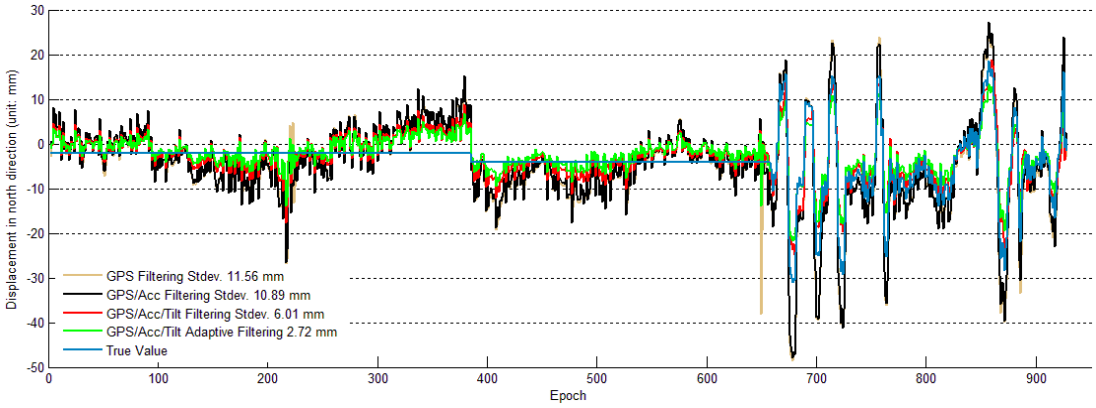

Fig. 5-8 Movement in the north direction of the dynamical experiment

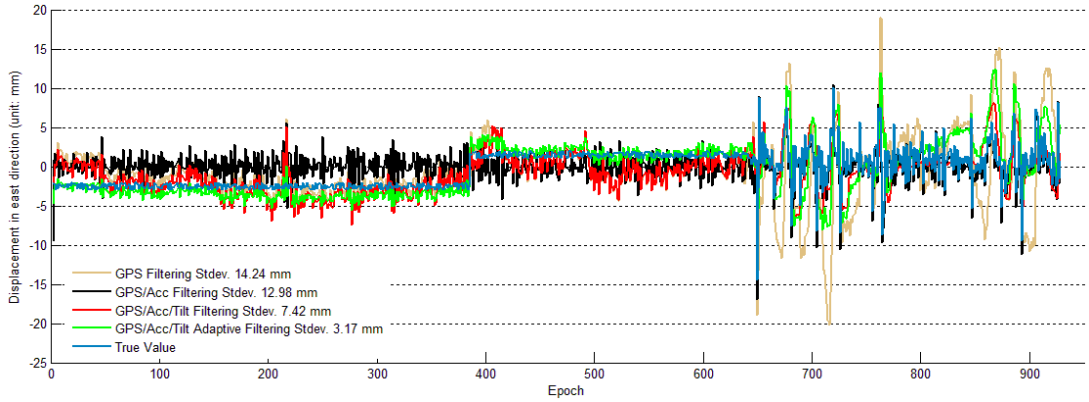

Fig. 5-9 Movement in the east direction of the dynamical experiment

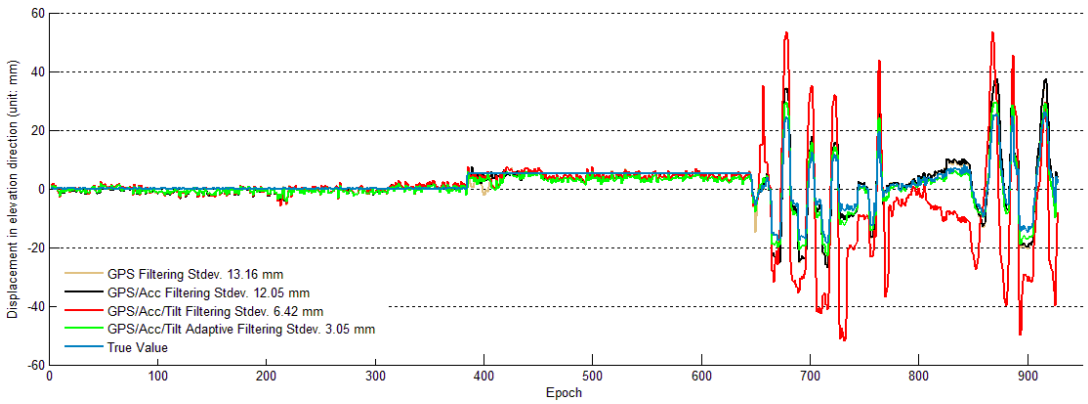

Fig. 5-10 Movement in the elevation direction of the dynamical experiment

As Figures 5-8, 5-9 and 5-10 show, the results of the GPS filtering and the GPS/Acc filtering are quite different from the true value. The result of the GPS/Acc/Tilt filtering is slightly better and the GPS/Acc/Tilt adaptive filtering can accurately track the changes of the vibration. Subtracting the true value from the result, we get the standard deviation (Table 5-4). Compared with the GPS filtering, GPS/Acc filtering improves the accuracy by 6%, 8.3% and 8.8%, the GPS/Acc/Tilt filtering improves the accuracy by 57.8%, 47.8%, 51.2% and the GPS/Acc/Tilt adaptive filtering improves the accuracy by 76.5%, 77.7%, 76.8% in the north, east and elevation directions, respectively. This verifies that the tilt-meter observation can improve the precision of algorithms. The adaptive factor can balance the weight ratio of the observation and suppress abnormal observations.

Table 5-4. Standard deviations of the four algorithms in the dynamical experiment. (unit: mm)

	GPS Filtering	GPS/Acc Filtering (Improve)	GPS/Acc/Tilt Filtering (Improve)	GPS/Acc/Tilt Adaptive Filtering (Improve)
North	11.56	10.89 (5.8%)	6.01 (48.0%)	2.72 (76.5%)
East	14.24	12.98 (8.8%)	7.42 (47.9%)	3.17 (77.7%)
Elevation	13.16	12.05 (8.4%)	6.42 (51.2%)	3.05 (76.8%)

5.7 Discussions and Conclusions

Based on the complementarity among the accelerometer, tilt-meter and GPS in high dynamic deformation monitoring, this chapter proposes two new fusion algorithms for these three sensors:

One is the GPS/Acc/Tilt filtering, which is established by adding tilt-meter observation to the GPS/Acc algorithm.

The other one is the GPS/Acc/Tilt adaptive filtering, which is formed by introducing an adaptive factor to the GPS/Acc/Tilt dynamic filtering algorithm to adjust the weight ratio of the observed information and the dynamic information.

We also compare the algorithms with different GPS observation precisions and using different numbers of satellites by simulation experiments. The results show that the GPS/Acc/Tilt dynamic filtering and GPS/Acc/Tilt adaptive dynamic filtering can improve the reliability of the monitoring system, especially when the GPS observation is abnormal and the satellites are insufficient. For example, if 4 observable satellites are used, the accuracy of displacement can be improved by about 60%. If the GPS accuracy is poor, less than 10mm, the new algorithms can improve accuracy by 60%. In the case study, the GPS/Acc/Tilt filtering algorithm and GPS/Acc/Tilt adaptive filtering algorithm can improve the accuracy by 50% and 70%, respectively, compared with the GPS filtering. In the simulation experiments, it can been found that, GPS/Acc/Tilt filtering and GPS/Acc/Tilt adaptive filtering with only 4 GPS satellites available can work as well as using only GPS data with 9 satellites observed. In simulation experiments

and case study, it has verified that the tilt-meter observation can improve the precision of algorithms, and the devised adaptive factor can balance the weight ratio of the observation and suppress abnormal observations.

CHAPTER 6 CONCLUSIONS AND FUTURE WORK

6.1 Conclusions

Structural health monitoring usually utilises multi-sensor technology to extract structural parameters, such as stress, strain, deformation, displacement, velocity or acceleration. This thesis combines GPS, tilt-meter and accelerometer for structural health monitoring and processes their observation with our new integrating algorithm.

In this thesis, integration between GPS, tilt-meter and accelerometer sensors in the observation domain has been carried out. This approach is different from traditional research. The innovation and contributions of this thesis are summarised as follows:

1) This study combined a multi GPS antenna system with a tilt-meter and proposed data processing model. Verification experiments show that when the GPS observation is abnormal, the integration algorithm can improve the precision by 37%, and the improvement in the elevation direction is the most significant.

2) This study combined stacked multi tilt-meters with GPS and tilt-meter observations to reduce the effect of multi-path error. A new constrained least squares algorithm is proposed.

An adaptive factor is given to adjust the contribution of the GPS observation and the tilt-meter observation to the parameter estimation, which provides a new way for multi sensor data fusion. The case study show, when the GPS observation is abnormal, the standard deviation of results obtained by the adaptive fusion algorithm was reduced by about 40% in all the three directions (north, east and elevation).

3) This study suggested a Kalman filter-based model with constraints to integrate observations of different sensors. Experiment results show that this algorithm can improve the precision by 60% when the GPS observation is abnormal and accuracy is poor (less than 10mm).

4）This stduy propose an adaptive filtering algorithm with constraints for the fusion of GPS, accelerometer and tilt-meter when the weighting scheme is iteratively estimated. Simulation experiments with different GPS observation precisions and different numbers of satellites in simulation experiments show that the proposed algorithm can significantly improve the reliability of the monitoring system, especially when the GPS observation is abnormal and satellites are insufficient.

6.2 Recommendations for Future Work

Structural health monitoring requires the combination of a lot of information including structural loads, structural static response, dynamic characteristics of the structure, therefore, traditional monitoring technologies are unable to meet the needs of long-term health monitoring of a structure. The monitoring

technology with sensors cannot provide sufficient information, because some affecting factors are difficult to detect. This makes the monitoring cost high and online monitoring is unavailable. This thesis mainly focused on the static index without considering the structural dynamics and the following aspects need future study:

1) Optimisation of the sensor placement. The placement of sensors affects the economic cost, structure operation and the data processing algorithm. How to install minimum sensors properly to acquire maximum reliable information should be studied in detail.

2) Structure damage detection. The structure damage signal is different from and to the original signal. Based on this, we can use wavelet analysis and EMD method to detect the frequency changes at, before and after the damage moment to identify other damage information.

3) Prior information fusion. The description of the uncertainty of prior information in the structure health monitoring needs further study. Areas such as interval constraints, ellipsoid constraints and set constraint will require significant study. These constraints can be combined with the multi sensor measurement and be used for structure health monitoring.

REFERENCES

Amiri-Simkooei A.R.,Tiberius C.C. J.M. (2007), Assessing receiver noise using GPS short baseline time series. GPS Solutions, 11(1):21-35

Axealrad P., Comp C.J.,Macdoran P.F. (1996), SNR-based multipath error correction for GPS differential phase. IEE Trans Aerospace Electronic System 32:650-660

Barnes J.B., Cross P.A. (1998), Processing models for very high accuracy GPS positioning. Journal of Navigation, 51(2): 180-193.

Betaille D.F., Cross P.A., Euler H.J. (2006), Assessment and improvement of the capabilities of a window correlator to model GPS multipath phase errors. IEEE Transactions on Aerospace Electronic Systems, 42(2):705-717.

Bjornar V., Fossen T.I. (2000), A nonlinear observer for integration of GPS and inertial navigation systems. Modeling Identification & Control. 21(4):193-208

Brian D. (1976), Vibration condition monitoring techniques for rotating machinery. The Shock and Vibration Digest. London: SpingerLink. 8 (12): 3. doi:10.1177/058310247600801203

Brunner F.K., Hartinger H., Troyer L. (1999), GPS signal diffraction model-ling: the stochastic SIGMA-D model. Journal of Geodesy, 73:259-267.

Casciati F., Fuggini C. (2009), Towards global positioning system-based structural health Monitoring. In Trends in Civil and Structural Engineering Computing, Topping BHV, Costa Neves LF, Barros RC (eds)(eds.).. Saxe-Coburg Publications: Scotland, Stirlingshire.

Cazzaniga N.E., Pinto L., Forlani G., Abruzzi P. (2005), Monitoring oscillations of slender structures with GPS and accelerometers. Proceedings of the FIG Working Week (2005) and GSDI-8, Cairo, Egypt, 16–21 April,

Celebi M. (1998), GPS measurements-Case congress and/or strong and weak motion structural response studies, Proceedings of Structural Engineers World San Francisco,CA, CD-ROM.

Çelebi M. (2000), GPS in dynamic monitoring of long-period structures. Soil Dynamics and Earthquake Engineering. Volume 20, Issues 5–8, December 2000, Pages 477–483

Celebi M., Prescott W., et al. (1999), GPS monitoring of dynamic behavior of long-period structures. Earthquake Spectra, 15:55-66.

Celebi M., Sanli A. (2002), GPS in pioneering dynamic monitoring of long-period structures. Earthquake Spectra, 18:47.

Chan W.S., Xu Y.L., Ding X.L., Dai W.J. (2006), An integrated GPS-accelerometer data processing technique for structural deformation monitoring. J Geodesy (2006) 80:705-719. DOI: 10.1007/s00190-006-0092-2.

Chan W.S., Xu Y.L., Ding X.L., Xiong Y.L., Dai W.J. (2005), Dynamic displacement measurement accuracy of GPS for monitoring large civil engineering structures. Proceedings of SPIE (2005) 5765, San Diego, PP 54–65.

Chan W.S., Xu Y.L., Ding X.L., Xiong Y.L., Dai W.J. (2006), Assessment of dynamic measurement accuracy of GPS in three dimensions. Journal of Surveying Engineering, 132 (3): 108-177.

Chan W.Y., Man K.L., Wong K.Y. (2001), Real-time kinematic spans the gap, GPS World.

Charles F.(2005) Structural health monitoring publications. (https://www.lanl.gov/projects/ national-security-education-center/engineering/publications/shm-pub.php)

Chen Q.J., Zhang Q., Cheng Y.H. (2013), Railway track irregularity measuring by GNSS/INS integration Proceedings of the 26th international technical meeting of the satellite division of the institute of navigation (ION GNSS+ 2013), Nashvile, TN, September :2180-2194)

Chen Y.Q., Huang D.F., Ding X.L. (2001), Measurement of vibration of tall building with GPS: a case study. Proceedings of SPIE. No.4337:477-483.

Chueng M.S., Tadros G.S., Brown T.G. (1997), Field monitoring and research on performance of the confederation bridge. Canadian Journal of Civil Engineering, 24(6): 951-962

Chung K.T. (1999) A multi-sensor approach to the monitoring of machining processes. M.Phil. Thesis, City University of Hong Kong.

Chung K.T., Geddam A. (2003), A multi-sensor approach to the monitoring of end milling operations. Journal of Materials Processing Technology 139 15-20.

Clement O., Chris R., Wang J.L., Toward the implementation of on-line structural monitoring using RTK-GPS and analysis of results using the wavelet transform. The 10th FIG international symposium on deformation measurements.

Cobb H.S. (1997), GPS pseudolites: theory, design, and applications, PhD Dissertation, Stanford University.

Cohen C.E., Pervan B.S., Cobb,H.S., Lawrence D.G., Powell J.D., B.W.(1993), Parkinson real time cycle ambiguity resolution using a pseudo-lite for precision landing of aircraft with GPS, The Second international symposium on differential satellite navigation systems DSNS'93, Amsterdam, The Netherlands, March 30-April 2 171-178.

Cosser E., (2003), Bridge deflection monitoring and frequency identification with single frequency GPS receiver, Institute of Engineering Surveying and Space Geodesy, University of Nottingham

Dai W.J. et al. (2007), Single epoch ambiguity resolution in structure monitoring using GPS. Geomatics and Information Science of Wuhan University, 32(3): 234-237.

Dai W.J., WU X.X., LUO F.X. (2011), Integration of GPS and accelerometer for high building vibration monitoring. Journal of Vibration and Shock, 30(7): 224-225.

Dai, W.J., Ding, X.L., Li Z.W., Kwok K.C.S., Campbell S. (2006), Tropo-spheric effectson GPS measurements in monitoring tall buildings, Location, 1(5):36-39.

Daniel B., Fritzen C.P., Alfredo G. (2006), Structural health nonitoring. ISBN-13:978-1-905209-01-9 2006

Wang D. (1996), Resolving cycle slips with redundant satellites for kinematic Global Positioning System. Electronics and Commubications in Japan, Part 1, Vol. 79, No 5,1996:103-107.

Ellum C., Naser E.L.J. (2002), Inexpensive kinematic attitude determination from MEMS-base accelerometer and GPS-dervied accelerations. Navigation (Washington, DC) A, PP 117-126 ISSN: 0028-1522 CODEN: NAVIB3

El-Sheimy N. (2004), Inertial techniques and INS/DGPS integration, ENGO 623-Course Notes. Department of Geometrics Engineering, University of Calgary, Canada.

Fan L., Zhao G.C., Su Y.Q. (2013), Fruit fly optimization algorithm optimized general regression neural network in deformation monitoring and prediction. Bulletin of Surveying and Mapping, 11:87-89.

Fan Q., Fang X.H. (2010), Method of deformation monitoring data processing for high-rse building based on empirical mode decomposition denoising. Journal of Jiangnan University (Natural Science Edition), 9(5): 555-558.

Guo H.Z., Cong P.J. (2007), Application of hilbert-huang transform in analysis on monitoring data of dam. Geomatics and Information Science of Wuhan University, 32(9): 774-777.

Guo J.J., et al. (1997), Big building displacement monitoring with GPS. Geotechnical Investigation and Surveying, 146(3):48-51.

Han H.Z., Wang J.L., Meng X.L. (2015), Reconstruction of integrated GPS bridge dynamics using and accelerometer. Journal of China University of Mining & Technology, 44(3): 549-556.

Hera A., Hou Z. (2004), Application of wavelet approach for ASCE structural health monitoring benchmark studies. Journal of Engineering Mechanics, 130(1): 96-104.

Holland J.H. (1975), Adaptation in natural and artificial systems. Ann Arbor:The University of Michigan Press.

Hong X.M., Yang X.S., Huang Q. (2005), Using tilt-meters to measure bridge deflection. Journal of bridge engineering. DOI:10.1061/(ASCE)1084-0702(2005)10:5(564).

Hou Z., Hera A. (2002), Progress of phase II study of the ASCE health monitoring benchmark data using wavelet approach. In: Ling H I, ed. Proceedings of the 15th ASCE Engineering Mechanics Conference, New York, 2002-06-0205. Boca Raton: CRC Press. CD Version.

Hu J., Li X.P., Qu W.L. (2008), Analysis of time domain reflectometry monitoring signals based on composite wavelet transform. Journal of Wuhan University of technology, 30(6): 87-90.

Hu J.Y., Wen H.Y., Zhou L., et al. (2014), Study on dam prediction and inversion with multi-source monitoring data based on IPSO-BP model. Journal of geodesy and geodynamics, 34(4): 67-70.

Huang D.F., Ding X.L., Chen Y.Q. (2001), Wavelet filters based separation of UPS multi-path effects and engineering structure vibrations. Acta Ueodaetica et Cartographica Sinica, 30(1): 36-41.

Huang N.E. (1998), The empirical mode decomposition and the hilbert spectrum for nonlinear and non-stationary time series analysis. Proc. R. Soc. Lond. A March 8, 1998 454:903-995

Janusz B., Mariusz F., Grzegorz N., Marcin S., Maciej W. (2012), GNSS-based multi-sensor system for structural monitoring applications. J. Appl. Geodesy, Vol. 6 pp. 55–64.

Jia M., Tsakiri M., Stewart M. (2000) Mitigation multipath errors using semi-parametric models for high precision static positioning. IAG symposia. Geodesy beyond 2000 The challenges of the first decade, vol 212, pp 393-398

Kijewski C.T. (2003), Full scale measurement sand system identifieation: A time-frequency perspective. Department of Civil Engineering and Geologieal Sciences,University of Notre Dame,Notre Dame.

Kijewski C.T., Kareem A., Kochly M. (2006), Experimental verifi-cation and full-scale deployment of global positioning systems to monitor the dynamic response of tall buildings, Journal of Structural Engineering – ASCE, 132(8):1242-1253.

Ko J.M., Sun Z.G., Ni Y.Q. (2001), Simulaiton of damage method for idenitifeaiton using vibraiton based Kap Shui Mun Bridge. Earthquake Engineering and Engingeering Vibration, 21(4): 117-124.

Kunysz W. (2001), Advanced pinwheel compact controlled reception pattern antenna (AP-CRPA) designed for interference and multipath mitigation. In: Pro-ceedings of IONGPS 2001, Salt Lake City, Utah, 11-14 September, pp. 2030-2036.

Lau C.K., Mak W.P.N., Wong K.Y., Chan W.Y. et al. (1999), Structural health monitoring of three cable-supported bridges in Hong Kong. Structural Health Monitoring 2000. Pennsylvania: Technomic Publishing Co., 450-460

Lee K.S., Geem Z.W.(2005),A new meta-heuristic algorithm for continuous engineering optimization: harmony search theory and practice. Comput. Methods Appl. Mech. Engrg. 194 (2005) 3902–3933

Lee Y.H., Wang J.L., Chris R. (2002), GPS/Pseudolite/INS integration: Concept and first tests GPS solutions. 6:34-46 DOI 10.1007/s10291-002-0010-x

LI G., Qin Q., Dong C.(2000), Optimal placement of sensors ofr monitoring systems on suspension bridges using genetic algorithms. Engineering mechanics,17(1):25-33.

Li C.X., Shi X.F.(2016) Research of attitude algorithm method of the two-axis FOG continuous inclinometer. Electronic Measurement Technology, 2016, 39(3): 118-121.

Li J., Cheng J.H., et al., (2012), Brief introduction of back propagation neural network algorithm and its improvement. Advances in CSIE, Vol. 2, AISC 169, pp. 553–558.

LI S.J., Uzuki Y. (2003), Application of wavelet analysis to structural health monitoring. J. of HUST. (Urban Science Edition), 20(2): 32-35.

Li X.J, Peng G.D., Rizos C., Ge L.L. (2003), Integration of GPS, accelerometer and optical fibre sensors for structural deformation monitoring. Proceedings of 2003 International Symposium on GPS/GNSS, Tokyo, Japan, 617

Li X.J., Ge L.L., Ambikairajah E., Rizos C., Tamura Y., Yoshida A. (2006), Full-scale structural monitoring using an integrated GPS and accelerometer system.GPS Solutions, 10(4):233–247

Li Z., Zhu F., Chen J.J. (2011), Analysis and processing of wind shock deformation monitoring data for bridge based on wavelet transform. Bulletin of Surveying and Mapping, 11: 18-20.

Lin X., Luo G.C. (2016), A new adaptive multi-rate Kalman filter for the data fusion of displacement and acceleration. Chinese J Geophys. 59(5):1608-1615, doi:10. 60381 cjg20160506.

Liu H., Zhang H.Q., Liu B. (2014), A prediction method for the deformation of decp foundation pit based on the particle swarm optimization neural network. Journal of Jilin University; Earth Science Edition, 44(5):160}161}, doi:10.13278/j. cnki, jjucsc. 201405204.

Liu Y., Ji T.H., et al. (2016), Calibration and compensation for accelerometer based on kalman filter and a six-position Method. Piezoelectrics & Acoustooptics, 38(1): 94-98.

Llera C.D.L., Chopra K. (1995), Estimation of accidental torsion effects for seismic design of buildings. Journal of Structural Engineering, Vol. 121, No.1. January. ASCE ISSN 0733-9445/95/0001-0102-0114. Paper No. 7691.

Lovse J.W., Teskey W.F., Lachapelle G., Cannon M.E. (1995), Dynamic deformation monitoring of tall structure using GPS technology. J SurvEng (1995) 121(1):35-40. doi:10.1061/(ASCE)0733-9453 121:1(35)

Luan Y.Z., Luan H.X., et al. (2015), Research on wavelet denoising and kalman filter in bridge deformation monitoring data. Journal of Geodesy and Geodynamics, 35(6): 1041-1045.

Luo F.X., Dai W.J., et al. (2012), EMD-ICA with reference signal method and Its application in UPS multipath. Acta Ueodaetica et Cartographica Sinica, 41(3):366-371.

Ma M. Wang J., Li W., et al. (2014), Identification of potential landslide slippery surface morphology based on displacement monitoring data. Chinese Journal of Underground Space and Engineering, 10(6): 1455-1461.

Madhani P.H., Axelrad P., Krumvieda K. Thomas J. (2001) Mitigation of the near-far problem by successive interference cancellation. Proceedings of US Institute of Navigation GPS-2001, Salt Lake City, Utah, 11-14 Sept, 148-154.

Meng X.L. (2002), Real-time deformation monitoring of bridges using GPS/accelerometers. Phd. Thesis. (2002). Nottingham University.

Meng X.L., Dodson A., Roberts G. (2007), Detecting bridge dynamics with GPS and triaxial accelerometers. Engineering Structures,2007,29(11):3178-3184

Meng X.L., Roberts G.W., Dodson A.H., Cosser E. (2002), The use of pseudolites to augment GPS data for bridge deflection measurements. In: Proc 15th Int Tech Meeting Satellite Division US Inst Navigation, Portland, OR, 24–27 September, pp 851–862

Meng X.L., Roberts G.W., Dodson A.H., CosserE., Barnes J., Rizos C. (2004), Impact of GPS satellite and pseudolite geometry on structural deformation monitoring: analytical and empirical studies. Journal of Geodesy, 77:809-822.

Michael K., Kijewski K., James S. (2005), GPS monitoring in urban zones:calibration and quantifieation of multipath effects.SPIE

Model List for NovAtel Receivers. NovAtel Inc. Effective Date: 17 October, 2011

Moschas F. Stiros S. (2011), Measurement of the dynamic displacements and of the modal frequencies of a short-span pedestrian bridge using GPS and an accelerometer, Engineering Structures, 33(1):10-17.

Nakamura S. (2000), GPS measurement of wind-induced suspension bridge girder displacements. J StructEng 126:1413-1419.

Ni Y.Q., Xia Y., Liao W.Y., Ko J.M. (2009), Technology innovation in developing the structural health monitoring system for GuangZhou new TV tower. Structural Control and Health Monitoring. 2009. DOI:10.1002/stc.303.

Nobuaki K. (2009), Advantage of velocity measurements on instantaneous RTK positioning. GPS Solut(2009) 13:271-280.

Pan G.R., Gu C. (2007), Wavelet neural network prediction method of deformation monitoring data. Journal of Geodesy and Geodynamics, 2007, 27(4): 47-50.

Park H.S., Sohn H.G., Kim I.S., Park J.H. (2008), Application of GPS to monitoring of wind-induced responses of high-rise buildings. The Structural Design of Tall and Special Buildings 2008; 17(1):117–132.

Petovello M., Cannon M., Lachapelle G. (2003), Benefits of using a tactical grade INS for high accuracy positioning. Navigation, Journal of The Institute of Navigation, 2003, 51(1):1-12

Qian J.R., Guo J.J., et al. (1998), Measurment researchs on dynamic property and on top displacement and acceleration during large wind for Diwang. Plaza.hina Cicil Engineering Journal, 31(6):30-38.

Qin H., Lu Y. (2006), Wavelet analysis for inclination monitoring. Journal of Highway and Transportation Research and Development, 2006, 23(8): 57-61.

Quan Y., Gu M., Tamura Y. (2005), Experimental evaluation of aerodynamic damping of square super high-rise buildings. Wind and Structures 2005;8(5):309–324.

Rangwala S., Dornfeld D. (1990), Sensor integration using neural networks for intelligent tool condition monitoring. Trans. ASME J. Eng. Ind. (1990) 112 (3) 219–228.

Rao Y.G., Jiang W.P., Chen H. et al. (2016), Research and realization of deformation monitoring algorithm with millimeter level precision based on BeiDou navigation satellite system. Acta Ueodaetica et Cartographica Sinica, 2016 .45(1):16-21. DOI:10. 11947/j. AUC'S. 2016. 20140649.

Ren C.H, Pan Y.J., et al.（2010） Study on fast precision orientation and incline metering with small diameter fiber gyro. Chinese Journal of Scientific Instrument 2010,31 (5): 1127-1130.

Roberts G.W., Dodson A.H., Ashkenazi V. (1999), Twist and deflection: Monitoring motion of Humber bridge. GPS World, 1999,10(10):24-34.

Roberts G.W., Meng X.L., Dodson A.H. (2004), Integrating a Global Positioning System and accelerometers to monitor the deflection of bridges. Journal ofSurveying Engineering 130(2): 65-72 DOI: 10.106/ (ASCE)0733-9453(2004)130:2(65).

Safak E., Hudnut K. (2006), Real-time structural monitoring and damage detection by acceleration and GPS sensors. Proceedings of the 8th US National Conference on Earthquake Engineering, San Francisco, California, USA, 18–22 April, 2006.

Satirapod C., Khoonphool R., Rizos C. (2003), Multipath mitigation of permanent GPS stations using wavelets. International symposium on GPS/GNSS, Tokyo

Seeber G. (2003), Satellite Geodesy, 2nd edition. Walter de Grupter GmbH & Co.KG, 10786, Berlin Germany.

Segawa R., Sone A., Masuda A., et al. (2001), System identificationof MDOF structures by wavelet transform. In: Yoshiaki K, ed. Proceedings of the US-Japan Joint Workshop and Third Grantees Meeting, Seattle, 2001-08-1516. MonbuKgagku-Sho and The National Science Foundation. CD Version, 2001.

Shao P. (2012), Theoretical and experimental investigation on error correction method of inclinometer. Wuhan University of Technology graduate Thesis.

Söderholm S., Juhola T., Saarnimo T., Karttunen V. (2001), Indoor navigation using a GPS receiver, Proceedings of US Institute of Navigation GPS-2001, Salt Lake City, Utah, 11-14 September, 1479-1486

Sohn H., et al. (2003), A review of structural health monitoring literature: 1996–2001. Los Alamos National Laboratory Report, LA-13976-MS, 2003

Song L., Qin Y. (2009), Six-position testing of MEMS accelerometer. Measurement & Control Technology, 2009，7: 5-9.

Souza E.M., Monico J.F.G. (2004), Wavelet shrinkage: high frequency multipathreduction from GPS relative positioning. GPS Solutions, 8:152-159.

State bureau of surveying and mapping. Specification for check off and test of GPS receiver of surveying model. CH8016-95 S. Beijing Surveing and Mapping Process 1995 1-3

Sumitro S., Okamoto T., Matsui Y., Fujii K. (2001), Long span bridge health monitoring system in Japan.Proc. SPIE.4337-67, 2001: 517-524

Tolman B.W., Craig B.K., (1997), An integrated GPS/Accelerometer system for low dynamics, International Symposium on Kinematic Systems in Geodesy, Geomatics and Navigation, June 1997, Banff, Alberta, Canada.

Townsend B., Fenton P. (1994), A practical approach to the reduction of pseudo range multi-path error in a L1 GPS receiver. In: Proc ION GPS-94. 1994: 143-148

Tu R., Zhang Q., Wang L., Huang G.W. (2015), An improved method for tight integration of GPS and strong-motion records: Complementary advantages. Advances in Space Research 56 (2015) 2335–2344

VanDierendonck A.J., Fenton P., Ford T. (1992), Theory and performance of narrow correlator spacing in a GPS receiver. Navigation 39(3):265-283.

Wand D.C., Qu G.Q., Yin H.T. (2016), High-rate GPS dynamic monitoring of bridge and feature information recognition. Journal of Shandong University of Technology (Natural Science Edition), 2016, 30(2): 45-48.

Wang L., et al. (2011), Experiment results and analysis of the dynamic of a kind of landslide based on GPS deformation monitoring technology. Geomatics and Information Science of Wuhan University, 2011, 36(4): 422-426.

Wang X., Liu W.S., Wang C. (2011), Processing of monitoring data of building deformation based on wavelet threshold denoising. Engineering of surverying and mapping, 2011, 20(1): 44-46.

Wu J.B., Zhou S.J. (2016), The de-noising study based on empirical mode decomposition and independent component analysis. Science of Surveying and Mapping, 2016, 41(7): 197-201.

Wu S.H. Hu Z.R., Cheng P.G. (2015), Application of the non-equal interval weighted gray combination of linear regression model in deformation monitoring based on the genetic neural network. Geotechnical Investigation ＆ Surveying, 2015,12: 55-59.

Xiao G.Y., Liu L.L., Chen Q.Q. (2011), Using GPS for dynamic monitoring tall-building's structures based on wavelet analysis. 2011 Seventh International Conference on Natural Computation.

Xie Z.N., Gu M. (2009), Across-wind dynamic response of high-rise building under wind action with interference effects from one and two tall buildings.The Structural Design of Tall Special Buildings 2009;18(1):37–57.

Xu F., Wang C.C., Zhang F. (2012), Application of particle swarm optimization-BP neutral network in dam displacement prediction. Science of Surveying and Mapping, 2012, 37(4): 181-183.

Xu J., Huang S.X., Ma F.H. (2010), The Dynamic characteristics analysis for the large bridge based on the improved hilbert-huang transformation. Geomatics and Information Science of Wuhan University, 2010, 35(7): 801-805.

Xu P.L., Shi C. Fang R.X., et al. (2013), High-rate precise point positioning (PPP) to measure seismic wave motions: an experimental comparison of GPS PPP with inertial measurement units. Journal of Geodesy, 2013, 87(4):361-372

Yan S.H., Chen S.S. (2009), Application of wavelet neural networks to forecast deformation monitoring. Hydrographic Surveying and Charting, 2009, 29(3): 71-73.

Yang J.N., Lei Y., Huang N.E. (2001), Damage identification of civil engineering structures using Hilbert-Huang transform. In:Chang F K, ed. Proceedings of the 3`d International Workshop on Structural Health Monitoring, Stanford, 2001-09-1214. Boca Raton: CRC Press, 2001. 544553

Yang J.N., Lei Y., Lin S., et al. (2004), Hilbert-huang based approach for structural damage detection. Journal of Engineering Mechanics, 2004, 130: 85-95.

Yang J.N., Lin S.L., Pan S.W. (2002), Damage identification of structures using hilbert-huang spectral analysis. In: Ling H I,ed. Proceedings of the 15th ASCE Engineering Mechanics Conference, New York, 2002-06-0205. Boca Raton: CRC Press, 2002. 7077.

Yang Y., Song L., Xu T. (2002), Robust parameter estimation for correlated geodetic observations. Selected Papers for English Edition, Acta Geodeatica Cartography Sinica, 31(2)：18-24.

Yang Y.X., Gao W.G. (2006), A new learing statistic for adaptive filter based on predicted residuals. Progress in Nature Science, 2006, 16(8): 833-837.

Yang Y.X., Gao W.G. (2006), An optimal adaptive Kalman filter. J Geodesy, 2006, 80: 177-183[DOI]

Yao L.H., Gao J.X., Wang J. (2011), New wavelet threshold noise reduction model of dynamic deformation signal. Engineering of surverying and mapping, 2011, 20(5): 18-21.

Ye S.R., Zhao L.W., Chen D.Z. (2016), Real-time deformation monitoring data processing based on BDS triple-frequency observations. Geomatics and Information Science of Wuhan University, 2016, 41(6): 722-727.

Yi T., et al. (2010), Recent research and applications of GPS based technology for bridge health monitoring. M. Sci. China Technol. Sci. (2010) 53: 2597. doi:10.1007/s11431-010-4076-3

Yi T.H., Li H.N., Gu M. (2013) Recent research and applications of GPS-based monitoring technology for high-rise structures. Structural control and health monitoring. Control Health Moniting.2013;20:649–670

Yigit C.O., Cevat I., Yetkin M. (2008), Monitoring of tall building's dynamic behaviour using precision inclination sensors. 13th FIG Symposium on Deformation Measurement and Analysis.

Yu J.R., Shao X.D., Meng X.L., et al. (2014), Experimental research on dynamic monitoring of bridges using GNSS and accelerometer. China Journal of Highway and Transport, 2014, 27(2): 63-69.

Yu J.Y. (2014), GNSS and RTS technologies based structural dynamic deformation monitoring of bridges. Hunan University, 2014.

Zheng D.W., Zhong P., Ding X.L., Chen W. (2005), Filtering GPS time series using a vondrak filter and cross-validation. Journal of Geodesy, 79:363-369.

Zhong P., Ding X.L., et al. (2010), Sidereal filtering based on single differences for mitigating GPS multipath effects on short baselines Journal of Geodesy. February 2010, Volume 84, Issue 2, pp 145–158

Zhong P., Ding X.L., Zheng D.W., Chen W., Huang D.F. (2008), Adaptive wavelet transform based on cross-validation method and its application to GPS multipath mitigation. GPSSolut12:109-117. doi: 10.1007/s10291-007-0071-y

Zhou J., Huang Y., Yang Y., Ou J. (1997), Robust least squares methods. Publishing House of Huazhong University of Science and Technology, Wuhan.

Zhou X.W., Yang Y.M. (2012), Application of BFGS-BP in tunnel deformation monitoring data processing.Science of Surveying and Mapping, 2012, 37(3): 108-109.